THE ENERGY BUDGET AT THE EARTH'S SURFACE

Part II

Production Research Report No. 72

Agricultural Research Service
U.S. DEPARTMENT OF AGRICULTURE
In Cooperation With
NEW YORK STATE COLLEGE OF AGRICULTURE
and
THERM ADVANCED RESEARCH DIVISION,
THERM, INC.
for
Meteorology Department
U.S. ARMY ELECTRONIC PROVING GROUND

USAEPG SUMMARY

DA Task: 3A99-27-005-08 Micrometeorology (USAEPG)
Title: The Energy Budget at the Earth's Surface: Part II
Originator: Agricultural Research Service, U.S. Department of Agriculture, Ithaca, N.Y.

The general objective of the studies conducted by the Agricultural Research Service, Ithaca, N.Y., is to evaluate plant, soil, and meteorological interactions involved in the partition of thermal energy at the earth's surface. This report presents in part the results of research conducted with the particular objective of evaluating the aerodynamic surface roughness and relating it to the elastic and geometric characteristics of the surface cover.

Theoretical and experimental investigations of the turbulent transfer characteristics of the airstream near the ground are reported. It is shown that the surface boundary layer must be divided into two regions: the freestream above the surface where the various forms of turbulent transfer are nearly independent of height, and the airstream within the vegetative canopy where sources and sinks are present. Several theoretical models for canopy flow are reported and compared with observations. A numerical method for determining the aerodynamic characteristics and their standard errors in the freestream is described. Experimental results for freestream and canopy flow are reported.

It is concluded that canopy flow is fully turbulent and that the observations satisfy best a theoretical model in which the mixing length is a function of height above the ground surface. Experimental data show that the aerodynamic surface roughness varies with the windspeed and the variations depend upon the geometric and elastic characteristics of the vegetation. Elastic vegetation shows decreasing roughness with increasing windspeed and shearing stress is nearly independent of windspeed. Semirigid vegetation has increasing roughness and shearing stress with increasing windspeed. The results of these studies serve to emphasize that the concept of "roughness length," although very useful, is in reality an artifact.

No recommendations are stated.

METEOROLOGY DEPARTMENT
USAEPG

This study was conducted under Interdepartmental Cross Service Order No. 2-61 and cooperative agreement No. 12-14-100-2477(41). The first three sections herein were issued essentially the same as Therm Advanced Research Reports TAR-IR 601 (March 1960), TAR-IR 602 (July 1960), and TAR-IR 611 (February 1961).

605527

THE ENERGY BUDGET AT THE EARTH'S SURFACE

Part II

Studies at Ithaca, N.Y., 1960

Agricultural Research Service
U.S. DEPARTMENT OF AGRICULTURE
In Cooperation With
The Department of Agronomy
NEW YORK STATE COLLEGE OF AGRICULTURE
Cornell University
and
THERM ADVANCED RESEARCH DIVISION, THERM, INC.
for
Meteorology Department
U.S. ARMY ELECTRONIC PROVING GROUND
Fort Huachuca, Ariz.

Prepared by:
Edgar R. Lemon, USDA
Principal Investigator

Contributions by:
Winton Covey, USDA
S. D. Ling, Therm, Inc.
D. E. Ordway, Therm, Inc.
A. Ritter, Therm, Inc.
D. A. Spence, Therm, Inc.
Jerry Stoller, Cornell University
H. S. Tan, Therm, Inc.

Production Research Report No. 72

Washington, D.C. September 1963

CONTENTS

THE ENERGY BUDGET AT THE EARTH'S SURFACE

Part II

INTRODUCTION

Unfortunately, the evaluation of the partition of solar radiation into other forms of energy at the earth's surface has to depend, in part, upon indirect means. For example, energy exchange calculations based upon aerodynamic principles have to be used to estimate sensible heat exchange. The principles are customarily used also to estimate latent heat and momentum exchange. More recently, the photochemical fixation of carbon dioxide in the process of photosynthesis has been evaluated from aerodynamic exchange calculations of carbon dioxide transfer to vegetated surfaces.

Historically, the aerodynamic exchange principles were first developed in wind tunnel and laboratory fluid flow studies, then applied to atmospheric exchange studies at the earth's surface either over water or over land where the vegetation was generally short or sparse. It has been commonly accepted that such calculations are more complicated over water because of its surface instability. This arises from the fact that in the exchange calculations commonly used, it is necessary to know certain boundary conditions, i.e., have knowledge of a reference plane where the turbulent boundary layer begins. One can readily see that on land surfaces the problem should be much simpler, since the stable soil surface can serve as the reference plane.

Recent investigations over more lush vegetative surfaces of the land, however, have demonstrated that these surfaces may theoretically and experimentally be more difficult to handle than water surfaces simply because of changing geometric characteristics (plant growth, leaf fall) and changing elastic properties (stalk bending, leaf flutter, and streamlining). Of course, these problems are amplified with larger plants; i.e., prairie grass, farm crops, and forests.

When one wants to evaluate the heat budget over extended periods of time—for days and months as we are attempting to do—it is practically impossible at present to use any aerodynamic technique other than the so-called log profile methods. Since this method depends upon knowledge of the surface reference plane where the turbulent boundary layer begins (and we are particularly interested in the energy exchanges with extensive vegetative surfaces), it is necessary to resolve the new complications that have naturally developed. This requires a systematic research effort into the turbulent exchange characteristics within and above the dynamic vegetative canopy. This report takes up in detail the theoretical and experimental approaches used in 1960 to understand further the aerodynamic exchange processes within and above the plant canopy. The studies were carried out in addition to the routine collection of heat budget data for the 1960 growing season over an alfalfa field and a cornfield. The results of the heat budget studies will be taken up in another publication.

The first three sections in the present study take up the theoretical development and supporting experimental results concerning the airflow characteristics within the source and sink region of the turbulent boundary layer at the earth's surface, as well as the airflow characteristics just above the source and sink region. Two models for "canopy flow" (in the source and sink layer) were developed. It was later found that the model based upon fully turbulent flow within the plant canopy most realistically applies to nature. To facilitate experimental studies, it was postulated that the turbulent structure could be broken down into two classifications: (1) a transient state and (2) a quasi-steady state. To date, only the quasi-steady state has been investigated. The turbulent canopy flow model postulated a linear growth of diffusivity within the canopy flow layer, rather than the log velocity profile (which holds above the canopy flow layer). The theory and experimental results demonstrate a curvature reversal of the velocity profile deep in the canopy layer.

The last two sections discuss the complexity of the relationship of the logarithmic velocity profile characteristics above the canopy to the dynamic surface properties of lush vegetation. To facilitate the study of the relationships involved, a machine computation method was worked out and described (p.28). From the method one can evaluate the friction velocity, roughness length, and effective displacement parameters along with their standard errors. The last section takes up the experimental findings from log profile studies over alfalfa, wheat, and corn. An amazing phenomenon was discovered in that both the alfalfa and wheat demonstrated a constant friction velocity with increasing windspeed once a "critical" windspeed was reached. Evidently, the elastic plants "streamlined" so that a decrease in roughness compensated for increasing windspeed.

The last section also takes up an evaluation of the distribution of shear and the momentum transfer coefficient within the vegetative canopy in wheat and corn. These studies focus attention on the fact that shear originates within the roughness volume, and not at some empirical plane. Further studies are to be made to evaluate also the source and sink distribution for sensible heat, latent heat, and carbon dioxide within the canopy layer.

EFFECTS OF TURBULENCE AND PHOTOSYNTHESIS ON CO_2 PROFILES IN THE LOWER ATMOSPHERE

By D. E. Ordway, A. Ritter, D. A. Spence, and H. S. Tan

BACKGROUND

The two causes of turbulence in the atmosphere are (1) forced convection, through the boundary layer type shear flow instability (effect of velocity profile), and (2) free convection, through the buoyancy force-type instability (effect of heating from below).

At present much literature on the study of turbulence exists on forced convection, but little definitive knowledge is available regarding the second type. In the present study, it is our purpose to limit the first phase of the investigation to the effect of the forced convective, or boundary-layer type turbulence only, on atmospheric CO_2 distribution. We are considering the problem of steady state atmospheric boundary layer flow and shall now introduce a principle of "flux conservation."

This principle states in essence that the transport equation for any physical quantity Q must be of the form

$$\frac{dQ}{dt}=\frac{\partial Q}{\partial t}+q.\nabla Q=\mathrm{div}(K\nabla Q)+S\equiv 0 \qquad (1)$$

where K is the flux coefficient, S the distributed source distribution, t is time, and q the flow velocity. In other words, particle derivative of Q must vanish. This is indeed a generalization of the well-known constant flux hypothesis (*29*) [1] long adopted by micrometeorologists, to include the distributed source contribution.

Under the usual hypothesis of flow stratification, application of this principle to the steady state distribution of CO_2 concentration, E, with height, z, immediately gives

$$q.\ \rho\nabla E=\frac{\partial}{\partial z}\left[D\frac{\partial E}{\partial z}\right]+w\equiv 0 \qquad (2)$$

where w is distributed sink or source of CO_2 due to photosynthesis and respiration, and D the total diffusivity; i.e., sum of molecular diffusion (laminar, D_L) and eddy mixing (turbulent, D_T).

Application of the same principle to x-momentum with u as wind velocity gives

$$q.\ \rho\nabla u=\frac{\partial\tau}{\partial z}-\vartheta\equiv 0 \qquad (3)$$

where ϑ is distributed shear source, i.e., leaf drag, and τ is the shear stress, given by

$$\tau=(\mu+\epsilon)\frac{\partial u}{\partial z} \qquad (4)$$

with μ denoting laminar viscosity and ϵ, eddy viscosity.

The validity of this principle can most easily be seen from the limiting behavior of equation 3. Indeed, for outer flow where $\vartheta\equiv 0$, this equation leads to a constant shear requirement that is famous for the logarithmic velocity profile in turbulent wall flow and linear velocity profile in laminar Couette flow. On the other hand, when $\vartheta\neq 0$, this equation directly gives the differential equation of canopy flow velocity distribution.

Equations 2 and 3 will form the basis of our mathematical study of the atmospheric carbon dioxide concentration and the canopy flow, respectively.

ATMOSPHERIC CARBON DIOXIDE CONTENT STUDY

CO_2 content in the lower atmosphere controls and is in turn controlled by the life process on earth. The mechanism that keeps local CO_2 content from becoming deficient or excessive is the process of molecular (laminar) and eddy (turbulent) diffusion. The differential equation governing the steady state CO_2 concentration, E, assuming adequate CO_2 for saturation requirement of photosynthesis, can therefore be written in general as follows:

$$\frac{\partial}{\partial z}\left(D\frac{\partial E}{\partial z}\right)+w=0 \qquad (5)$$

$$w=-f(z)E+g(z) \qquad (6)$$

where D denotes the total diffusivity, w the rate of CO_2 assimilation or production as a result of photosynthesis (f) and respiration (g). Functions f and g are defined by:

$$f(z)=\text{photosynthetic rate coefficient}=C_1L(z)\sigma'(z) \qquad (7)$$

[1] Italic figures in parentheses refer to Literature Cited, p. 48.

$$g(z) = \text{rate of respiration} = C_2\sigma'(z). \tag{8}$$

Here $L(z)$ is the light intensity function (5), $\sigma'(z)$ the leaf area density function, and C_1 and C_2 are constants.

With $w=0$ for $z>h$ (h=plant height), it is evident that the plane $z=h$ separates the atmosphere into two regions, inside each of which different laws govern the CO_2 distribution, namely.

The outer flow, $z>h$—

$$\frac{\partial}{\partial z}\left(D\frac{\partial E}{\partial z}\right)=0 \tag{9}$$

The inner flow, $z<h$—

$$\frac{\partial}{\partial z}\left(D\frac{\partial E}{\partial z}\right)-f(z)E+g(z)=0. \tag{10}$$

Equations 5 and 6 show clearly the respective roles played by turbulence and photosynthesis on the atmospheric CO_2 distribution: the effect of turbulence appears in the diffusive term $\frac{\partial}{\partial z}\left(D\frac{\partial E}{\partial z}\right)$ through D, the eddy diffusivity coefficient. The effect of photosynthesis that depends on leaf area, light intensity, and atmospheric CO_2 concentration appears as the linear term $f(z)E$ of the differential equation. The nonhomogeneous term $g(z)$ represents the effect of respiration, which is independent of light and CO_2 contents.

Now, the kinetic transport mechanism for mass (diffusion), momentum (shear), and energy (heat conduction) are identical. Upon introducing the concept of constant turbulent Schmidt number defined by

$$S_{c_T}=\frac{\epsilon}{\rho D_T} \tag{11}$$

we can usually establish some correlation between CO_2 concentration profile $E(z)$ and velocity profile $u(z)$. Let us consider now the two flow regimes.

Outer Flow, $z>h$

Since outer flow is nothing but the turbulent wall flow, where $\tau=\tau_0$, $\epsilon=Cz$, on introducing the Schmidt number, equation 9 takes the form

$$\frac{\partial}{\partial z}\left(z\frac{\partial E}{\partial z}\right)=0 \tag{12}$$

giving

$$E-E_0=C\ln z. \tag{13}$$

Like the velocity distribution, E also has a logarithmic profile.

However, one must be careful in not pushing the analogy too far. Equation 12 is indeed identical with that governing the velocity distribution, but the analogy stops here. Whereas the nonslip condition over the datum plane of velocity profile necessarily represents a momentum sink, the boundary condition over the datum plane of concentration profile can be either source or sink, depending solely on the relative rate of respiration and photosynthesis. Moreover, even the datum planes for the two cases are usually at different locations. Thus, the only conclusion one can safely draw from the similitude of the two differential equations is that the two solutions must belong to the same family of curves.

Inner Flow, $z<h$

In this region, $\tau\neq$constant. As can be seen by comparing with the canopy flow equation derived in the discussion of the laminar flow model study, p. 5, the differential equation for E differs essentially from that for u. Thus little correlation between the two profiles can be expected. Here, two cases should be considered separately, depending on the linear term in the differential equation.

1. Respiration Profile (Nighttime).

In this case,

$$f(z)=L(z)\equiv 0,\ g(z)\neq 0. \tag{14}$$

Equation 10 reduces to the following form,

$$\frac{\partial}{\partial z}\left(D\frac{\partial E}{\partial z}\right)+g(z)=0. \tag{15}$$

The solution to this equation can be obtained through integration, as follows:

$$\frac{\partial E}{\partial z}=\frac{1}{D}\left[C-\int g(z)dz\right]$$

$$E-E_0=\int^z\frac{1}{D}\left[C-\int g(z)dz\right]dz. \tag{16}$$

2. Photosynthesis Profile (Daytime).

In this case, if

$$f(z)\neq 0,\ g(z)\neq 0, \tag{17}$$

the full equation 10 must be retained; i.e.,

$$D\frac{\partial^2 E}{\partial z^2}+\frac{\partial D}{\partial z}\frac{\partial E}{\partial z}-f(z)E=-g(z). \tag{18}$$

A general solution to this equation usually presents great complication and difficulty. However, if we make the approximation D=constant, which has been commonly adopted by various investigators (*32*), this equation simplifies to the following generalized Hille's equation:

$$D\frac{d^2E}{dz^2}-f(z)E=-g(z). \tag{19}$$

Although this assumption is admittedly crude, nevertheless, it should provide a good first approximation.

A solution to equation 19 can be obtained by introducing a Fourier spectrum for $f(z)$ and expressing the complementary solution in the form

$$Y=e^{\alpha_1 z}\sum^{\infty}a_n e^{\mathrm{i}nz}+e^{\alpha_2 z}\sum^{\infty}b_n e^{\mathrm{i}nz}=Y_1+Y_2. \tag{20}$$

The determination of characteristic exponents α_i by Hille determinant and the recursion formulas connecting the a_n's and b_n's are discussed in detail by Whittaker and Watson (*39*). For the particular solution, by writing

$$Y=v_1Y_1=v_2Y_2 \tag{21}$$

and applying the method of variation of parameters, it can be shown that (*10*)

$$v_1=-\int\frac{Y_2}{\Delta(Y_1,Y_2)}\,g(z)dz$$

$$v_2=\int\frac{Y_1}{\Delta(Y_1,Y_2)}\,g(z)dz \tag{22}$$

where $\Delta(Y_1,Y_2)$ is the Wronskian of Y_1 and Y_2.

CANOPY FLOW VELOCITY DISTRIBUTION STUDY

We define canopy flow as the flow inside the plants ($0<z<h$), which consists mainly of a turbulent layer at the upper part and a wake-type flow at the lower part. It is clear that a really satisfactory study must be a statistical one, of ensemble average type approach. However, as a crude approximation, it seems also plausible that we can replace the distributed plant leaves by a fictitious distribution of shear centers and solve the differential equation corresponding to this model. This approach is by nature speculative. At the present moment there are two models of approach under consideration.

Laminar Flow Model

The differential equation for velocity u can be written:

$$\mu\frac{d^2u}{dz^2}-F(z)u^2=0 \tag{23}$$

where μ is the laminar viscosity and $F(z)$ is some function of the plant characteristics. The indirect solution to this equation can be obtained by quadrature after certain transformations and expressed in terms of elliptic functions as follows:

$$\left(\frac{du}{dz}\right)^2=\frac{2}{\mu}\int_0^u F[z(u)]u^2du+k_1$$

so,

$$z=\int_0^u\frac{du}{[G(u)+k_1]^{1/2}}+k_2. \tag{24}$$

A detailed discussion and some typical results of this model are given below.

In the first model of the canopy flow velocity distributions study, an approximate solution to the velocity profile $u(z)$ in the base flow within the plants has been considered. At the upper edge of the flow, say $z=z_l$, we see that the outside turbulent flow effectively "drags" the canopy flow, analogous to a moving wall with a velocity u_l. If we replace the leaves by an effective distribution of infinitesimal "shear centers," we can write an equation of horizontal force equilibrium from figure 1. We assume that τ, the fluid dynamic shear, is due mainly to the molecular momentum transport of laminar flow and $\overline{D}$, the average drag per unit volume of the shear centers, is turbulent in nature. In nondimensional form, this yields,

$$0=\frac{d^2\bar{u}}{d\bar{z}^2}-S(\bar{z})\,\frac{\bar{u}^2}{2} \tag{25}$$

where $\bar{u}\equiv u/u_l$, $\bar{z}\equiv z/z_l$ and

$$S(\bar{z})\equiv\overline{C}_D\,Re_l\,\frac{d\sigma(\bar{z})}{d\bar{z}}. \tag{26}$$

$\overline{C}_D$ is a mean drag coefficient of the shear centers, which is turbulent and is independent of $\bar{u}$; Re_l is the Reynolds number dependent on u_l and z_l, and $d\sigma(\bar{z})/d\bar{z}$ is an effective, equivalent local leaf area density. Equation 25, together with the boundary

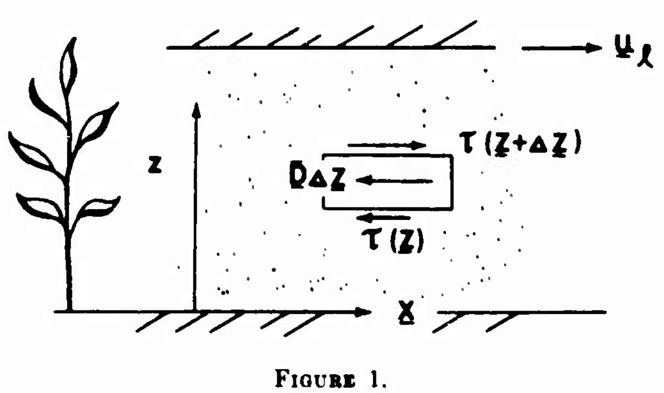

FIGURE 1.

673752 O—63——2

conditions at z_l and 0, respectively,

$$\bar u(1)=1 \tag{27}$$

$$\bar u(0)=0 \tag{28}$$

then determines the velocity profile in the canopy flow. Since the solution is characterized only by $S(\bar z)$, we call $S(\bar z)$ the "shape function." Because it is always positive, we see that the variation of the slope is always negative. That is, the velocity profile is always concave backwards as opposed to the typical laminar boundary layer, which is concaved forward.

Equation 25 is a quasi-nonlinear differential equation of second order. In general, the solution has not been found. However, for constant S or $S(\bar z)=\bar S$, a suitable transformation to the velocity gradient as the independent variable and the velocity as the dependent variable permits integration. The result is

$$\left[\frac{\bar S k}{\sqrt{3}}\right]^{1/2}\bar z=F\left[\cos^{-1}\frac{(\sqrt{3}-1)k-\bar u}{(\sqrt{3}+1)k+\bar u},\ \frac{2+\sqrt{3}}{4}\right]$$
$$-F\left[\cos^{-1}(2-\sqrt{3}),\ \frac{2+\sqrt{3}}{4}\right] \tag{29}$$

where k is related to $\bar S$ and the profile slope at the ground; i.e., the ground shear by

$$k^3=\frac{3}{\bar S}\left(\frac{d\bar u}{d\bar z}\right)^2\Bigg]_{\bar z=0} \tag{30}$$

and F is the elliptic function of the first kind. For a given value of the constant shape function, the parameter k, and hence the ground shear, is determined *in general* by satisfying equation 27. The results are plotted in figure 2 over a representative range. A typical velocity profile for $\bar S=141$ has also been computed and is illustrated in figure 3.

Turbulent Flow Model

This model has been suggested under the heuristic argument that on the leaf scale, the flow may appear laminar; on plant scale, it must appear turbulent. The corresponding differential equation takes the form:

$$\frac{d}{dz}\left(\epsilon\frac{du}{dz}\right)-F(z)u^2=0 \tag{31}$$

where $\epsilon(z)$ is the eddy viscosity.

For a first approximation, we may take ϵ as constant (several orders of magnitude greater than μ (*33*)), thus reducing equation 31 to equation 24, only with a different scale.

Further study of both models should be carried out. A final choice can only be made after sufficient field data have been gathered to confirm the theoretical model.

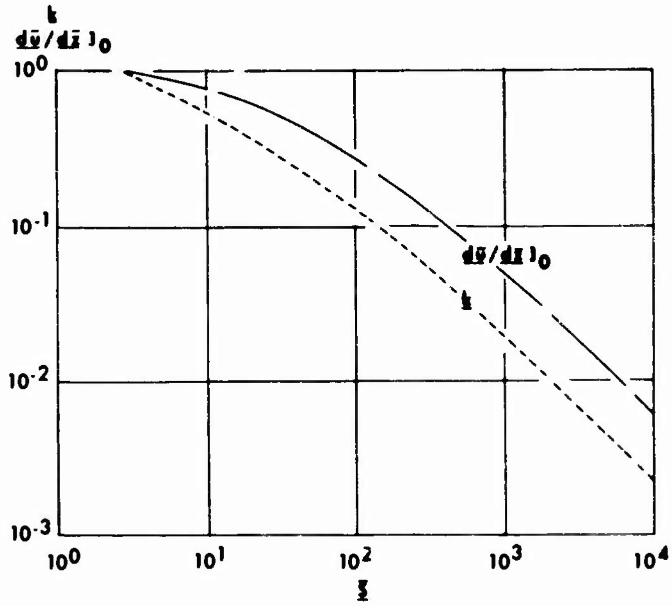

FIGURE 2.—Canopy flow wall shear for a constant shape function.

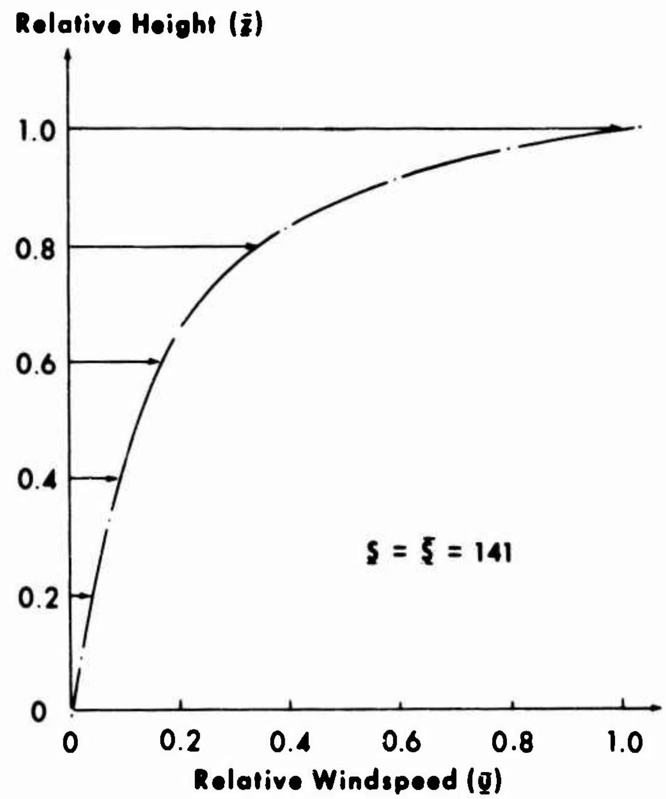

FIGURE 3.—Canopy flow velocity profile.

QUASI-STEADY MICRO-METEOROLOGICAL ATMOSPHERIC BOUNDARY LAYER OVER A WHEATFIELD

By H. S. TAN and S. C. LING

THEORETICAL MODEL

Concept of Relevant Scale

In the study of turbulent transport process in the lowest part of the earth's atmosphere, one of the most important concepts is the "relevant scale" of the micro-structure of the wind. Indeed, any typical wind record taken at a point in a cornfield or wheatfield exhibits (fig. 4) at least two distinct ranges of eddy scales: (1) a high frequency fluctuating velocity component of small-scale eddies superimposed on (2) a lower frequency gusty wind composed of large eddies. To a cosmic observer in the large or meteorological sense, both these eddies, with scales of different orders of magnitude, are nothing but turbulence. However, to an observer sitting at the top of a wheat crop in the small or micro-meteorological sense, the picture is different. What he recognizes here is a turbulent (high frequency), gusty (low frequency) wind. The recognition of such a "relevant scale" is important if we recall that the term "turbulence" is so vaguely defined. Indeed, P. A. Sheppard brought this point out most clearly in his final address to the International Symposium on Atmospheric Turbulence in the Boundary Layer (7). He points out as follows:

> The atmosphere . . . shows simultaneously many modes of motion, varying in scale from the "long waves" of the westerlies down through depressions and anticyclones, convective motions and so on, to small scale turbulence . . .
>
> Now the motions which we commonly study under the name of turbulence are so much smaller in scale than depressions and the like that we make little or no attempt to pick out individual elements of the flow, except quite formally as: e.g., in a power spectrum. But who doubts that if we magnified the field sufficiently, drew a series of "synoptic charts," in fact, we should in general find recognizable structures and changes in those structures with time . . .

If we study the wind structure in its spectrum over a relatively short time, we notice that the energy of turbulence usually resolves itself into two widely separated wave packets (fig. 5). This phenomenon can be interpreted from a micro-meteorological point of view as follows: E_1, associated with small-scale eddies, carries the turbulent mixing part of the kinetic energy that controls both the vertical and horizontal transport processes; E_2 associated with large-scale eddies,

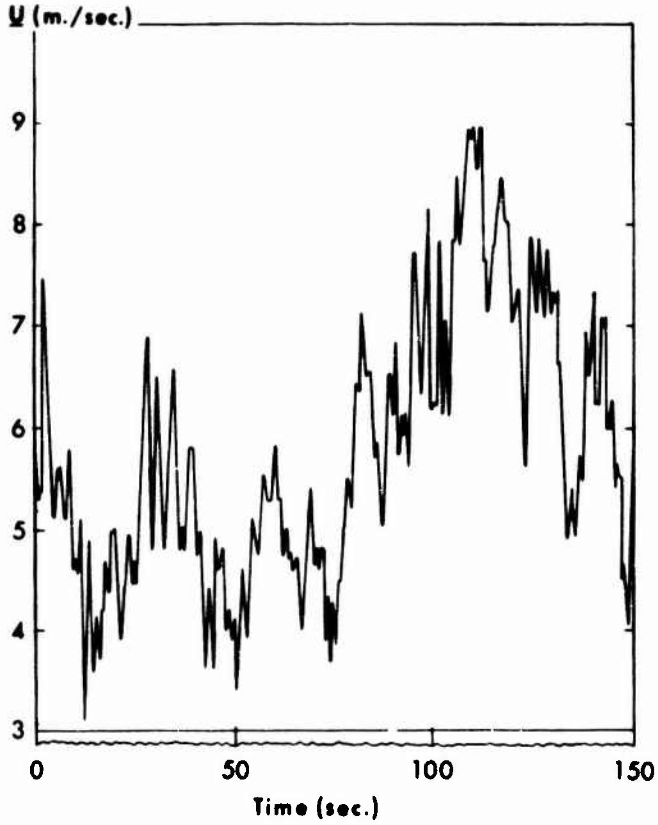

FIGURE 4.—Horizontal wind (u) at 7-meter height.

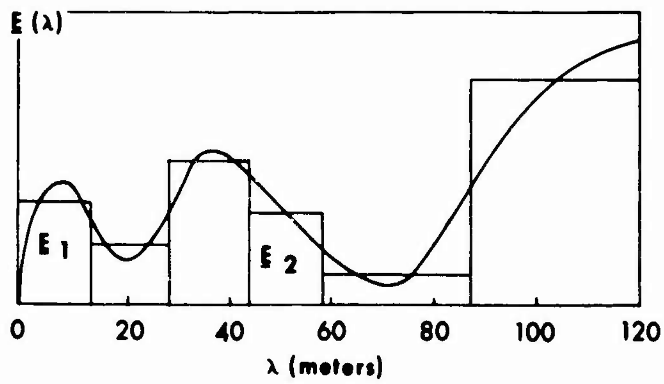

FIGURE 5.—Typical spectrum of horizontal wind.

represents the part of the kinetic energy carried away by gusty winds, which can only affect the horizontal transport. This separation of two distinct eddy scales responsible for the vertical and the horizontal transport processes, respectively, was also arrived at by A. Monin (*20*).

Subdivision of Atmospheric Boundary Layer: Synoptic Versus Micro-Layers

Whenever there is a fluid flow past a surface, a boundary layer will develop. Now the structure of the atmospheric wind consists of components of large- and small-scale eddies embedded in the synoptic (geostrophic) wind. The large-scale turbulence present in the synoptic wind boundary layer is caused by the presence of large-scale roughness elements, such as terrain irregularities, and the layer thickness usually extends to a height of a few kilometers. The relatively smaller scale micro-meteorological, or gusty winds, are nothing but these large-size turbulent eddies in the synoptic layer. Indeed these are actually air lumps of the size of a few hundred meters, sweeping across the field and leaving behind the gust front a growing micro-boundary layer. This layer quickly reaches a quasi-steady state a few meters behind the propagating front and resembles very much the steady flow leading edge boundary layer over a flat plate. The thickness of this micro-boundary layer inside the micro-meteorological wind usually extends to about 10 meters. Further, the small-scale turbulence inside this layer with eddy sizes ranging in decameters is caused by small-scale roughness elements, such a plant crops.

On the average, a gusty wind of 10 meters per second with a steady interval of several minutes and a turbulent fluctuating component having a frequency of a fraction of a cycle per second are typical. On the other hand, a micro-wind in a field is never steady. However, the relatively well-defined edge of gusts (air lumps) indicates that a frontal theory can be developed. The highly transient portion behind the gust front extends about 10 meters, after which a quasi-steady state is quickly established. This means that a 10-second average field measurement taken in the middle portion of a 1-minute period gusty wind should indicate a consistent steady state logarithmic velocity profile outside the crop. The validity of this scaling idea has now been amply verified by field measurements.

The classification of eddy sizes and definition of a quasi-steady condition can be quantitatively expressed in terms of the micro-boundary layer thickness, δ, and the relaxation time, t, in the following manner.

Quasi-steady condition considered reached at:

$$U_0 t > \delta \text{ where } \delta \doteq 10 \text{ m.},$$

$$t > \frac{\delta}{U_0} \text{ sec.}$$

$t=0$ at the gust front.

Now let λ denote the eddy size, or wavelength, and then we have the following scheme:

Scale	*Eddy classification*
$\frac{\lambda}{\delta} < 2.0$	Turbulent eddies.
$2.0 < \frac{\lambda}{\delta} < 20$	Unsteady gusts.
$\frac{\lambda}{\delta} > 20$	Quasi-steady wind.

Proper Averaging Period

In a natural field, over a sufficiently long period, all scales of eddies will appear and the spectrum will be continuous. A velocity mean taken over an arbitrary period of time is thus meaningless. The proper averaging period must be arrived at by "relevant scale" conside..tions in accordance with the process involved. For example, in the vertical transport process that is controlled solely by small-scale turbulence (wavelength of meter size and period of seconds), extraneous effects of the large-scale turbulence (gusty winds) will be introduced if the averaging period is taken in hours.

This will utterly ruin the statistical behavior of the relevant small-scale eddies. On the other hand, for the horizontal transport process that is governed by all scales of turbulence, averaging periods of less than a minute will give no trend at all. Moreover, the results will be meaningless since, under such an averaging process, the largest energy-carrying eddy scales in the spectrum are completely left out.

The technique proposed in the present report therefore involves a selective sampling procedure, in order to insure the proper quasi-steady behavior. It must be remarked at this point that this quasi-steady state study alone is not sufficient for complete knowledge of the vertical transport process; this must be augmented by a further study of the transient; i.e., an accelerating and decelerating regime. The final effective eddy diffusivity will have to be evaluated as a weighted sum of the quasi-steady and nonsteady measurements, and should more or less deviate from that corresponding to the classical logarithmic velocity profile. For the study of the nonsteady regime, frontal theory might be expected to play an essential role. However, such a study will not be attempted before we enter the second phase of our research program.

FIELD MEASUREMENTS

Experimental Considerations

As stated earlier, in a natural field over a sufficiently long time, the entire spectrum of eddy scales appears and hence, theoretically, the relevant scale encompasses the complete spectrum. Such longtime averages of atmospheric measurements are definitely of interest in the study of weekly or seasonal variations of atmospheric phenomena and, in particular, of horizontal transport processes. On the other hand, over a relatively short interval, we can usually identify two distinct, dominating ranges of eddy scales, of which the smaller one alone controls the vertical transport process in the earth's atmosphere. Thus, inasmuch as we restrict our study to the vertical atmospheric distribution, the long period averages can be ruled out as improper. The "relevant scale" for the vertical distribution study is the small one; the corresponding averaging time is the short periods; i.e., of the size of meters and period of 10 seconds.

Based on the above reasoning, a new approach for handling this problem was proposed: separation of the transient part of the wind from the steady part and a study of their characteristics as separate entities. In order to envision more clearly the picture involved, one may consider the atmospheric boundary layer as consisting of three distinct cascading layers, as follows:

(1) Laminar sublayers, at the surface of the leaf and stalk;

(2) Micro-meteorologic, turbulent boundary layer (over plant top and canopy flow within plants);

(3) Synoptic, turbulent boundary layer of earth's atmosphere.

These three layers embrace different scales of eddies and have different mean velocity gradients. The roughness of leaf and stalk surfaces as seen by the laminar sublayer does not directly influence the mixing mechanism of the micro-turbulent layer. On the other hand, the fluctuating velocity in the laminar sublayer is directly the result of the eddies of the micro-turbulent layer. In the same manner the roughness of plants as seen by the micro-turbulent layer plays no direct role in the mixing mechanism of the larger synoptic atmospheric boundary layer. However, the large eddies of the synoptic layer are responsible for the gustiness of the micro-turbulent layer. This is precisely why the micro-turbulent layer is never steady. The turbulence in the synoptic layer is controlled essentially by the roughness scale of much larger magnitude, such as terrestrial irregularities (hills and valleys), other disturbances generated by temperature gradients (buoyant motion), and continental pressure fields.

The small-scale eddies in the micro-turbulent layer are now solely responsible for the vertical diffusion of carbon dioxide, vapor, and heat around plants. This is the layer that is to be studied in detail, in order to understand the mechanism of lower atmospheric diffusion. As mentioned earlier, this layer is influenced by the large eddies of the outer synoptic boundary layer, and therefore the state of flow varies constantly between the transient and the quasi-steady. During the transient stage, the wind shear is not constant over the height, so that the logarithmic wind profile does not exist. However, with eddies of sufficient size, a period of quasi-steady state exists and this then enables one to measure the steady-state flow-parameters.

As a first step toward the understanding of a complex problem, this report is limited to the study of the quasi-steady state.

The wheatfield selected for the present study is situated on top of Mount Pleasant, 5 miles east of Ithaca, N.Y. Measurements of wind profiles were taken during July 1960, starting when the heads of wheat were level with the top leaves, and continuing up to the time when the heads were 30 cm. above the top leaves. The average peak-plant-height ranged from 95 to 130 cm. Average plant density was 60 stalks per square foot.

The instrument mast was located near the center of a 200- by 200-meter field. Small-cup anemometers, 9 cm. in diameter, were used. They were seated at 10, 20, 40, 80, and 160 cm. above the peak level of crop. Counters for all anemometers were read simultaneously at every 30-second interval. Attempts were made to select the wind-profile record only when a quasi-steady wind existed. That is, a wind record was selected when it was preceded and followed by a 30-second wind record with approximately the same average wind velocity as measured by the top anemometer.

From the experimental record it was evident that for a considerable part of the time the wind profiles over the crop were transient.

Five representative steady wind-profiles of different mean-velocity ranges are plotted in figure 6. One important characteristic is that the mean velocity gradient at the peak level of the crop changes only slightly with increase in mean velocity. In addition, the characteristics of these profiles are insensitive to thermal conditions and stages of plant growth.

Logarithmic Wind Profiles

Steady wind velocity profiles over a crop can be expressed by

$$U(Z, U_0)=\frac{U_*(U_0)}{k}\log\frac{Z-d(U_0)}{Z_0(U_0)} \qquad Z>h \quad (32)$$

where

$k=0.42$, von Kármán's constant;
Z=height above ground;
h=peak level of crop;
U_0=mean velocity outside of boundary layer (at 10-meter height based on logarithmic profile);

$U_* = \ln(10)\cdot\sqrt{\frac{\tau}{\rho}}$, friction velocity;
d = zero-plane displacement;
Z_0 = roughness length;
τ = shear stress;
ρ = mass density.

U_*, d, and Z_0 are to be determined from the measured wind profiles, and they are found to be dependent on U_0. The value of d is obtained from equation 33, where the mean velocity gradients at two different heights are obtained from measurements.

$$d=\frac{\left(\frac{\partial U}{\partial Z}\right)_2 Z_2-\left(\frac{\partial U}{\partial Z}\right)_1 Z_1}{\left(\frac{\partial U}{\partial Z}\right)_2-\left(\frac{\partial U}{\partial Z}\right)_1}. \quad (33)$$

U_* is computed, after d is known, as follows:

$$U_*=k\cdot\frac{U_1-U_2}{\log\frac{(Z_1-d)}{(Z_2-d)}}. \quad (34)$$

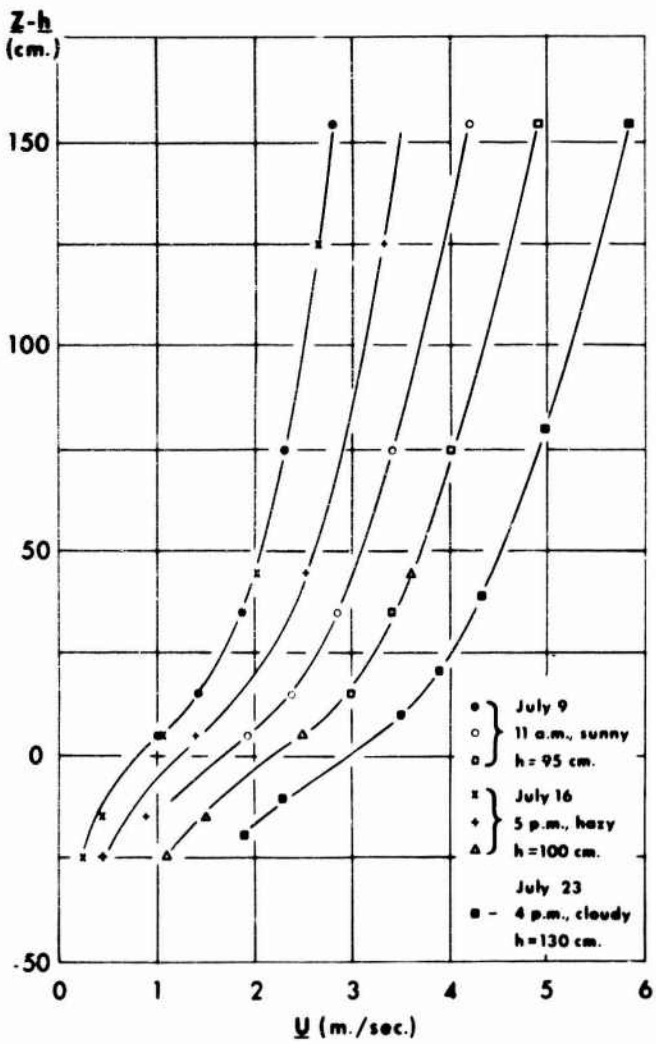

FIGURE 6.—Mean velocity profiles over winter wheat.

Z_0 is computed after d and U_* are found.

$$Z_0=\frac{Z_1-d}{10^{kU_1/U_*}}. \quad (35)$$

When the three parameters have been computed for each experimental wind profile, the value of U_0 (at 10 meters height) can be computed from equation 32.

Values of Z_0, U_*, and $\frac{d}{h}$ are plotted in figure 7 as a function of U_0. Both $\frac{d}{h}$ and U_* are found to be insensitive to free-stream velocity. On the other hand, Z_0 decreases rapidly with increase of U_0 and remains constant when U_0 increases beyond 8 meters/sec. The drag coefficient

$$C_D=[\ln(10)]^2\,\frac{\tau}{\frac{\rho U_0^2}{2}}=2\left(\frac{U_*}{U_0}\right)^2$$

is plotted as a function of U_0 in figure 7. The reduction of C_D with increasing U_0 is evident.

Canopy Flow

The basic differential equation for canopy flow (*35*) is

$$\frac{\partial}{\partial Z}[\epsilon(Z)+\mu]\frac{\partial U}{\partial Z}=A(Z)\,\frac{C'_D\rho U^2}{2} \quad (36)$$

where

$\epsilon(Z)$ = eddy viscosity, a function of Z;
μ = dynamic viscosity, a constant;
$A(Z)$ = total vertical plane area of plants/unit volume, a function of Z;
C'_D = drag coefficient of plant;
ρ = mass density of air;
U_h = mean velocity at height, h.

Within the flow range considered, C'_D can be taken as independent of Reynolds number. Equation 36 can be rearranged as

$$\frac{\partial^2\bar U}{\partial\bar Z^2}=\frac{U_h h^2 A(\bar Z)C'_D\rho\bar U^2/2-\frac{\partial\epsilon(\bar Z)}{\partial\bar Z}\frac{\partial\bar U}{\partial\bar Z}}{\epsilon(\bar Z)+\mu}\equiv S(\bar Z)\,\frac{\bar U^2}{2} \quad (37)$$

where $\bar U$ and $\bar Z$ are U and Z normalized by U_h and h, respectively. We consider $S(\bar Z)$ to be the parameter (shape function) of the differential equation. For wheat, $A(\bar Z)$ can be considered as independent of ($\bar Z$), because the area density of the plant is practically constant with height. The eddy viscosity $\epsilon(\bar Z)$ may be taken as being a constant for the top quarter of $\bar Z$, for the reason

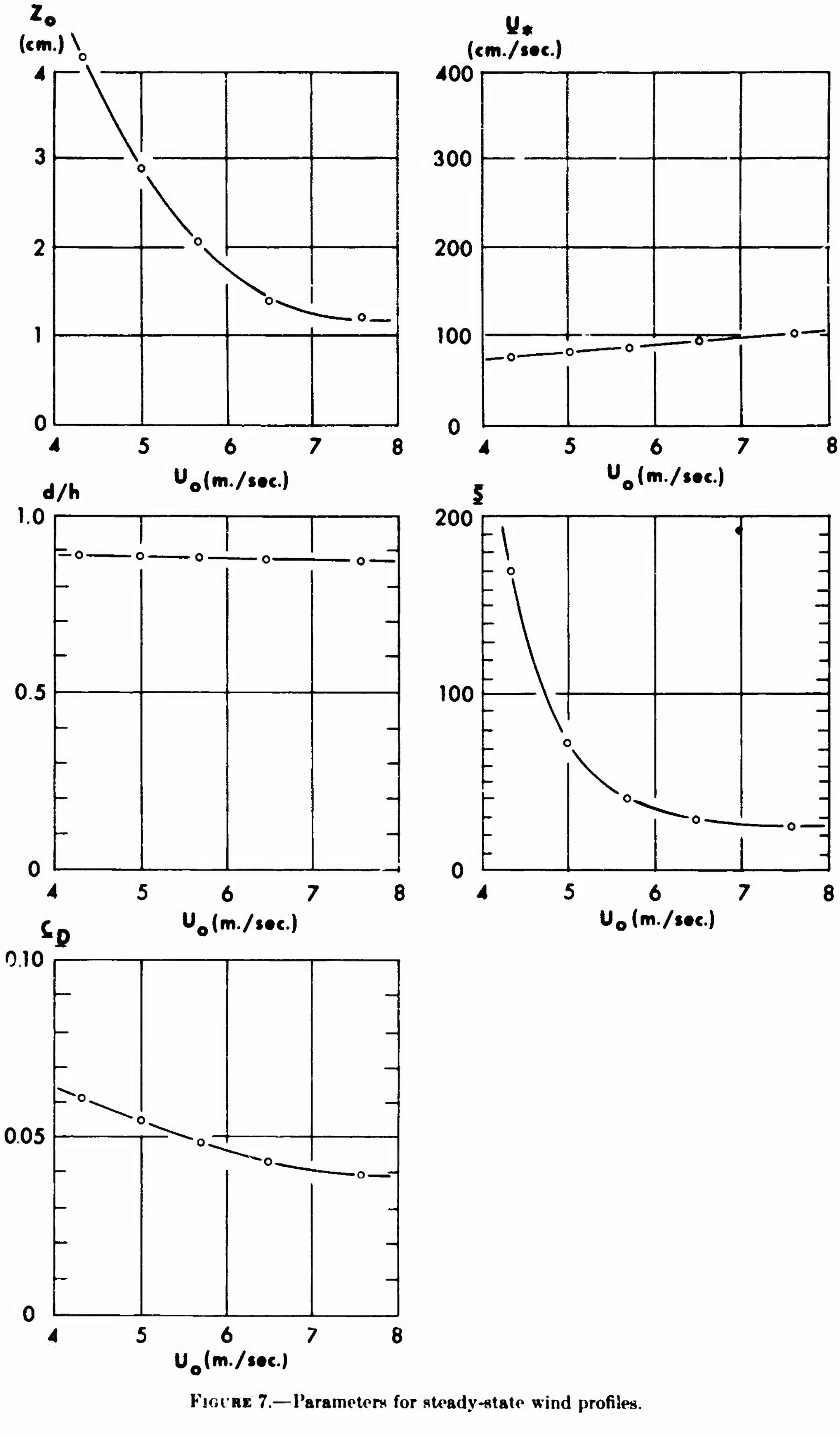

FIGURE 7.—Parameters for steady-state wind profiles.

that the energy-carrying eddies are not expected to be modified extensively as they penetrate into the plants. Hence $S(\overline{Z})$ may be taken as a constant $\overline{S}$.

With boundary conditions

$$\overline{U}|_{\overline{Z}=1}=1$$

$$\overline{U}|_{\overline{Z}=0}=0$$

equation 37 is unique and can be solved for each value of $\overline{S}$. The canopy wind profiles are plotted in figure 8 for various shape functions from 10 to 1,000. The velocity gradient at h, $\left.\frac{\partial \overline{U}}{\partial \overline{Z}}\right|_h$, is plotted in figure 9.

The velocity gradient of the wind profiles at h must match the velocity gradient at the edge of the canopy flow (fig. 9). From this condition the shape function, $\overline{S}$, as a function of outer boundary-layer velocity, U_o, can be found and is plotted in figure 7. This completes the tie between the wind profile and canopy flow once the steady wind, U_o, is given.

The shape function, $\overline{S}$, drops rapidly with increase of U_o and tends to reach a terminal value above a 7-meter/sec. windspeed. In figure 8, one notes that the canopy profiles are more curved for high $\overline{S}$ and low U_o, and approach asymptotically a straight line for low $\overline{S}$ and large U_o. $\overline{S}$ varies directly as C_D', and inversely as $\epsilon(\overline{Z})$; the reduction of $\overline{S}$ at large U_o means a reduction in C_D' and an increase in $\epsilon(\overline{Z})$. This in turn means that the flow is more turbulent. We see therefore that the field measurements exhibit trends similar to those anticipated from the theory.

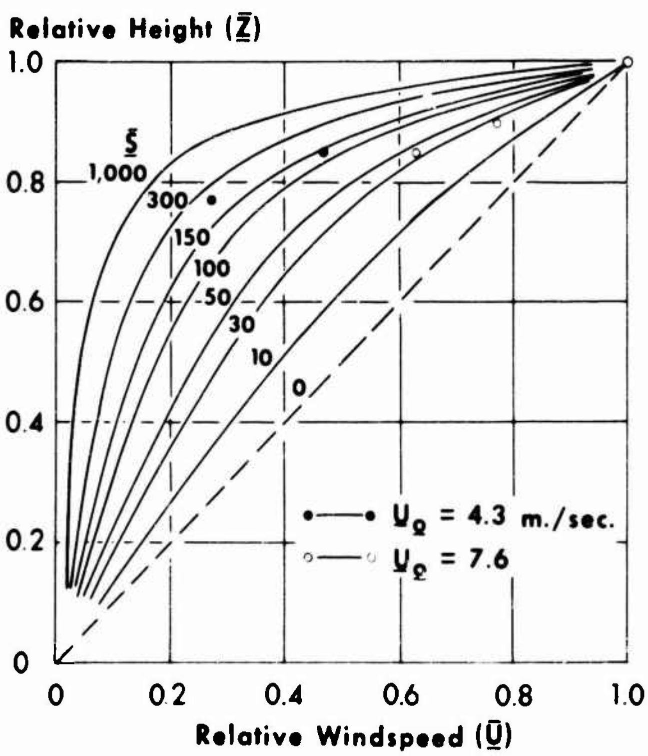

FIGURE 8.—Canopy wind profiles for various constant shape functions, $\overline{S}$.

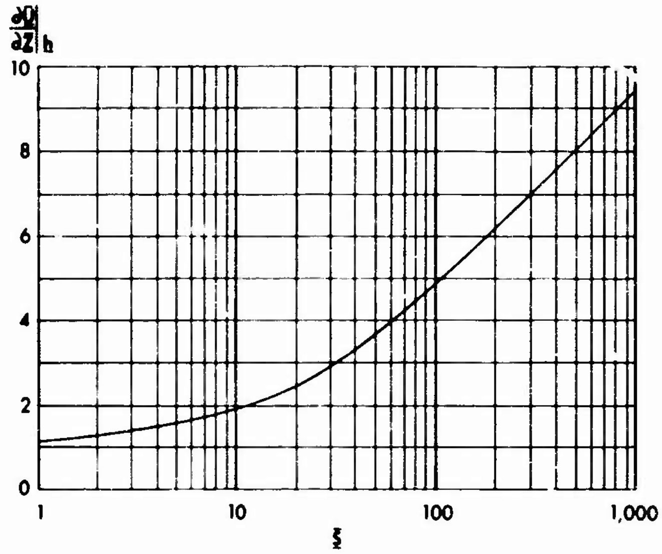

FIGURE 9.—Velocity gradients at peak-plant-height as a function of shape function, $\overline{S}$.

Accurate measurement of canopy flow has not yet been made, but from some preliminary measurements there seems to be a tendency for the canopy wind profile to cross from a lower $\overline{S}$ value to a higher $\overline{S}$ value curve, as $\overline{Z}$ goes below 0.8. This would mean that $\epsilon(\overline{Z})$ may not be a constant, but should be reduced as $\overline{Z}$ is lowered. Thus far, experimental data are not sufficient to evaluate $\epsilon(\overline{Z})$.

From the known value of the $\overline{S}$ factor, for a given U_h and plant density, the value of eddy viscosity can be computed. For the range of data presented, the ratio of eddy viscosity to dynamic viscosity ranges from 1×10^3 to 3×10^4. The eddy viscosity at peak plant height, ϵ_h, can be computed from the logarithmic equation, equation 32,

$$\epsilon_h=\rho k(h-d)U_*/\ln(10). \tag{38}$$

The ratio of eddy viscosity to dynamic viscosity obtained by this method is considered to be more accurate, and it was found to range from 0.9×10^3 to 2.2×10^3. The values at high range do not agree well with those computed by canopy flow. The error is probably due to the assumption of constant $\epsilon(\overline{Z})$. More experimental measurements and analytical study on $\epsilon(\overline{Z})$ will be conducted.

A STUDY OF ATMOSPHERIC TURBULENCE AND CANOPY FLOW

By H. S. TAN and S. C. LING

In the present study the following two aspects are stressed: (1) To furnish the "relevant scale" concept with a more rigorous foundation and (2) to improve the canopy flow model by postulating the linear growth of diffusivity rather than the logarithmic velocity profile as the basic property of turbulent wall flow. It is gratifying to find that the predicted velocity profile curvature reversal deep in the canopy flow was indeed observed and pointed out repeatedly by several investigators (*22*).

It might not be out of place to mention at this point that until now we have not approached the diffusion problem with source distribution, the photosynthesis problem, and the thermo-instability problem as seriously as we would like to. The main reason behind this is the heavy dependence of these phenomena on the atmospheric turbulence, of which little is definitely known and much has yet to be clarified before we can satisfactorily formulate a working model of atmospheric transport.

An introductory discussion of turbulent diffusivity in shear flow is provided by Dr. Spence.

Our study so far has been restricted to the quasi-steady part of the mean motion (time mean). A tentative shear wave model for treating the nonsteady problem has been suggested by Dr. Ling, and included.

TURBULENT TRANSPORT IN LOWER ATMOSPHERE

Equation of Turbulent Transport

The transport of any physical quantity in the atmosphere is governed by the following basic differential equation:

$$\frac{d\theta}{dt}\equiv\frac{\partial\theta}{\partial t}+q\cdot\nabla\theta=\nabla\cdot(K\nabla\theta)+S(\theta) \qquad (39)$$

in which θ denotes the transported quantity, q the wind velocity, K the coefficient of diffusivity, and S the source function. Physically the equation states that:

(a) The total derivative of quantity θ is given by the sum of divergence of flux and rate of production of θ;
(b) The flux of θ is in turn proportional to the gradient of θ;
(c) The flux per unit gradient is named the coefficient of diffusivity.

In connection with this transport equation, the following two studies are of particular interest:

(a) Simplification of the equation to correspond with specific physical problems;
(b) Effect of turbulence on diffusivity, K, and hence on its solution θ.

For lower atmospheric study the following simplifications are usually obtained.

1. Vertical stratification and horizontal wind

$$\nabla=k\frac{\partial}{\partial z},\quad q=iU:\ \text{so}\ q\cdot\nabla\theta\equiv0$$

and equation 39 becomes

$$\frac{\partial\theta}{\partial t}=\frac{\partial}{\partial z}\left(K\frac{\partial\theta}{\partial z}\right)+S(\theta), \qquad (40)$$

which, upon putting $S\equiv0$, forms the basic equation for usual nonsteady, micro-meteorology study:

$$\frac{\partial\theta}{\partial t}=\frac{\partial}{\partial z}\left(K\frac{\partial\theta}{\partial z}\right). \qquad (40a)$$

2. Steadiness condition, $\frac{\partial}{\partial t}\equiv0$

Equation 39 further reduces to

$$\frac{\partial}{\partial z}\left(K\frac{\partial\theta}{\partial z}\right)+S(\theta)=0. \qquad (41)$$

Equation 41 actually forms the basis for the first two sections of this report (pp. 3 and 7) and for the present investigation. Upon putting $S\equiv0$, equation 41 simplifies to

$$\frac{\partial}{\partial z}\left(K\frac{\partial\theta}{\partial z}\right)=0; \qquad (41a)$$

i.e., the well-known "constant flux" equation for steady earth surface layer.

For the present report, θ will denote either carbon dioxide concentration in photosynthesis study or horizontal windspeed, u, in velocity distribution study.

It is clear from the above that our study naturally separates into two regions by the crop height, $z=h$. For the outer flow ($z>h$), $S=0$, the governing equations for both $[CO_2]$ and u are given by equations 40a and 41a; i.e., the well-known atmospheric diffusion equation. For quasi-steady case, we have simply:

$$\frac{\partial}{\partial z}\left(K\frac{\partial\theta}{\partial z}\right)=0. \tag{42}$$

For the inner flow ($z<h$), on the other hand, $S\neq0$. In this case it has been shown that for quasi-steady flow we have (*35*):

$$[CO_2]\text{ study: }\frac{\partial}{\partial z}\left(K\frac{\partial\theta}{\partial z}\right)+C(z)\theta+g(z)=0; \tag{43}$$

$$u\text{ study: }\frac{\partial}{\partial z}\left(K\frac{\partial\theta}{\partial z}\right)+S(z)\theta^2=0. \tag{44}$$

Turbulence and Diffusivity

The role played by turbulence in atmospheric transport takes on the form of coefficient of diffusivity, K. Prandtl first introduced his famous mixing length theory for the mechanism of turbulence transport and showed that K is actually proportional to his mixing length, l. By further postulating that in the neighborhood of a solid wall, mixing length, l (and, consequently, diffusivity, K) grows linearly with distance z from the wall, he was able to deduce from equation 42 that the velocity profile for turbulent wall flow must follow a logarithmic law; i.e.,

$$u=\frac{u^*}{k}\ln\left(\frac{z}{z_0}\right). \tag{45}$$

This velocity profile has indeed been confirmed by many observations.

In the last 20 years, however, there has been a noted trend among investigators toward taking a diametrically opposite view in discarding the mixing-length hypothesis completely and accepting the logarithmic law as the basis for theoretical development, from which the "austausch coefficient" K can be shown to grow linearly with z. So far as the outer flow is concerned, it makes no difference which point of view to take. However, as soon as we enter into the inner flow region, where there are distributed sources, both approaches face impossible difficulty. On the other hand, by extending Prandtl's linear growth hypothesis instead to the canopy flow diffusivity, i.e., $K\sim z$, equation 44 becomes:

$$\frac{\partial}{\partial z}\left(z\frac{\partial u}{\partial z}\right)+Su^2=0. \tag{44a}$$

So we were able to compute the theoretical velocity profile and predict a curvature reversal deep in the crop, which has been amply verified by various field measurements.

This fact is considered to be of great significance toward justifying Prandtl's mixing length concept in general,[2] and pointing to the basic correctness of our theoretical canopy flow model in particular, i.e., turbulent flow with linearly growing diffusivity, K.

Theory of Average and Its Applications

1. *Theorems*

The following definitions and theorems are intended for clarifying some basic questions concerning the process of ensemble, space, and time averages employed in the atmospheric turbulence study.

Definition.—The mean value of a bounded fluctuating function f is defined by:

$$\hat{f}(t)|_{2T}=\frac{1}{2T}\int_{t-T}^{t+T}f(t')dt'. \tag{46}$$

Theorem 1.—It is evident that

$$\text{(a)}\quad \hat{f}(t)|_{T\to0}=f(t);$$

$$\text{(b)}\quad \hat{f}(t)|_{T\to\infty}=\text{const.};$$

$$\text{(c)}\quad \hat{f}(t)|_{T}\ =fn(t,T). \tag{47}$$

Theorem 2.—The mean of a simple periodic function retains its periodicity, T_0, but the amplitude falls off according to $(T/T_0)^{-1}$. It may be noted that there exists a set of eigen-functions:

$$\hat{f}(t)|_{T=nT_0}\equiv0. \tag{48}$$

Definition.—The spectrum of a fluctuating function f is defined by:

$$f(\omega)|_T=\int_0^T f(t)e^{i\omega t}dt=f(\omega,T); \tag{49}$$

$$f(k)|_X=\int_0^X f(x)e^{ikx}dx=f(k,X). \tag{49a}$$

Theorem 3.—It is evident that $f(\omega,\infty)=f(\omega)$, $f(k,\infty)=f(k)$; i.e., the Fourier Spectra.

Definition.—We define the two following time and space correlation functions:

$$R(\tau)=\frac{1}{\overline{u'^2}}\overline{u(x,t)u(x,t+\tau)}; \tag{50}$$

[2] Indeed it would be interesting to introduce a parametric representation of the "Austausch" coefficient as follows: $K\sim z^\alpha$ where α is a function of S. $\alpha\to1$ as $S\to0$. $\alpha(S)$ can be determined by correlating the canopy flow velocity profile with varying crop density.

$$R(\xi)=\frac{1}{\overline{u^2}}\overline{u(x,t)u(x+\xi,t)}; \tag{51}$$

where $(^-)$ denotes ensemble average.

Theorem 4.—Ergodic Principle: If a turbulent field has a steady time mean and a uniform space mean, then the field is ergodic; that is, the ensemble average can be replaced by either time or space average.

In the present case this gives

$$R(\tau)=\lim_{T\to\infty}\frac{1}{\overline{u'^2}}\frac{1}{T}\int_0^T u(x,t)u(x,t+\tau)dt; \tag{50a}$$

$$R(\xi)=\lim_{T\to\infty}\frac{1}{\overline{u'^2}}\frac{1}{T}\int_0^T u(x,t)u(x+\xi,t)dt. \tag{51a}$$

Infinite extent of T or X cannot be reached, and so a real-steady, uniform mean does not exist. This state can, however, be approximated by a quasi-steady and quasi-uniform mean over $\overline{T}$ and $\overline{X}$. $\overline{T}$ denotes the maximum averaging period or length of record and $\overline{X}$ the actual field extent.

For a turbulent field with quasi-steady, quasi-uniform mean, quasi-ergodic hypothesis permits the following replacement:

$$\overline{f(\ )}=\frac{1}{N}\sum_{n=1}^{N}\frac{1}{T}\int_0^T f(x_n,t)dt \tag{52}$$

where T is the finite averaging period, $x_n=x(t_n)$, and $t_n-t_{n-1}>T$. This gives—

Theorem 5.—

$$R(\tau)=\frac{1}{\overline{u'^2}}\frac{1}{NT}\sum_{n=1}^{N}\int_0^T u(x_n,t)u(x_n,t+\tau)dt=R_\tau(T); \tag{53}$$

$$R(\xi)=\frac{1}{\overline{u'^2}}\frac{1}{NT}\sum_{n=1}^{N}\int_0^T u(x_n,t)u(x_n+\xi,t)dt=R_\xi(T). \tag{54}$$

Theorem 6.—For a bounded, fluctuating function $f(x, t)$ with quasi-steady, quasi-homogeneous mean, we postulate the following similarity law:

$$R_\tau(T)\sim R_\xi(T); \tag{55}$$

i.e., as functions of averaging period, T, the space and time correlation functions behave in similar manner.

The general behavior of R_τ and R_ξ, as functions of T in the lower atmospheric turbulence, is shown in reference (*24: fig. 1.2.1, p. 40*) and reference (*3: fig. 3.4.15, p. 201*), respectively. From the figures given in the references, it is evident that both R_τ and R_ξ are monotonically increasing functions of T, and, indeed, $\lim_{T\to\infty} R_{\tau,\xi}(T)=R(\tau,\xi)$. This means $R_{\tau,\xi}(T)$ is a faster decreasing function than $R_{\tau,\xi}$ with increasing τ, ξ.

Hence, by the Birkhoff Ergodic Theorem (*12*), the applicability of a quasi-ergodic hypothesis is assured.

Theorem 7.—Eddy scale L is defined by (*27*):

$$L=\int_0^\infty R_\xi(T)d_\xi=L_\xi(T) \tag{56}$$

$$=\alpha\int_0^\infty R_\tau(T)dT=\alpha L_\tau(T) \tag{56a}$$

from theorem 6. Thus, the recognizable eddy scale grows with the interval of average T.

Theorem 8.—In equation 56a, we can put

$$\alpha=\overline{U}. \tag{57}$$

By field measurements, Cramer (*4*) established the following remarkable relationship,

$$R_\tau(T)=R_\xi(T), \xi=\overline{U}\tau, \tag{58}$$

based on a 20-minute sampling interval (T) with $\overline{U}$ the 20-minute mean windspeed. These correlation curves fit approximately the Kolmogoroff Law for inertial subrange; i.e.,

$$1-R\sim\tau^{2/3} \tag{59}$$

and the agreement improves with increasing turbulence level, indicating that isotropy extends further into lower frequency range with higher turbulence intensity.

2. *Application to atmospheric turbulence analysis*

An atmospheric wind record exhibits random fluctuations containing many frequencies, and usually a few dominant ones. The maximum averaging period, $\overline{T}$, is limited from above by the length of the record available.

An instrument has finite resolution and, hence, can only read a corresponding average with $T>0$. The minimum averaging period, $\underline{T}$, is thus limited from below by the instrument sensitivity.

An ideal spectrum $\sqrt{\overline{u'^2}}(\omega)$ corresponds to $\overline{T}\to\infty$, $\underline{T}\to 0$. Now what are the effects of finiteness of $\overline{T}$ and $\underline{T}$ on a spectrum?

Theorem 5 shows that the maximum recognizable eddy scale is limited by $\overline{T}$. [Indeed $L(T)$ is a monotonically increasing function of T.] Thus, $\overline{T}$ effectively offers a low frequency (low-wave number) cutoff, in the sense that beyond this point the spectrum function defined by equation 39 only holds formally and loses its physical significance.

Theorem 2 and equation 49 show that the multiplying factor for averaging over period T of a periodic function with periodicity T_0 varies as $(T/T_0)^{-1}$. Thus, because of the inevitable averaging character of an instrument, the spectrum of higher frequency ($T_0<T$) or small-scale fluctuating components are effectively suppressed. In other words, this averaging process removes a large part of the time dependence due to small-scale eddies, but retains the time dependence of large-scale eddies. The $\underline{T}$ of instrument sensitivity, therefore, imposes the high frequency (high-wave number) cutoff.

In relation to the relevant eddy scale, $L(T)$, for vertical atmospheric turbulent transport processes, the smaller scale eddies play the role of turbulent mixing (austausch), while larger eddies appear as nonsteady wind.

If there were no dominant scales of atmospheric eddies, then the word "mean" would have little meaning. In the atmospheric surface layer, however, there are usually two natural dominant scales of eddies: the small-scale ones produced by the roughness elements, such as plant leaf and stalk; and the large-scale ones produced by the terrain irregularities, like hill and dale. The existence of these definitely separated ranges of eddy scale has been demonstrated by field record; it gives a unique meaning to the word "mean," and, moreover, it introduces in a natural way the concept of relevant scale and proper averaging period.

ANALYSIS OF ATMOSPHERIC WIND IN THE VICINITY OF PLANTS

Background Information of This Study

The atmospheric wind consists of a cascade of turbulent eddies, varying in size from a few meters at the plant to macroscale at the fringe of the atmosphere (*36*). The wind in the vicinity of a crop is influenced by all scales of atmospheric disturbances. Thus, strictly speaking, no stationary time average exists. However, if we limit our interest to a finite scale and period, a quasi-steady average can usually be found.

The basic turbulent mechanism in the vicinity of a crop is controlled primarily by the roughness effect of the crop alone. In addition, this mechanism is maintained by a driving wind, U_0, that, within a given period of interest, can be represented by a mean wind and Fourier spectrum of oscillating winds. This driving wind is a function of all external influences other than that of the crop. With this in view, it is possible to treat the turbulent, atmospheric boundary layer as three intermixed states of flow, namely: (1) steady; (2) quasi-steady; and (3) nonsteady.

The mean driving wind contributes to the local steady state, while the short-wave spectrum of the fluctuating wind constitutes its turbulent mechanism. A sustained local wind or a long wave of 1,000 meters can be taken as quasi-steady flow. A wavelength in the range of 40 to 1,000 meters is considered nonsteady. The oscillating components in this range propagate downward. Very little is known about nonsteady turbulent-boundary-layer flow. Indeed, the types of nonsteady boundary layers investigated are either laminar-boundary layers (*8*, *17*, *27*, *38*) or turbulent-boundary layers (*11*) driven by a nonturbulent, oscillatory flow field (potential flow). A boundary layer driven by a turbulent shear flow remains a subject yet to be studied.

The most important feature that governs the turbulent transport in the vicinity of a crop is the steady-state-velocity profile. To obtain these profiles by field measurement, the sampling period required should be greater than the relaxation period of the boundary layer. The relaxation period will be defined in the section on shear-wave theory. For flow over a crop, this relaxation time is approximately 10 seconds. An averaging period of 30 seconds should smooth out the high-frequency waves due to turbulent eddies. If the averaging period is extended to cover the maximum range of the nonsteady wind, the time dependent factor of this component can again be eliminated. However, it can be shown from field measurements (fig. 10) that the intensity of nonsteady as well as quasi-steady winds is, in general, beyond the linear perturbation range. Consequently, the result of a long averaging period is to include nonlinear effects in the steady-state average.

So far, the short-period averaging seems to be most logical for this study, but this must be accompanied by a selective sampling technique to eliminate the nonsteady components as well as the nonlinear effects due to extreme variation of wind velocities. The method used in this report embraces the method of selecting samples from periods of 30-second duration preceded and followed by approximately the same time average. Field data, obtained by this means, were found to be quite consistent. This, in a way, verified the basic concept of selective short-time average.

Wind-profile measurements over a wheatfield and a cornfield were conducted with multiple small-cup anemometers of 9-cm. diameter, in conjunction with Hasting thermocouple-anemometers.[3] The cup anemometers were appropriately mounted at various heights within and above the crop. Thermocouple anemometers were used within the crop where the windspeed was considered too low for cup anemometers.

[3] The use of this or other patented equipment in this study does not imply approval of the product to the exclusion of others that may also be suitable.

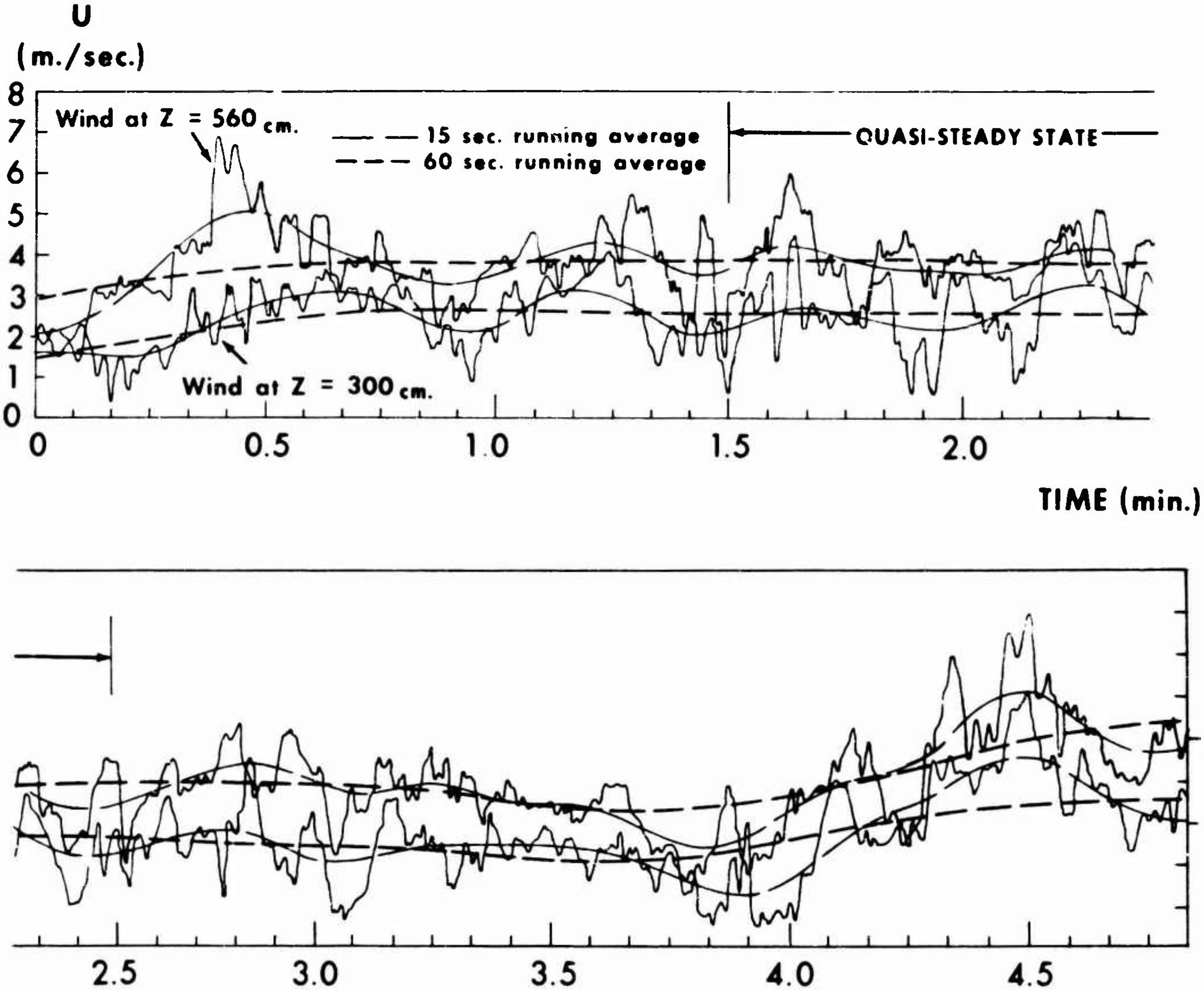

FIGURE 10.—Simultaneous horizontal-wind recording at two different elevations above a corn crop.

Simultaneous, integrated readings from these anemometers were recorded at 30-second intervals. The average wind profiles were obtained from these measurements. The selected samples representing quasi-steady wind profiles for a wheat field and a cornfield are shown in figures 11 and 12, respectively. The range of wind profiles presented here is limited to the most common prevailing winds encountered in a typical field. Data for extremely low and high winds are incomplete, and, therefore, not presented.

The wheatfield was situated on top of Mount Pleasant unobstructed on all sides, whereas the cornfield was situated in Ellis Hollow. (See last section, p. 37.) The wind profile characteristics, by virtue of the sampling technique employed, are expected to be independent of the geographical terrain.

Most of the field data and the instrumentation work used in this report were carried out with the assistance of J. Stoller, New York State College of Agriculture, under the direction of E. R. Lemon, ARS, USDA. A considerable amount of field data had been compiled during the summer months of 1960, but only a small part of the information was analyzed and presented herein, as a consequence of limited time and effort.

The general theory and experimental results of steady state and quasi-steady state winds in the vicinity of a crop are presented in the next subsection.

Boundary-Layer Profiles

1. Logarithmic wind-profile over a crop

The logarithmic-boundary-layer theory of Prandtl (*23*) applies very well to the steady-boundary-layer flow above a crop. In the original theoretical model, it was assumed that the mixing length or the equivalent eddy viscosity of turbulent mixing grows linearly with the height. This assumption is now extended all the way from

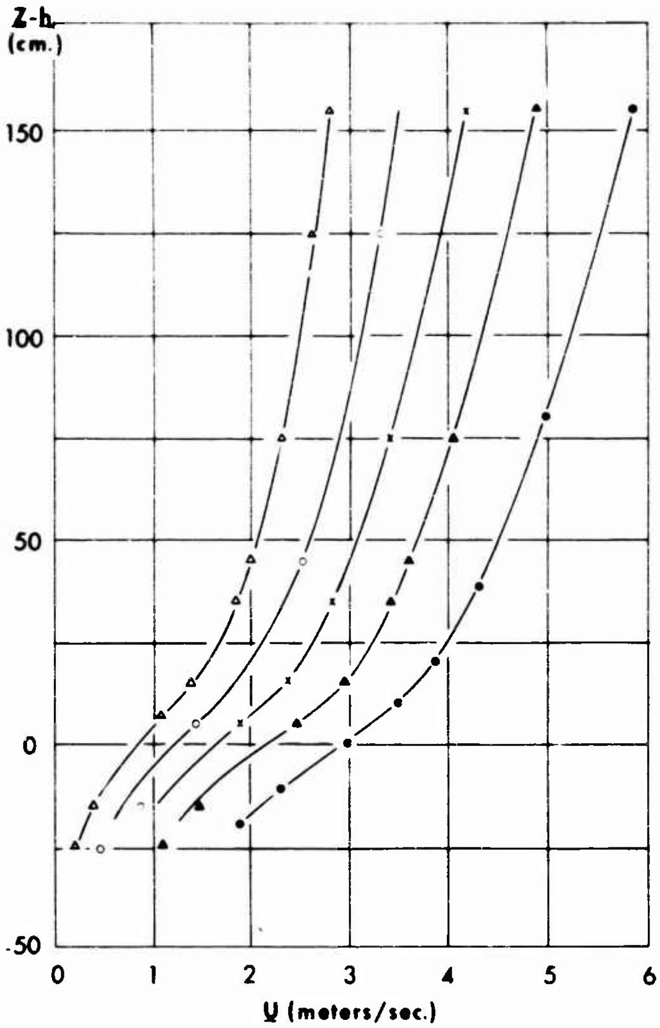

FIGURE 11.—Wind profiles over a wheat crop, 1960.

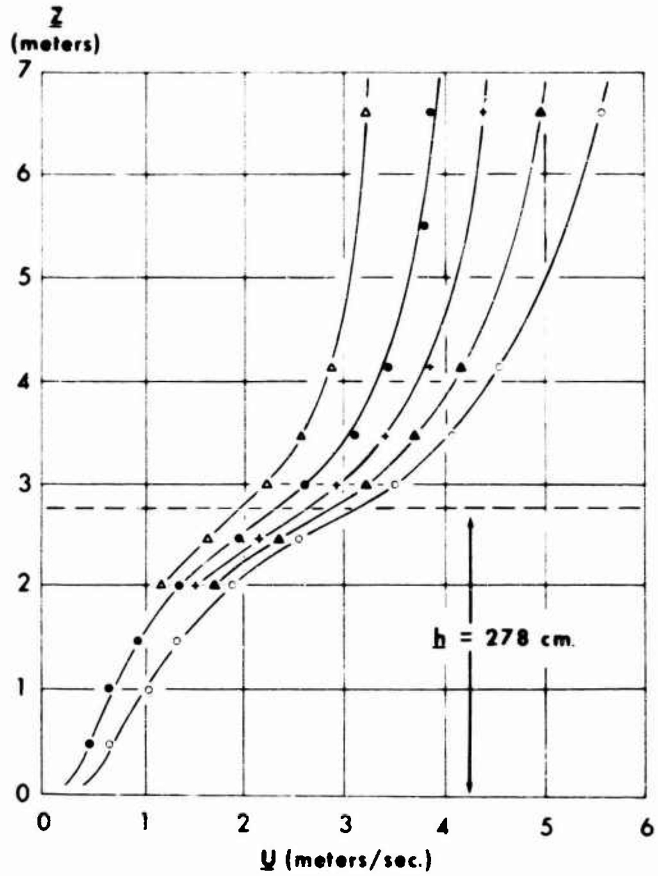

FIGURE 12.—Wind profiles over a corn crop, 1960.

within the crop through the inner boundary layer up into the outer turbulent-flow layer (*21*). By virtue of our stratification hypothesis; i.e., vanishing pressure gradient $\frac{\partial P}{\partial x}$, we have

$$\frac{\partial \tau}{\partial Z}=0;$$

i.e., the flow is maintained through the shearing action of eddy viscosity. Now this leads to

$$\tau=\epsilon(Z)\frac{\partial U}{\partial Z}=\text{constant}. \qquad (60)$$

Introducing the friction velocity as

$$U_*\equiv\sqrt{\frac{\tau}{\rho}}, \qquad (61)$$

the eddy viscosity $\epsilon(Z)$, as

$$\epsilon(Z)=\rho U_* k(Z-d), \qquad (62)$$

and incorporating equations 61 and 62 in equation 60, we obtain the well-known logarithmic-boundary-layer equation through integration of equation 60.

$$\frac{U(Z,U_0)}{U_*(U_0)}=\frac{1}{k}\ln\frac{Z-d(U_0)}{Z_0(U_0)}, \quad Z>h \qquad (63)$$

where

$k=0.42$ Von Kármán's constant;
$Z=$height above ground level;
$U_0=$mean wind velocity at 10-meter reference level;
$h=$peak plant height, defined as 1.1 times the mean plant height, $\bar{h}$;
$d=$zero-plane displacement, a function of U_0;
$Z_0=$roughness length, a function of U_0;
$\rho=$mass density of air.

The constants, U^*, Z_0, and d are called the characteristic parameters of a steady-state-wind profile.

In order to provide a convenient reference level in place of a boundary thickness, the conventional height of 10 meters, Z_{10}, was chosen as the nominal limit of the surface layer. Ratios formed with Z_{10} are to be taken as of approximate order of magnitudes.

The three wind-profile parameters, d, U_*, and Z_0, can be determined from the measured wind profiles, as shown in figures 11 and 12, and they are obtained through the following equations:

$$d=\frac{\left[\frac{\partial U}{\partial Z}\right]_2 Z_2-\left[\frac{\partial U}{\partial Z}\right]_1 Z_1}{\left[\frac{\partial U}{\partial Z}\right]_2-\left[\frac{\partial U}{\partial Z}\right]_1} \qquad (64)$$

$$U_*=k\,\frac{U_1-U_2}{\ln\frac{(Z_1-d)}{(Z_2-d)}} \qquad (65)$$

and

$$Z_0=\frac{Z_1-d}{e^{kU_1/U*}}. \qquad (66)$$

These equations are derived directly from the basic logarithmic equation 63. The values of these parameters as a function of reference wind, U_0, for a wheatfield and a cornfield are plotted in figures 13 and 14, respectively. It is to be noted that values given in the above figures are for a typical wheatfield and a cornfield having an approximate plant density of 60 plants and 0.5 plant per square foot of ground, respectively.

The value of kinematic-eddy viscosity, K_m, known also as the coefficient of eddy diffusivity, is of basic interest in the study of diffusion of CO_2, water vapor, and heat. Direct measurement of this coefficient was planned, but only crude measurements were possible at the time of this report. In general, they check well with those obtained indirectly from the wind-profile parameters. The equation for eddy diffusivity is, from equation 62,

$$K_m=\frac{\epsilon(Z)}{\rho}=U_*(U_0)k[Z-d(U_0)]. \qquad (67)$$

Values of U_* and d can be obtained from figures 13 and 14 for a given U_0 and field condition.

The drag coefficient defined as

$$C_D=\frac{\tau}{\frac{\rho U_0^2}{2}}=2\left[\frac{U_*}{U_0}\right]^2 \qquad (68)$$

is also plotted in figures 13 and 14.

Comparing the behavior of flow parameters between a wheat and a cornfield, it is noticed that the zero-plane displacement, d, decreases with an increase of U_0; this characteristic is controlled primarily by the mechanism of the canopy flow. The values of friction velocity, U_*, are of about the same magnitude and characteristic for both the wheatfield and the cornfield. This indicates that the characteristics of turbulence above either crop are of approximately the same scale and intensity. The value of roughness parameter, Z_0, behaves differently for the two crops. For the wheatfield, Z_0 tends to decrease with U_0, whereas the reverse is true for the cornfield. It is postulated that the behavior of Z_0 depends on the flexibility of the plant as well as plant density. The wheat plant is more flexible and tends to bend and "streamline" itself under a high wind, but the corn is relatively stiff and does not "streamline" itself as readily. The difference in effective plant density, or leaf area density between wheat and corn, exercises a strong influence on the canopy flow that indirectly affects the characteristic of Z_0. The different dependence of C_D on U_0 between a wheatfield and a cornfield is similar to the variation of Z_0 with U_0. Therefore, the same tentative explanation regarding plant flexibility is applicable.

2. *Canopy flow within a crop*

The basic analytical model for a canopy flow has been mentioned in the introductory section of this report. Basically, it is assumed that the flow within the crop is maintained by the action of eddy viscosity, and that the mixing length theory, which is applied to the outer flow, is also valid in this zone. The differential equation governing the flow is,

$$\frac{\partial\tau}{\partial Z}=C'_D A(Z)\,\frac{\rho U^2}{2} \qquad (69)$$

where

$A(Z)$ = total vertical plane area of plants/unit volume, a function of Z; and

C'_D = drag coefficient of plant.

The term on the right represents the drag force offered by leaves and stalks of the crop. Within the flow range considered, C'_D can be taken as independent of Reynolds number, and the drag force is proportional to the square of the velocity.

Introducing equation 60 into equation 69, we have

$$\frac{\partial}{\partial Z}\left[\epsilon(Z)\,\frac{\partial U}{\partial Z}\right]=C'_D A(Z)\,\frac{\rho U^2}{2}. \qquad (70)$$

Let

$\overline{Z}=\frac{Z}{h}$, normalized height variable, and

$\overline{U}=\frac{U}{U_h}$, normalized wind, where U_h = wind at peak-plant height,

and introducing these new variables in equation 70, we have

$$\left[\frac{\partial}{\partial\overline{Z}}\,\epsilon(\overline{Z})\right]\frac{\partial\overline{U}}{\partial\overline{Z}}+\epsilon(\overline{Z})\,\frac{\partial^2\overline{U}}{\partial\overline{Z}^2}=h^2U_hA(\overline{Z})C'_D\,\frac{\rho\overline{U}^2}{2},$$

$$\overline{Z}<1. \qquad (71)$$

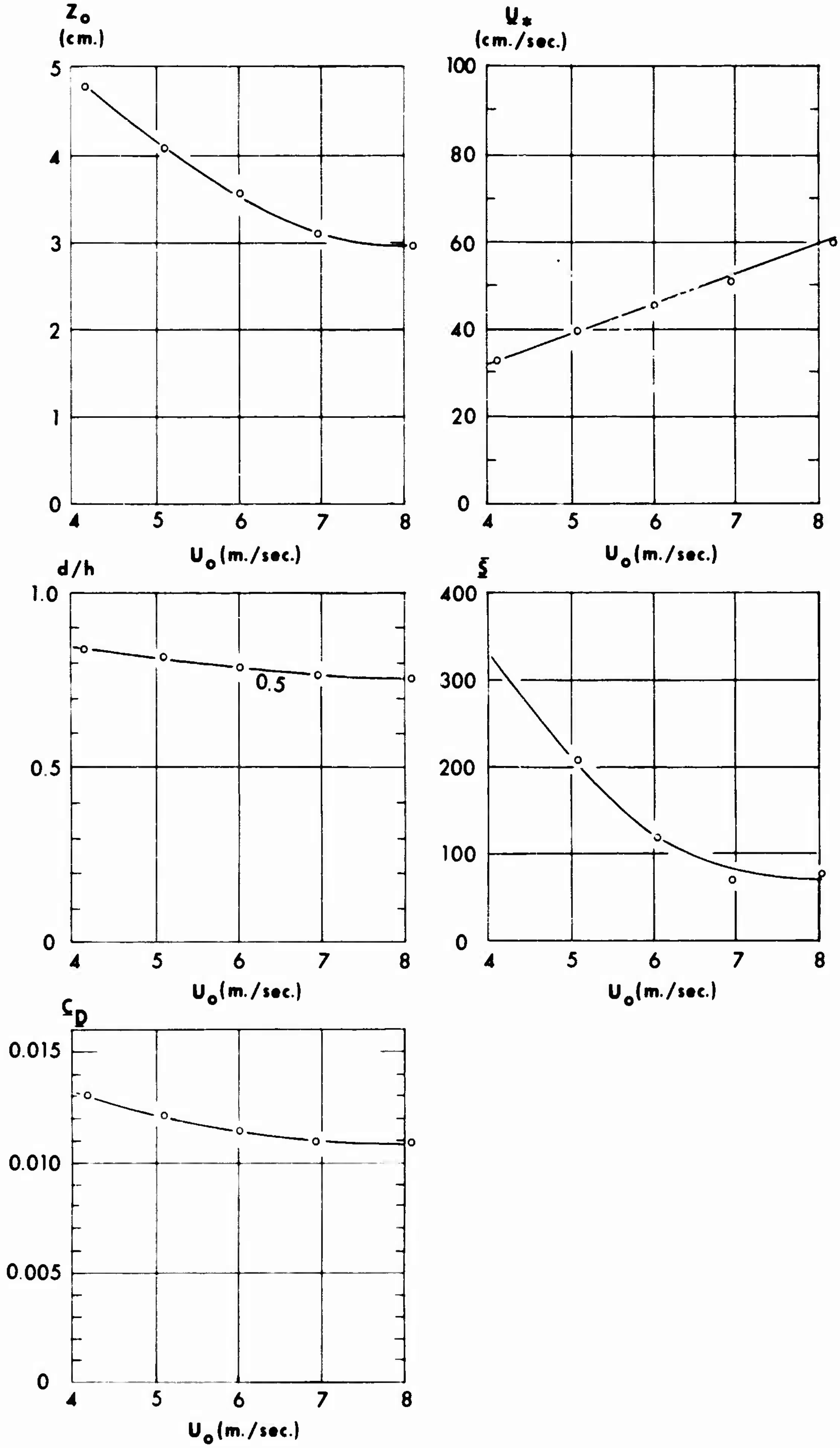

FIGURE 13.—Parameters for steady-state wind profiles for winter wheatfield.

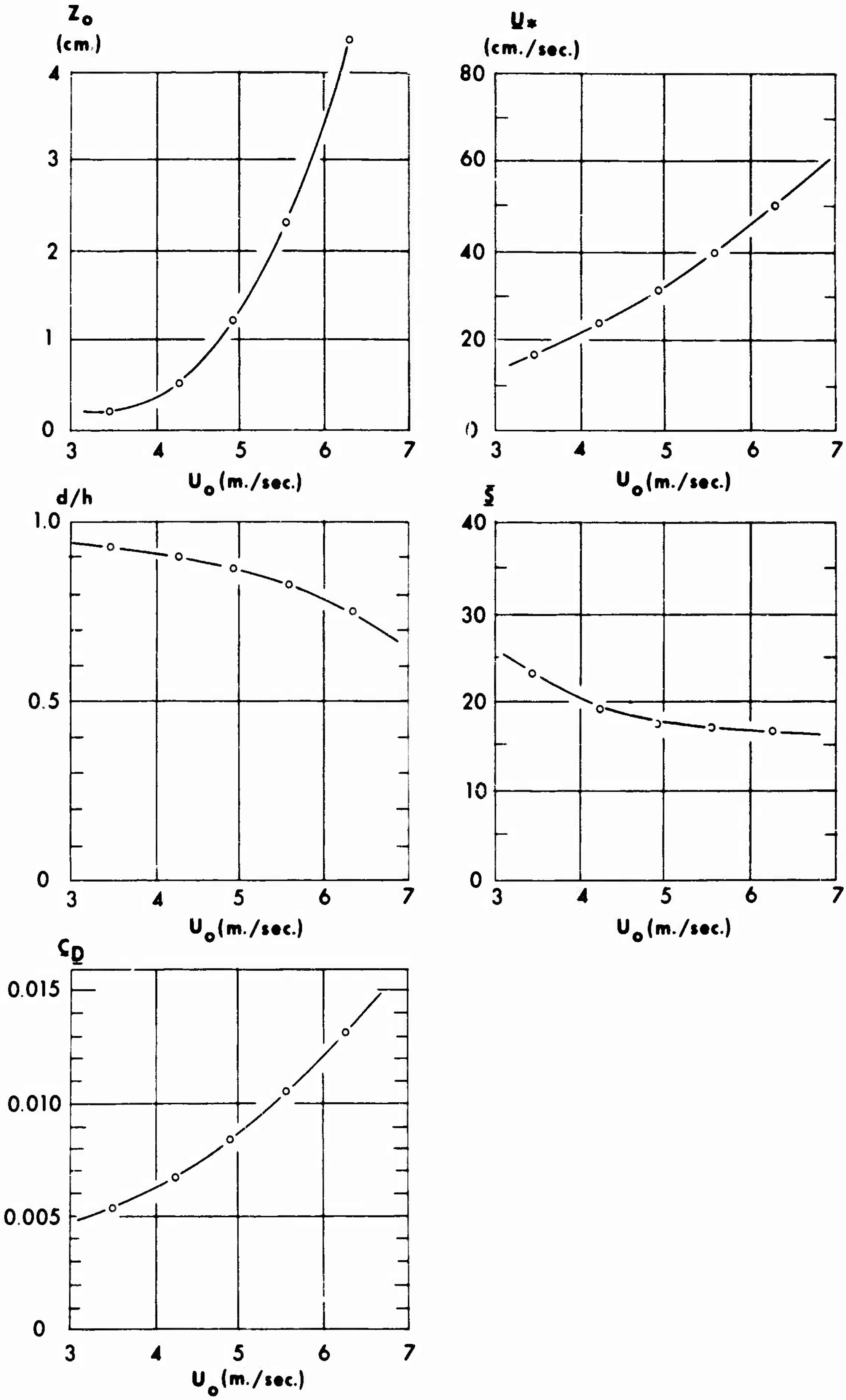

FIGURE 14.—Parameters for steady-state wind profiles for cornfield.

673752 O—63——4

In order to define statistically the value of peak-plant height, some sampling data on the probability density distribution of corn height, $P(h)$, were taken and plotted in figure 15. The peak-plant height has a value of about 1.2 times the mean height of plants. However, instead of taking this figure, a value of 1.1 times the mean height of plants is taken as the definition of h. It was assumed that this definition is also applicable to wheat.

The area distribution function, $A(Z)$, can be obtained statistically for a given crop. However, for simplicity, it was assumed a priori that the average vertical projection area of a single plant (with the vertical plane making an angle of 45° between the planes of maximum and minimum projected area) has an area distribution that is uniform from the root of a plant to 85 percent of its height; from that point on, the area reduces uniformly with height to zero at the tip. By combining this standard area function with the plant height distribution function, the statistical

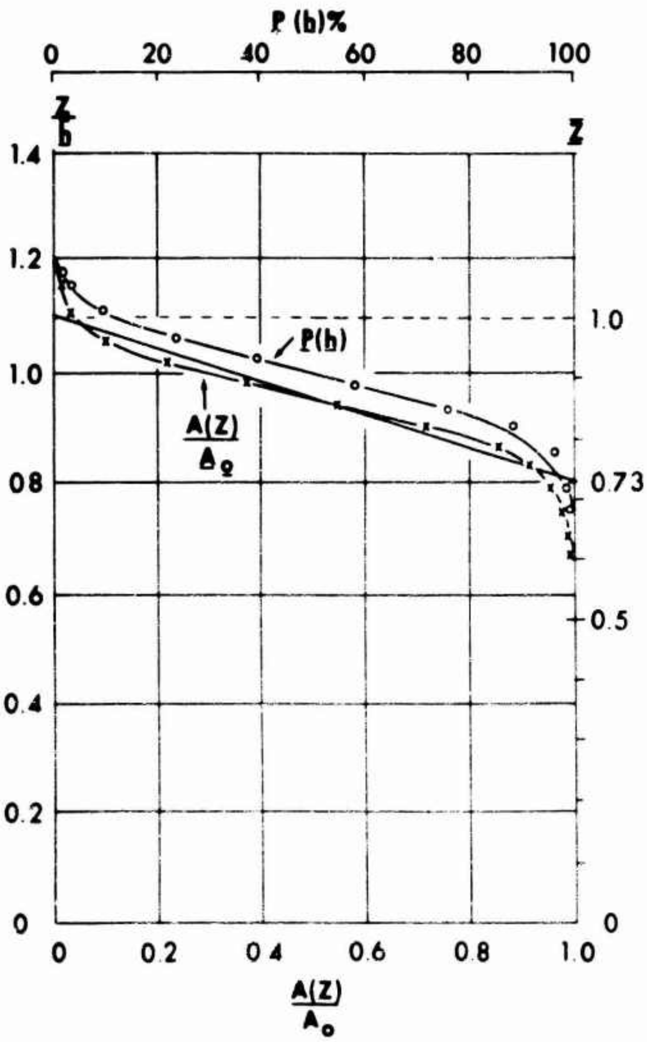

FIGURE 15.—Plant area and height distribution functions for corn.

area distribution function, $A(Z)$, is obtained and plotted as a ratio of area density, A_0, at the midplant height. This function is shown with "x" marks in figure 15. The area distribution function again, for the sake of simplicity, was approximated by a straight line shown in the above figure. This simplified area function gives zero area at 1.1 times the mean-plant height, and hence this height was used for the definition of peak-plant height.

If we introduce the linear growth of eddy viscosity with height,

$$\epsilon(\bar{Z}) = \bar{Z}\epsilon_h,$$

where ϵ_h is the eddy viscosity at height, h, and with the above simplified function of $A(\bar{Z})$, equation 71 is written for two zones:

$$\frac{\text{for } 0<\bar{Z}<0.73}{A(\bar{Z}) = A_0, \text{ constant}},$$

$$\frac{\partial \bar{U}}{\partial \bar{Z}} + \bar{Z}\frac{\partial^2 \bar{U}}{\partial \bar{Z}^2} \equiv \bar{S}\frac{\bar{U}^2}{2}; \qquad (72)$$

$$\frac{\text{for } 0.73<\bar{Z}<1.0}{A(\bar{Z}) = A_0\left[1-\frac{(\bar{Z}-0.73)}{0.27}\right]},$$

$$\frac{\partial \bar{U}}{\partial \bar{Z}} + \bar{Z}\frac{\partial^2 \bar{U}}{\partial \bar{Z}^2} \equiv \bar{S}\left[1-\frac{(\bar{Z}-0.73)}{0.27}\right]\frac{\bar{U}^2}{2}; \qquad (73)$$

where $\bar{S}$ is the dimensionless parameter of the differential equation. It is to be called the shape factor of canopy flow, namely,

$$\bar{S} \equiv \frac{\rho h^2 U_h A_0 C'_D}{\epsilon_h}. \qquad (74)$$

Equations 72 and 73 are nonlinear, differential equations of the second order. They are, however, unique and can be solved by numerical integration for the following boundary conditions:

$$U_{\bar{Z}=1} = 1;$$

$$U_{\bar{Z}=0} = 0.$$

Relaxation method (*28*) was used to obtain the characteristic canopy-wind profiles for various values of shape factors. The result, plotted in figure 16, covers the range of $\bar{S}$ from 5 to 1,000.

In all these cases, the ground shear was neglected in comparison to the leaf drag. For $\bar{S}$ <5, ground effect comes into play. When $\bar{S}\rightarrow 0$, ground shear alone controls the flow, and we obtain the normal logarithmic wind profile.

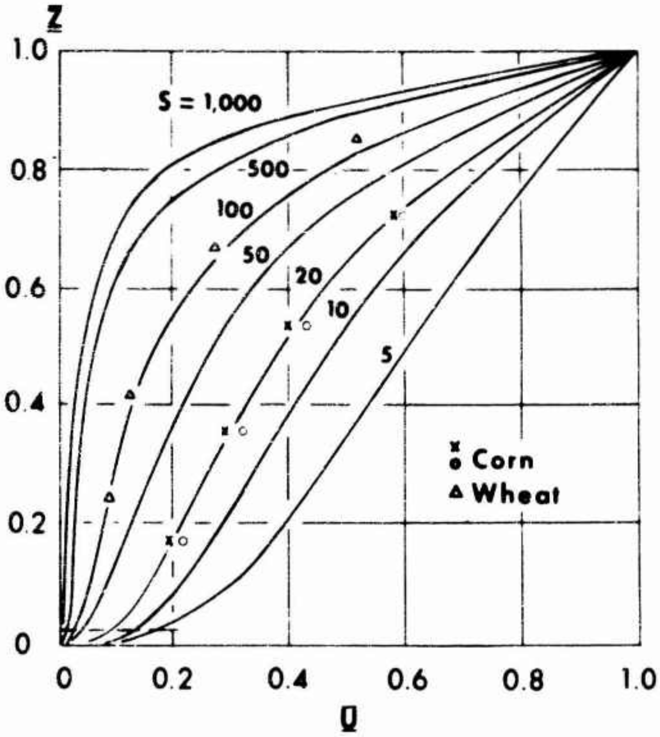

FIGURE 16.—Canopy wind profiles for various shape factors $\bar{S}$.

3. *Combination of canopy and logarithmic-wind profile*

The canopy flow and the logarithmic-profile flow above are actually one continuous system. The matching point between the two flow fields is at the peak-plant height, h, where the wind velocity and the velocity gradient must match. This means that, for a given logarithmic-wind profile, there will be a canopy profile of a given shape factor that will match it at h. The value of ϵ_h in equation 74 must also match the value of $\epsilon(Z)_h$ determined by equation 62 of the logarithmic-wind profile.

The velocity gradient $\left.\frac{\partial \bar{U}}{\partial \bar{Z}}\right|_{\bar{Z}=1}$ for the canopy flow is plotted in figure 17 as a function of shape factor $\bar{S}$. From that plot, the matching shape factors for the wind profiles, shown in figures 11 and 12, are plotted in figures 13 and 14, respectively. The trend of shape factor for the cornfield and the wheatfield turns out to be the same; that is, it tends to decrease with an increase of reference wind, U_0. The corresponding $\bar{S}$ values of wheat are about 10 times those of corn. The reason for this difference is that the effective area density, A_0, of the wheatfield is much higher than that of the cornfield.

In figure 16 the measured-canopy flow profiles for corn and for wheat are plotted. They fit well with the computed wind profiles. This validates

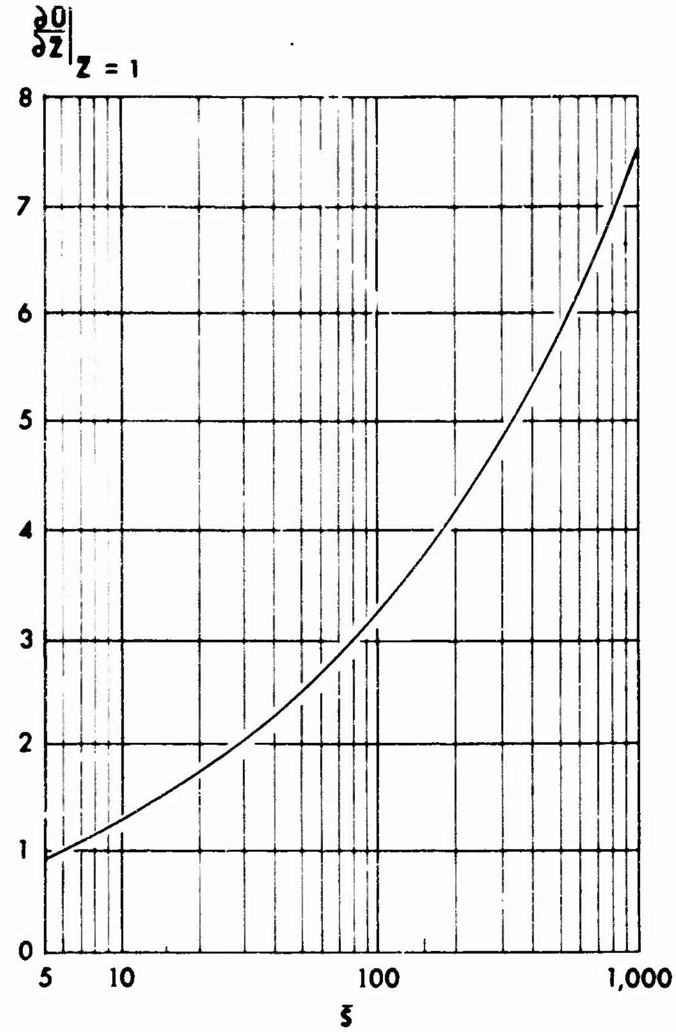

FIGURE 17.—Velocity gardients at peak-plant height as a function of shape factor $\bar{S}$.

the assumption of the turbulent mixing-length concept used in the analytical model.

For both the wheatfield and the cornfield, the ratio of eddy viscosity at peak-plant height to the viscosity of air varies from 1,000 to 8,000 within the range studied. The assumption of a fully turbulent model, and, consequently, the application of mixing-length theory to the study of air motion in the vicinity of a crop, are, therefore, valid.

Shear-Wave Theory

During the course of this study, a very crude shear-wave theory was proposed to study one phase of the nonsteady state phenomena. This idea was generated by field measurements of the wind profiles when it was observed that wind components at different heights exhibited phase lags, thereby suggesting a propagating shear-wave. Figure 10 shows two simultaneous recordings of the horizontal wind at two vertical positions—Z=560 cm. and Z=300 cm.—within a cornfield.

The lines containing high frequencies are instantaneous recordings from anemometers with a response time of less than one second. The second set of lines in long dashes represents the running average of 15 seconds, and the third set represents a running average of 60 seconds. For the 60-second running average, all wavelengths under 60 seconds are averaged out, and only the wave spectrum greater than 60 seconds remains. These long-period waves vary nearly in phase with each other, and are defined as quasi-steady flow. The 15-second average line, which oscillates about the 60-second average line, represents the spectral components between 15-second and 60-second waves.

These waves are seldom in phase between the two levels under observation. The top wave may either lead or lag behind the lower waves. It is not easy to differentiate which is leading or lagging when waves of multiple periods are intermixed. However, when there is a sudden increase in wind intensity, the wind on the upper level generally can be observed to be leading that of the lower level. This type of oscillating wind is identified as nonsteady wind.

The differential equation for shear-waves propagating in the Z direction can be obtained through the modified Navier-Stokes equation by replacing eddy viscosity for molecular viscosity and neglecting pressure gradients and velocity gradients in the x and y directions.

$$\rho\frac{\partial U}{\partial t}=\frac{\partial}{\partial Z}\left[\epsilon(Z)\frac{\partial U}{\partial Z}\right]=\frac{\partial\tau}{\partial Z}. \tag{75}$$

Differentiating equation 75 with respect to Z and multiplying each side by $\epsilon(Z)$, we have

$$\frac{\partial}{\partial t}\epsilon(Z)\frac{\partial U}{\partial Z}=\frac{\epsilon(Z)}{\rho}\frac{\partial^2\tau}{\partial Z^2}$$

or

$$\frac{\partial\tau}{\partial t}=K(Z)\frac{\partial^2\tau}{\partial Z^2}. \tag{76}$$

The eddy diffusivity $K(Z)$ may be taken as linearly proportional to Z; however, this leads to a rather complex solution for the shear wave. To simplify the situation, it is expedient to consider that $K(Z)$ is a constant, with an average value of K_0 within the range considered. Equation 76 is then reduced to

$$\frac{\partial\tau}{\partial t}=K_0\frac{\partial^2\tau}{\partial Z^2}, \tag{77}$$

with the boundary conditions:

$$\frac{\partial\tau}{\partial Z}=0, \qquad Z=0$$

and τ at reference height Z_{10} oscillates about a mean shear τ_0 as

$$\tau=\tau_0+\tau'\sin(\omega\tau).$$

The steady state solution for equation 77 is similar to the well-known, periodic-heat-transfer problem of a flat slab (2).

$$\tau(Z,t)=\tau_0+\frac{\tau'\cosh\omega'Z(1+i)}{\cosh\omega'Z_{10}(1+i)}, \tag{78}$$

where

$$\omega'=\left[\frac{\omega}{2K_0}\right]^{1/2}.$$

When the frequency factor $\omega'Z_{10}$ is less than 0.5, the absolute magnitude of oscillating shear, $\tau'(Z)$, differs only 2 percent at $Z=0$ from τ' at Z_{10}. The corresponding phase lag at these levels is 14°. That is, when the frequency factor is less than 0.5, constant-shear condition can be assumed.

It can be shown that the above shear wave will propagate downward with a speed of

$$v_\tau=\frac{\omega}{\frac{\partial}{\partial Z}\left[\arg\frac{\cosh\omega'Z(1+i)}{\cosh\omega'Z_{10}(1+i)}\right]}. \tag{79}$$

The speed of wave propagation is not constant with respect to height. However, it can be shown that for a good approximation, V_τ may be taken as

$$V_\tau\approx\sqrt{2K_0\omega}, \qquad \frac{Z}{Z_{10}}>0.2. \tag{80}$$

The shear-wave length in the Z direction can be defined as

$$\lambda_\tau=\frac{2\pi V_\tau}{\omega}=2\pi\sqrt{\frac{2K_0}{\omega}}. \tag{81}$$

The ratio of Z_{10} to λ_τ is

$$\frac{Z_{10}}{\lambda_\tau}=\frac{1}{2\pi}Z_{10}\sqrt{\frac{\omega}{2K_0}}=\frac{Z_{10}\omega'}{2\pi}. \tag{82}$$

For the limiting case of constant shear, $\partial\tau/\partial Z\approx 0$, where $Z_{10}\omega'$ is less than 0.5, the ratio of

$$\frac{Z_{10}}{\lambda_\tau}\leq\frac{0.5}{2\pi}=0.08.$$

That is, when the shear-wave length is more than 12 times the reference height, Z_{10}, constant-shear condition exists (quasi-steady state). The shear-wave length required for this state of flow is

$$\lambda_\tau\geq\frac{Z_{10}}{0.08}=125 \text{ meters}.$$

From equation 81 the frequency of oscillation, f, for quasi-steady condition can be obtained.

$$f \leq \frac{4\pi K_0}{\lambda_r^2} \tag{83}$$

For a typical condition where $U_o = 500$ cm./sec., $\lambda_r = 12{,}500$ cm., and $K_0 = 50{,}000$ cm.²/sec., the corresponding value of f from equation 83 is

$$f = \frac{4\pi 50{,}000}{12{,}500^2} = 4 \times 10^{-3} \text{ cycles/sec.}$$

Under the conditions when the time and space coordinates are interchangeable, the equivalent velocity wavelength can be defined as

$$\lambda_U = \frac{U_0}{f} = \frac{500}{4 \times 10^{-3}} = 125{,}000 \text{ cm.} = 1{,}250 \text{ meters.}$$

Hence, from the very crude shear-wave theory, an approximate boundary value for quasi-steady state condition is defined. That is, any wavelength greater than 1,000 meters may be considered as a quasi-steady wind.

The wind spectrum can now be divided into the following classification of eddy scales:

Scale Ratio	*Eddy Classification*
$\frac{\lambda_U}{Z_{10}} < 4$	Turbulent eddies.
$4 < \frac{\lambda_U}{Z_{10}} < 100$	Nonsteady wind.
$100 < \frac{\lambda_U}{Z_{10}}$	Quasi-steady wind.

The relaxation time, t_r, of a boundary layer, referred to at the beginning of this section, is defined as the time for the shear wave to propagate from the reference height down to the plant.

$$t_r = \frac{Z_{10} - h}{V_r}. \tag{84}$$

For the typical example as given above, the value for t_r is 14 seconds. Winds of higher frequency or shorter wavelength will, of course, give shorter periods. The phase-time relationship of waves of 30 seconds duration, as shown in figure 10 (in long dashes), is about 4 seconds between the two recording levels. Equation 84 gives a relaxation time of about the same magnitude. This checks well with the experimental data.

ON THE DIFFUSION OF HEAT AND MASS IN A TURBULENT SHEAR FLOW

By D. A. Spence

The feature that distinguishes turbulence from laminar flow is its randomness: In any given case it is possible to give, at the very best, only a statistical description of the way in which the distributions of velocity, pressure, temperature, and density vary about their means. Fortunately, such a description is usually good enough, since one is only interested in the behavior of properties averaged over a time that is long compared with that of a turbulent fluctuation. Exactly as in statistical mechanics, one is only interested in the mean properties of an ensemble, and one not only could not but would not want to say how an individual particle behaves.

The analogy with statistical mechanics is a natural one, and led Prandtl to introduce the notion of a mixing length as a counterpart of the mean free path, but it is nowadays generally agreed that although this concept has dimensional validity, it is a great oversimplification of the transfer processes at work in a turbulent flow. For this reason, one is on dangerous ground in trying to predict the results of a new experiment—for example, in applying suction or blowing to a turbulent boundary layer—by means of mixing length theory, even though it can be used very successfully to rationalize some well-known observations, the most notable being the logarithmic law of the wall.

Turbulence presents a much more difficult problem than the mean motion of molecules in a gas, however, since the motion of one fluid particle affects that of every other, and the simplification of "molecular chaos" is not available. Moreover, the governing equations are nonlinear, and the fluctuating motion is always three-dimensional, even in a one—or two—dimensional mean flow. For this reason, substantial progress in predicting the development of a field of turbulence from a statistically known initial state has only been possible in the simplest case: that of decaying homogeneous isotropic turbulence. Definitive accounts of this subject are given by Batchelor (*1*) and Lin (*19*), and mention should also be made of the review by Liepmann (*16*).

The primary aim of workers in this field is to predict the form and time variation of the turbulent energy spectrum. In this way they obtain some insight into the mechanisms by which energy is transferred by the inertia terms in the equations of motion from large eddies with low-wave numbers through an intermediate range to the high-wave numbers at which dissipation takes place by viscous action. The well-confirmed existence of an inertial subrange in which the spectrum depends only on the rate of dissipation and the wave number, k—and is, therefore, found by a simple dimensional argument to vary as $k^{-5/3}$—shows that the process is a continuous one; i.e., that energy is passed successively down the whole wave-number scale without bypassing any part of the range. To make further progress, however, some physical hypothesis—for example, that the velocity correlations of a certain order are those given by joint normal distributions—must be made, and nothing completely satisfactory seems to have emerged, so the theory of homogeneous turbulence is, at present, something of a standstill.

In the meantime, however, the same methods have been used to acquire a considerable insight into the qualitative nature of turbulence in the important class of flows in which the mean motion is sheared, as between fixed boundaries in a pipe or channel, free boundaries, or in wakes or jets, and one fixed and one free in a boundary layer. A comprehensive survey of these flows was given by Townsend (*37*) in 1956. From his work a fairly definite picture has emerged of the way eddies compare in size with the width of the layer extract energy from the mean flow and hand it down through eddies of progressively smaller size to those in which it is ultimately dissipated. (The latter are not, as was once thought, necessarily isotropic even in a shear flow.) The net rate of production of turbulent energy per unit mass is $u\frac{\delta\tau}{\delta y}$, the product of mean velocity and shear stress gradient, and if it were possible by considering the structure of the turbulence to say how this quantity depends on the local velocity and pressure gradients, the calculation of mean flow as a shear layer would be fully determinate; a further relation being provided by the Navier-Stokes equations. But Townsend and his coworkers are still quite a long way from being able to make any quantitative predictions of the transport properties in terms of local mean quantities. ("Transport" is used so as to include heat and mass diffusion into shear force; i.e., momentum transport, in the discussion.)

Actually, it is not at all clear that a representation in terms of local quantities is physically meaningful, even though it is always formally possible by means of an eddy diffusion coefficient. Transport of any quantity is brought about to different extents by eddies of different sizes. Intuitively one has a picture of a lump of fluid carrying with it some property having the mean value appropriate to its initial surroundings and being convected by an eddy to a point where the mean properties are different, and where it then shares the transported property with the surrounding fluid. The distance traveled by the lump is then the mixing length, and the flux of the transportable property should be proportional on this argument to the mean gradient over the length.

But lumps converted by different eddies will travel different distances. At least in the case of the layer eddies, an exchange coefficient based on the local gradient at one point in the shear layer does not seem appropriate, both because the eddies are comparable in width to the shear layer and because the exchange process takes place continuously by molecular action wherever there is a local concentration gradient, not waiting for the lump to reach its final position. In fact, Townsend's experiments (see Hinze (*9*), *pp. 288–289*) indicate that momentum transport is primarily due to gradient-type diffusion by small-scale turbulence (presumably because the u and v components in the large eddies tend to be uncorrelated), whereas heat is transported both by gradient diffusion and by the bulk mechanisms associated with large eddies.

Thus, as pointed out by Lighthill (*18*) in reviewing Townsend's book, it is physically quite significant to define an eddy viscosity, ϵ, by

$$-\rho\overline{u'v'}=\epsilon\,\frac{\partial u}{\partial y},$$

and to expect ϵ to depend on local quantities. To this is added the viscous contribution to shear stress, giving altogether

$$\tau=(\mu+\epsilon)\,\frac{\partial u}{\partial y},$$

and the analogy between the gradient diffusion due to eddy and molecular motions is clear. By analogy with the first equation, an eddy conductivity K and an eddy diffusion coefficient D (for a primary mixture) may be defined in terms of the fluxes of enthalpy, h, and mass, denoted by concentration, c, of one species, due to the turbulent motion by

$$-\rho\overline{h'v'}=K\,\frac{\partial h}{\partial y},\quad -\rho\overline{c'v'}=D\,\frac{\partial c}{\partial y}.$$

The corresponding molecular transport coefficients are denoted by k and D, say. (Note that the specific heat C_p has been absorbed in the definitions of k and K.) The kinetic theory for a dilute gas at room temperatures shows that the ratios

$$Pr=\frac{\mu}{k},\quad Le=\frac{\rho D}{k},\quad Sc=\frac{\mu}{\rho D}$$

are all of order unity (between 0.7 and 1.4, roughly) and one is, therefore, able to treat the diffusion of heat or mass by analogy with that of momentum. For example, Reynold's analogy, which holds exactly for $Pr=1$, states that, when suitably nondimensionalized, skin friction is equal to heat transfer for a boundary layer.

For turbulent flows one naturally seeks to use the same type of analogy, even though for the reasons discussed, it rests on less certain physical grounds. Nevertheless, it is possible to give quite good quantitative answers to practical problems in chemical engineering, micro-meteorology, etc., by relating the fluxes of heat and matter to the shear stress by means of the corresponding parameters

$$(Pr)_{\text{turb}}=\frac{\epsilon}{k},\quad (Le)_{\text{turb}}=\frac{\rho D}{k},\quad (Sc)_{\text{turb}}=\frac{\epsilon}{\rho D}$$

which, in view of the broadly analogous exchange mechanisms, should all be somewhere near unity. General surveys of this approach have been given by Lees (*13*) and by Spalding (*30*), the latter being particularly concerned with combustion problems. The usual practice is to give the ratios constant values in any given shear flow. In this way the present author (*31*) was able to relate the distribution of enthalpy to that of shear stress, both being regarded as functions of velocity, in terms of an arbitrary value α for the turbulent Prandtl number. If the energy equation was integrated, it was then possible to express both the recovery and Reynold's analogy-factors in terms of α, and by taking $\alpha=0.85$, which is midway between unity and $(Pr)_{\text{molecular}}$, good agreement with the known experimental results for air was found.

In view of the differences in transport mechanisms for heat and momentum, it would be surprising if Pr_{turb} actually were constant across the layer and the above value should probably be looked on as a weighted means. The transport must depend on the eddy structure, and this varies across the layer. For the region where small eddies predominate (close to the sublayer), gradient diffusion would probably be the main mechanism, and one might expect to find $(Pr)_{\text{turb}}\sim(Pr)_{\text{molecular}}$, but near the outer edge of a shear layer large eddies are predominant and transport is primarily by bulk motions, so it seems more probable that the Prandtl number should then approach unity. The integration of reference (*31*) can actually be carried out formally for an arbitrary variation of $(Pr)_{\text{turb}}$, as is shown in the notation below, giving a result of some generality for zero-pressure gradient flows. Like most such results, they are not suitable for application without some physical hypothesis. In this case, the dependence of $(Pr)_{\text{turb}}$ on the shear stress may be a suitable representation of the local eddy structure.

The same methods can be used to estimate the diffusion of mass across a shear flow in terms of shear stress and velocity in terms of an arbitrary Schmidt number, and, in the absence of definite experimental information, one would take a value somewhere between unity and the molecular value as the most likely. Meteorologists usually use mixing lengths having some prescribed-height dependence to obtain the distribution of velocity and shear stress, as detailed by Priestley (*25*). When this is known, one can proceed exactly as in the heat diffusion case to calculate the flux of a foreign gas through the atmosphere due to turbulent mixing.

Integration of the energy equation in a zero-pressure gradient, with variable turbulent Prandtl number.—The energy equation with the usual notation is

$$\rho u\frac{\partial h}{\partial x}+(\rho v+\overline{\rho' v'})\frac{\partial h}{\partial y}=\frac{\partial q}{\partial y}+\tau\frac{\partial u}{\partial y},$$

and if $h=h(u)$, this can be written,

$$\frac{1}{\tau}\frac{d\tau}{du}\frac{dh}{du}=\frac{1}{\tau}\frac{dq}{du}+1.$$

The heat flux,

$$q=(k+K)\frac{\partial h}{\partial y}=k_{\text{eff}}\frac{\partial h}{\partial y},$$

say, and likewise

$$\tau=\mu_{\text{eff}}\frac{\partial u}{\partial y}.$$

If we write $\frac{\mu_{\text{eff}}}{k_{\text{eff}}}=\alpha$, then α is a function of the

$$Pr_{\text{turb}}=\frac{\epsilon}{k}=\frac{\mu_{\text{eff}}-\mu}{k_{\text{eff}}-k}.$$

In terms of α the energy equation is

$$\frac{d^2h}{du^2}+\left[(1-\alpha)\frac{d}{du}\ln\left(\frac{\tau}{\tau_w}\right)-\frac{d}{du}(\ln\alpha)\right]\frac{dh}{du}=-\alpha.$$

(The wall stress τ_w has been brought in for convenience.)

Denote by ϕ the Stieltjes integral

$$\int_\sigma^\alpha\left(ln\ \frac{\tau}{\tau_w}\right)d\alpha.$$

Then, if we set $\alpha=\sigma$ at the wall $u=0$, the result of integrating the energy equation twice is

$$h-h_w=\frac{1}{\sigma}\left(\frac{dh}{du}\right)_w\int_0^u\alpha\left(\frac{\tau}{\tau_w}\right)^{\alpha-1}e^{-\phi}du$$
$$-\int_0^u\alpha\left(\frac{\tau}{\tau_w}\right)^{\alpha-1}e^{-\phi}du\int_0^u\left(\frac{\tau}{\tau_w}\right)^{1-\alpha}e^{\phi}du.$$

If α=constant, this reduces to the usual Crocco integral.

It can also be integrated in a fairly straightforward manner if α is assumed to be a simple function of $\frac{\tau}{\tau_w}$. For instance, it might be physically realistic to assume a linear dependence, by setting

$$\alpha=1-(1-\sigma)\left(\frac{\tau}{\tau_w}\right),$$

which goes to unity at the free boundary and to σ at the wall.

A METHOD FOR THE COMPUTATION OF LOGARITHMIC WIND PROFILE PARAMETERS AND THEIR STANDARD ERRORS

By WINTON COVEY

The logarithmic wind profile equation may be written:

$$V=V_* \ln\left(\frac{z+D}{z_0}\right). \tag{85}$$

Here, z is height above the ground, V is mean windspeed over a short (e.g., 15-minute) time-interval. Equation 85 is observed to fit observations well when:

(1) The anemometry is good,
(2) Thermal stratification is adiabatic,
(3) The measuring site is amid a uniform patch of ground,
(4) The lowest anemometer is not too low, and
(5) The highest anemometer is not too high.

Requirements 3 and 4 lead some people, including the author, to view the logarithmic profile as applying basically to area-average profiles, rather than to point profiles. Requirements 3 and 4 are then looked upon as requirements for obtaining area-average profiles with a minimum of instrumentation.

The interpretation put upon the three parameters—V_*, z_0 (sometimes called roughness length), and D (sometimes called displacement height)—has been extremely diverse during the past 24 years. Extreme views have been that roughness length is "a constant of integration" on the one hand, and a physical parameter of the ground surface on the other. The parameter V_* has generally been identified as:

$$V_*=\frac{1}{k}\sqrt{\tau/\rho} \tag{86}$$

where k is Von Karman's constant, ~ 0.4; τ is shear stress in the surface layer; and ρ is air density. Let z_s be the value of z at which equation 85 gives $V=0$. Then:

$$0=V_* \ln\frac{z_s+D}{z_0},$$

or,

$$z_s=-D+z_0. \tag{87}$$

The parameter, D, is therefore related to the height at which the profile extrapolates to zero, differing by z_0, and having a change in sign.

For rough, rigid surfaces, z_0 appears to be a physical parameter of the surface and $z_s \doteq 0$. Recent work shows that for flexible elastic plant covers such as corn or rice, both z_0 and D vary with windspeed, as indicated by V_*, geostrophic wind, or speed at a reference height. The study of the manner of this dependence would be facilitated by a convenient means of determining V_*, z_0, D, and their standard errors from observations.

On receipt of some notes from Stephen M. Robinson and C. B. Tanner [4] at the University of Wisconsin, giving substantially the material in pages 1 to 5 of Technical Note No. 1 (*26*), a program for machine computation of adiabatic wind profile parameters was written here. This program accomplishes the same data reduction task as Mr. Robinson's, and is based on equations written by him. It has two major differences in technique that may prove useful. The subprogram for standard errors and the equations on which they are based are original contributions. The program is written in the Burroughs version of Algol, for the Burroughs 220 computer. This report discusses mathematical methods and not the details of the computer program.

REVIEW OF THE PROBLEM

The equation to be fitted to the adiabatic wind profile observations is:

$$V=V_* \ln\left(\frac{z+D}{z_0}\right). \tag{85}$$

Robinson's development is followed in general, with summation and mean value notation rather than vector notation. Data are speeds V_i for the n measuring heights, z_i.

The sum of the squares of errors to be minimized in evaluating V_*, D, and z_0 is:

$$E=\sum_{i=1}^{n}\left(V_i-V_* \ln\left(\frac{z_i+D}{z_0}\right)\right)^2. \tag{88}$$

Let:

$$w=\ln z_0,$$

$$x_i=\ln(z_i+D),$$

$$\bar{x}=\frac{1}{n}\sum_{i=1}^{n} x_i,$$

[4] Personal communication.

$$y_i = x_i - \bar{x},$$
$$u_i = V_i - \bar{V},$$
$$r_i = 1/(z_i + D).$$

Put the three partial derivatives simultaneously equal to zero:

$$\left\{\begin{array}{ll} \frac{\partial E}{\partial V_*} = -2\sum_{i=1}^{n}\{[V_i - V_*(x_i - w)](x_i - w)\} = 0; & (89) \\ \frac{\partial E}{\partial D} = -2V_*\sum_{i=1}^{n}\{[V_i - V_*(x_i - w)]r_i\} = 0; & (90) \\ \frac{\partial E}{\partial z_0} = \frac{2V_*}{z_0}\sum_{i=1}^{n}\{V_i - V_*(x_i - w)\} = 0. & (91) \end{array}\right.$$

In equations 89, 90, and 91, w is a function of z_0 and the x_i and r_i depend upon D. The set of values (V_*, D, z_0) is required that satisfies equations 89, 90, and 91.

In equation 91, averages are taken, and the equation is rearranged to give:

$$w = \bar{x} - \frac{\bar{V}}{V_*}. \qquad (92)$$

Equations 90 and 89 are rewritten and averaged, and the value of w from equation 92 is substituted in them. This gives:

$$0 = \overline{ur} - V_*\,\overline{yr} \qquad (93)$$

and

$$0 = \overline{uy} - V_*\,\overline{y^2}. \qquad (94)$$

From equation 93 comes the equation for V_*:

$$V_* = \frac{\overline{ur}}{\overline{yr}}. \qquad (95)$$

Combine equations 94 and 95 to obtain:

$$0 = \overline{uy} - \frac{\overline{ur}\,\overline{y^2}}{\overline{yr}}. \qquad (96)$$

Equation 96 is the implicit equation in the single unknown, D, which is to be solved. This is done by defining a function, $g(D)$, which has as a single real root the desired value of D, and by finding that root. Any of several functions $g(D)$ will do:

$$g'(D) = \text{constant} \cdot \{\overline{uy} - \overline{y^2}\,\overline{ur}/\overline{yr}\}$$

or

$$g''(D) = \text{constant} \cdot \{\overline{y^2}\,\overline{ur} - \overline{uy}\,\overline{yr}\},$$

for example.

A form of the latter function is chosen by Robinson. The choice,

$$g(D) = \text{constant} \cdot \left\{\frac{1}{\overline{y^2}} - \frac{\overline{ur}}{\overline{uy}\cdot\overline{yr}}\right\} \qquad (97)$$

has the merit that $g(D)$ so defined has, for reasonable data, a nearly linear form for a wide range of trial values of D. This near-linearity is convenient when new estimates of the root, D, are found by linear interpolations. Hence, equation 97 is used.

The second difference in technique is in finding the first two and subsequent estimates of D. Instead of a pair of reasonable guesses being supplied, the program automatically makes two extreme guesses, to bracket the root. New estimates are found alternately by linear interpolation and by bisection, until one of three criteria calls for making a final linear interpolation. Each new estimate is used to narrow the bracket.

The data format consists of integers (groups of digits) separated by spaces:

$$\text{aaa} \quad \text{bb} \quad \underbrace{\text{ccc} \quad \text{ccc} \quad \text{ccc} \quad \text{ccc}}_{\text{bb integers}}.$$

If the first integer (aaa) $\neq 0$, then (aaa) is the profile identification number, and the (ccc) are velocities, starting at the lowest anemometer height. The second integer (bb) is the number of measuring heights. If (aaa) $= 0$, then the (ccc) are anemometer heights, beginning with the lowest. The computer subsequently converts input data to floating point form, and the output has explicit decimal points. Units of V_* in the output are those of V_i in input; units of D and z_0 in the output are those of z_i in input. Units of centimeters per second and centimeters were visualized when writing the program, but are not essential.

The first and second trial values of D are $D_1 = -z_1 + 1$ and $D_2 = +z_1 - 1$. If these do not establish a bracket for D, the fact is noted and the next profile is read in.

The three criteria for making a final estimate of D by linear interpolation are:

(1) The absolute value of $g(D)$ less than a critical amount, or

(2) The size of the bracket less than a critical amount, or

(3) The number of trial values of D reaches a maximum allowed number.

With several sets of real data, all profiles having four or more measuring heights, and heights being measured from approximately the mean soil surface, seven trial values of D (including the first two) were always sufficient to evaluate the displacement height, D, to the nearest hundredth of a centimeter, if the least-squares value was within the original bracket (fig. 18).

A SAMPLE COMPUTATION

The same data are used as in Robinson's sample calculations. These are Lettau's mean adiabatic profile from the Johns Hopkins observations at O'Neill, Nebr., in 1953 (*15*).

z (cm.)	*V (mm./sec.)*
40	4,902
80	5,853
160	6,737
320	7,592
640	8,375

Successive estimates of D and corresponding values of—

$$g(D)=\frac{1}{\overline{y^2}}-\frac{\overline{ur}}{\overline{uy}\,\overline{yr}} \text{ are:}$$

Method:	*D*	*g(D)*	*Resulting bracket*	
	−39.0	+0.029518	....	....
	+39.0	−0.060772	−39.0	+39.0
By linear interpolation	−13.499818	+0.006182	−13.5	+39.0
By bisection	+12.750091	−0.030611	−13.5	+12.75
By linear interpolation	−9.088715	−0.000678	−13.5	−9.09
By bisection	−11.294266	+0.002713	−11.29	−9.09
By linear interpolation	−9.529773	−0.000006	−11.29	−9.529773

Then a final linear interpolation gave −9.53 cm. for D. The corresponding z_0 was 0.432 cm., and V_* was 1,151 mm./sec. Figure 18 shows the approximately linear dependence of $g(D)$ on D for the example above.

ESTIMATING THE ACCURACY OF V_*, D, AND z_0 FROM ADIABATIC WIND PROFILE DATA

Using a computer with eight significant-figure arithmetic does not lead to computational error in the profile parameters. Errors depend upon the data for the heights, z_i, and the speeds, V_i. The heights can be assumed to be accurate, and all the error of measurement (sampling and instrumental) can be assigned to the speeds. Then statistical analysis leads to estimates of the errors in computed parameters V_*, D, and z_0 as functions of the data. This statistical analysis involves only the assumptions already implied in the fitting of a least-squares profile.

The Error in D

Define

$$H(D, V_1, V_2, \ldots V_n)=\overline{uy}\;\overline{yr}-\overline{y^2}\;\overline{ur} \qquad (98)$$

where D is an arbitrary variable, and the V_i are measured velocities.

Then,

$$dH=\left.\frac{\partial H}{\partial D}\right|_{V_1, V_2, \ldots V_n} dD+\sum_{i=1}^{n}\left.\frac{\partial H}{\partial V_i}\right|_{V_{j\neq i}, D} dV_i. \qquad (99)$$

Divide equation 99 by dV_1, and put $0=dV_2=dV_3=\ldots dV_n=dH$. Then:

$$\left.\frac{\partial D}{\partial V_1}\right|_{V_2, V_3, \ldots V_n, H}=-\frac{\left.\frac{\partial H}{\partial V_1}\right|_{V_2, V_3, \ldots V_n, D}}{\left.\frac{\partial H}{\partial D}\right|_{V_1, V_2, \ldots V_n}} \qquad (100)$$

and, of course, similar equations apply with respect to V_2, V_3, . . . V_n. The error in displacement height, D, is given by:

$$E(D)=\frac{\partial D}{\partial V_1}E(V_1)+\frac{\partial D}{\partial V_2}E(V_2)+\ldots+\frac{\partial D}{\partial V_n}E(V_n)$$
$$+(\text{higher order terms})$$

where the derivatives are evaluated at the true values of the velocities.

The standard error of D is given (approximately) by:

$$SE(D)=\left\{\sum_{i=1}^{n}\left(\frac{\partial D}{\partial V_i}(SE(V_i)\right)^2\right\}^{1/2}. \qquad (101)$$

If the standard error of V_i is assumed constant with height, then:

$$SE(D)=\frac{SE(V)}{\frac{\partial H}{\partial D}}\left\{\sum_{i=1}^{n}\left(\frac{\partial H}{\partial V_i}\right)^2\right\}^{1/2}. \qquad (102)$$

Equations are required for

$$\left.\frac{\partial H}{\partial D}\right|_{V_1, V_2, \ldots V_n} \text{ and } \left.\frac{\partial H}{\partial V_j}\right|_{V_{i\neq j}, D}.$$

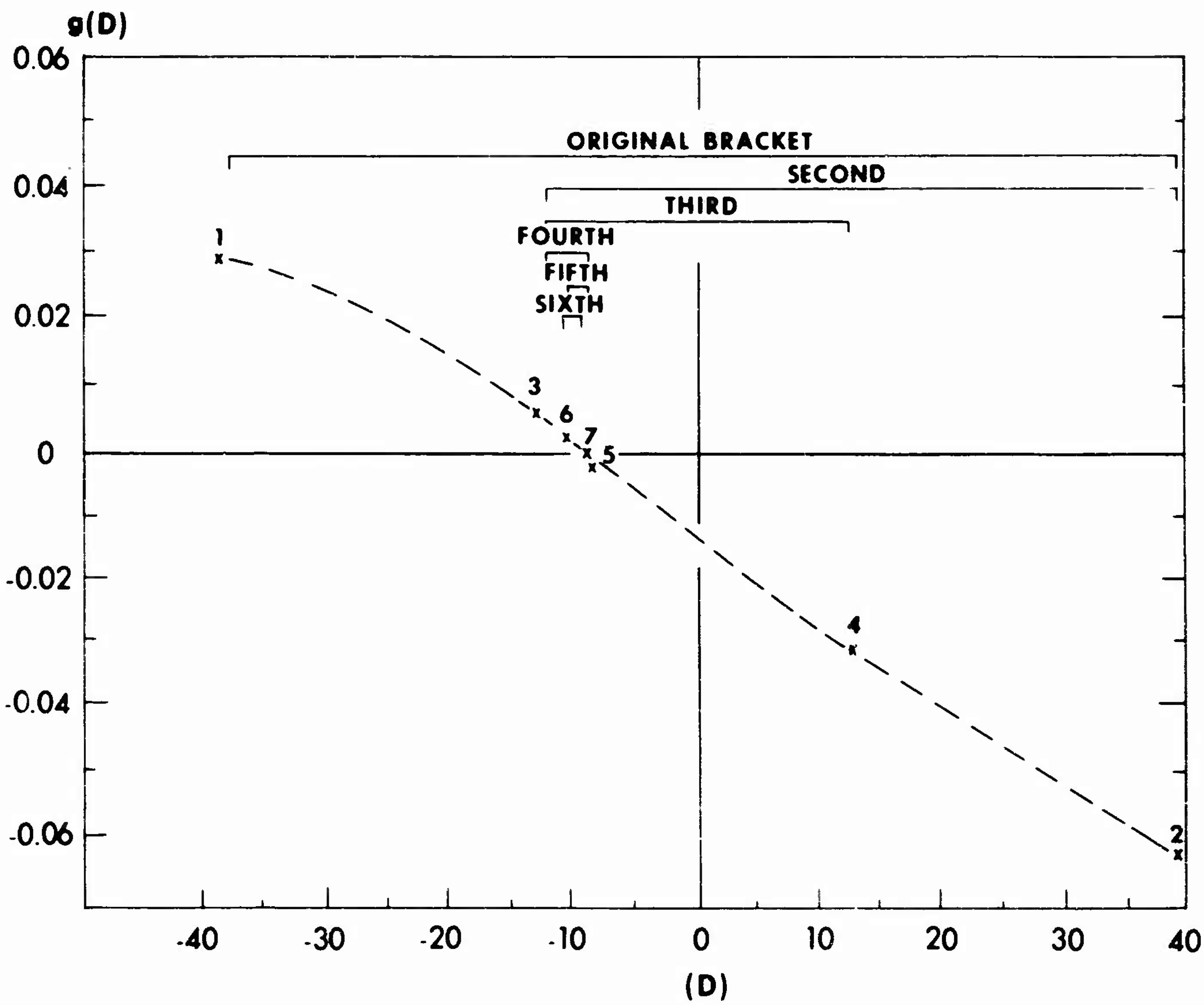

FIGURE 18.—The functions $g(D)$ for the sample computation.

Since

$$H=\overline{uy}\;\overline{yr}-\overline{y^2}\;\overline{ur},$$

therefore:

$$\frac{\partial H}{\partial D}=\frac{\partial \overline{uy}}{\partial D}\,\overline{yr}+\overline{uy}\,\frac{\partial \overline{yr}}{\partial D}-\frac{\partial \overline{y^2}}{\partial D}\,\overline{ur}-\overline{y^2}\,\frac{\partial \overline{ur}}{D}$$

or

$$\frac{\partial H}{\partial D}=\overline{us}\;\overline{yr}+\overline{uy}\;\overline{sr}-\overline{uy}\;\overline{yr^2}-2\,\overline{ys}\;\overline{ur}+\overline{y^2}\;\overline{ur^2}, \tag{103}$$

where $s_i=r_i-\bar{r}$. Evaluating at the true velocities so that $u_i=V_* y_i$, gives $\frac{\partial H}{\partial D}=V_*(\overline{y^2}\;\overline{sr}-\overline{ys}\;\overline{yr})$.

Similarly,

$$\frac{\partial H}{\partial V_i}=yr\,\frac{y_i}{n}-\overline{y^2}\,\frac{s_i}{n}, \tag{104}$$

so that

$$\left.\frac{\partial D}{\partial V_i}\right|_{V_j\neq i,\ H}=\frac{\overline{y^2}\,s_i-\overline{yr}\,y_i}{n\left.\dfrac{\partial H}{\partial D}\right|_{V_1,V_2,\ldots V_n}}.$$

The Error in V_*

V_* is computed from $V_*=\dfrac{\overline{ur}}{\overline{yr}}$

The standard error of V_* is:

$$SE(V_*)=\left(\sum_{i=1}^{n}\left[\left.\frac{\partial V_*}{\partial V_i}\right|_{V_j\neq i} SE(V_i)\right]^2\right)^{1/2}. \tag{105}$$

But,

$$\left.\frac{\partial V_*}{\partial V_j}\right|_{V_i\neq j}=\left.\frac{\partial V_*}{\partial D}\right|_{V_i}\left.\frac{\partial D}{\partial V_j}\right|_{V_i\neq j}+\left.\frac{\partial V_*}{\partial V_j}\right|_{V_i\neq j,\ D}. \tag{106}$$

Therefore,

$$\left.\frac{\partial V_*}{\partial V_j}\right|_{V_{i\neq j}}=\frac{-\overline{ur^2}\;\overline{yr}-\overline{ur}\;\overline{rs}+\overline{ur}\;\overline{y^2}}{(\overline{yr})^2}\left.\frac{\partial D}{\partial V_j}\right|_{V_{i\neq j}}+\frac{s_j}{n\overline{yr}}. \tag{107}$$

Evaluating at the true value of velocities,

$$\left.\frac{\partial V_*}{\partial V_j}\right|_{V_{i\neq j}}=-V_*\frac{\overline{rs}}{\overline{yr}}\left.\frac{\partial D}{\partial V_j}\right|_{V_{i\neq j}}+\frac{s_j}{n\overline{yr}}.$$

The Error in z_0

The roughness length, z_0, is given by:

$$z_0=\exp\left(\bar{x}-\frac{\bar{V}}{V_*}\right). \tag{108}$$

The standard error of z_0 is approximated by

$$SE(z_0)=\left(\sum_{i=1}^{n}\left[\left.\frac{\partial z_0}{\partial V_i}\right|_{V_{j\neq i}}SE(V_i)\right]^2\right)^{1/2}. \tag{109}$$

But,

$$\left.\frac{\partial z_0}{\partial V_j}\right|_{V_{i\neq j}}=\left.\frac{\partial z_0}{\partial D}\right|_{V_i}\left.\frac{\partial D}{\partial V_j}\right|_{V_{i\neq j}}+\left.\frac{\partial z_0}{\partial V_j}\right|_{V_{i\neq j},D}. \tag{110}$$

This leads to

$$\left.\frac{\partial z_0}{\partial V_j}\right|_{V_{i\neq j}}=z_0\left\{\left(\bar{r}+\frac{\bar{V}}{(\overline{ur})^2}[-\overline{ur^2}\;\overline{yr}-\overline{ur}\;\overline{rs}+\overline{ur}\;\overline{yr^2}]\right)\left.\frac{\partial D}{\partial V_j}\right|_{V_{i\neq j}}+\frac{1}{V_*}\left[\bar{V}\frac{s_j}{n\overline{ur}}-\frac{1}{n}\right]\right\}. \tag{111}$$

If we evaluate at true values,

$$\left.\frac{\partial z_0}{\partial V_j}\right|_{V_{i\neq j}}=z_0\left\{\left(\bar{r}-\frac{\bar{V}\,\overline{rs}}{V_*\overline{yr}}\right)\left.\frac{\partial D}{\partial V_j}\right|_{V_{i\neq j}}+\frac{1}{V_*}\left(\bar{V}\frac{s_j}{nV_*\overline{yr}}-\frac{1}{n}\right)\right\}.$$

To compute these standard errors of the profile parameters, several intermediate variables are required in addition to those found in computing the profile parameters. These are, for the least squares values of D, V_*, and z_0: $\bar{r}$, $\overline{sr}$, $\overline{ys}$, $\overline{s^2}$; and, at each measuring height, i: $s_i=r_i-\bar{r}$;

$$\left.\frac{\partial D}{\partial V_i}\right|_{H,V_{j\neq i}}$$

from equation 100;

$$\left.\frac{\partial V_*}{\partial V_i}\right|_{V_{j\neq i}}$$

from equation 107;

$$\left.\frac{\partial z_0}{\partial V_i}\right|_{V_{j\neq i}}$$

from equation 111.

The standard error of the windspeeds is also required, $SE(V_i)$. This may be estimated, for $n\geq 4$, by

$$SE(V_i)\doteq\frac{1}{\sqrt{n-1}}\left\{\sum_{i=1}^{n}\left(V_i-V_*\ln\left[\frac{z_i+D}{z_0}\right]\right)^2\right\}^{1/2}$$

$$=\sqrt{\frac{4n}{3n-1}}\,(\overline{u^2}-V_*\overline{uy})^{1/2}. \tag{112}$$

In any case, $SE(V_i)$ is at least as large as known anemometer errors. The parameters for the sample problem are now repeated, with their standard errors indicated:

$V_*=115.1\pm 1.4$ cm./sec.

$z_0=0.43\pm 0.04$ cm.

$D=-9.5\pm 1.2$ cm.

ANALYSIS OF A SET OF NEAR-ADIABATIC PROFILES

For a set of good adiabatic wind profiles, six measured at O'Neill, Nebr., in the summer of 1956 by Halstead and associates (*6*) were chosen. Data and results of analysis are tabulated below.

Date	*10 July*	*11 July*	*23 July*	*24 July*	*24 July*	*24 July*
Time	*1905*	*0605*	*1905*	*0605*	*0705*	*1905*
$T_{16m}-T_{.25m}$	+0.24°C	+0.23	−0.07	+0.48	−0.92	−0.18
u_{16m}	729 cm/sec	780 cm/sec	731 cm/sec	584 cm/sec	843 cm/sec	503 cm/sec
u_{8m}	639	689	635	532	763	427
u_{4m}	569	607	568	505	708	398
u_{2m}	497	543	----------	420	609	339
u_{1m}	432	474	437	380	552	291
$u_{.5m}$	373	411	377	336	501	259
$u_{.25m}$	299	340	310	289	426	224
V_*, cm/sec	108±4	113±5	108±6	75±6	107±6	Not computed
z_0, cm.	2.0±0.5	1.7±0.4	2.0±0.7	.65±.38	.61±.26	"
D, cm	9.0±5.3	12.0±6.0	12.4±8.5	5.3±10.3	9.6±8.0	>24

Compared to the mean profile first discussed, these six have appreciably higher standard errors for the parameters. That $D-z_0$ is positive is a minor puzzle. It indicates that the windspeeds at the highest levels are less than expected, while those at the lowest levels are greater. At the highest level, the log-law for area averages does not hold so well; at the lowest levels, the measurements are not sufficiently representative of area averages. In this instance. the tendency to avoid local obstacles and depressions in locating the anemometer mast appears to have led to selecting a spot with slightly higher winds than average near the surface. (These data were not taken with this manner of statistical profile analysis in mind. Subjective analysis of profile data generally weights the anemometer readings according to expected reliability.) These new computations show again that:

(a) Site selection and anemometry were good;

(b) The magnitude of displacement height, D, was small compared to median height of measurement; and

(c) z_0 was approximately 1 cm.

SUMMARY

Another program, based on Robinson's equations (*26*), has been written for evaluating logarithmic wind profile parameters. Two features in the technique differ from Robinson's: (1) the method of choosing the first estimates of D, and (2) the method of finding subsequent estimates of D. These perhaps are improvements. In addition, this program computes good estimates of the standard errors of the three parameters, provided—

(a) The accuracy of the anemometers is known, or

(b) A sufficient number of measuring heights are used.

TURBULENT TRANSFER CHARACTERISTICS OF THE AIRSTREAM IN AND ABOVE THE VEGETATIVE CANOPIES AT THE EARTH'S SURFACE

By Jerry Stoller and Edgar R. Lemon

Turbulent exchange calculations for sensible heat, latent heat (evaporation and condensation), and carbon dioxide (photosynthesis and respiration) are important in estimating some of the components of the energy balance near the earth's surface. Basic to these calculations is the determination of the transfer coefficient for momentum (*Km*) and applying it to the transfer of other molecular properties. In essence, one implicitly determines the value of *Km* in the turbulent boundary layer above the surface and uses it to calculate the exchange of other molecular properties, knowing their potential drop (gradient) across some known distance in the same boundary layer. The assumption is made that the momentum transfer coefficient is quantitatively equal to the other transfer coefficients, i.e., for heat, water vapor, and carbon dioxide.

Upon the accurate measurement of the momentum transfer characteristics of the turbulent boundary layer, then, rests the whole aerodynamic approach to the energy budget.

TURBULENT EXCHANGE ABOVE THE CROP CANOPY

Where vegetation exists at the earth's surface, the turbulent boundary layer has to be subdivided into two regions: One above the plant surfaces where no sources or sinks occur and the other within the vegetative canopy where sinks and sources do occur. Exchange calculations above the canopy rely upon the log wind profile law and the logarithmic law of vertical distribution of the other physical quantities. Three specific problems arise, however, in the use of this aerodynamic approach to exchange calculations above the vegetative canopy:

(1) The errors created by appreciable thermal gradients in the turbulent boundary layer;

(2) Instrument and interpretative limitations at low mean wind velocities; and

(3) The functional relationships of the log wind profile characteristics to both mean windspeed and surface properties (geometric and elastic properties of the roughness element).

When the temperature of the air near the vegetation rises significantly during the daytime, then thermal convective transfer processes ("free convection") become important in addition to the mechanical convective transfer processes ("forced convection"). [The forced convection processes are responsible for the log profile relationship.] Free convection superimposed on forced convection causes an underestimation of the transfer processes when the log profile law is used, and is especially pronounced at low wind velocities when the forced convection component is small. Sometimes the mean wind velocity is reduced to such a low level that it is not measurable by standard means (rotating cup anemometers). Under these conditions, the logarithmic law of vertical distribution of physical quantities no longer holds true and the calculated fluxes erroneously go to zero. The subject of "free convection" error will be dealt with in detail in a later report.

In addition to free convection and low windspeed problems associated with the log law application to transfer processes in the turbulent airstream, another problem arises out of the functional relationship between windspeed and the wind profile characteristics over vegetative surfaces. This problem is created by the changing geometric properties of the surface (plant growth) and the changing elastic properties of the surface (waving of stalks and leaf flutter). This functional relationship will be taken up in detail first.

The eddy flux across a plane of some entity (i.e., momentum) which is neither destroyed nor created in its transfer (not strictly true for momentum) can be written:

$$Q=K\frac{\partial c}{\partial z}, \tag{113}$$

where Q is the total amount of the entity passing downward through a unit area per unit time; K is the transfer coefficient, and $\partial c/\partial z$ is the gradient across the plane. The amount of the entity, c, is expressed on a per-unit-volume basis, and z is the axial distance normal to the plane.

For the flux of momentum (shearing stress), τ, the basic equation becomes:

$$\tau=Km\frac{\partial u}{\partial z}\rho \tag{114}$$

where u is the windspeed and ρ is the density of the air.

In the turbulent boundary layer immediately above the vegetation surface, the vertical gradient of wind is expressed by:

$$\frac{\partial u}{\partial z}=\frac{1}{k}\left(\frac{\tau_0}{\rho}\right)^{\frac{1}{2}}\frac{1}{z}, \qquad (115)$$

and upon integration gives the "logarithmic wind profile law" where the windspeed, u_z, at height z above the ground is represented by:

$$u_z=\frac{1}{k}\left(\frac{\tau_0}{\rho}\right)^{\frac{1}{2}}\ln\left(\frac{z+z_0}{z_0}\right), \text{ where } z>z_0, \qquad (116)$$

τ_0 is the shearing stress at the surface, z_0 is the roughness length, and k is the Von Karman constant (0.4).

Equations 115 and 116 imply that the windspeed profiles are functions of log height, z, above a given reference plane. As the ground vegetation grows, however, the turbulent boundary layer is displaced upward, causing the reference plane from which z is measured to be displaced upward also from the ground surface. It then becomes necessary to introduce a zero point displacement, d, and rewrite equation 116, thus:

$$u_{z_i+D}=\frac{1}{k}\left(\frac{\tau_0}{\rho}\right)^{\frac{1}{2}}\ln\frac{z_i+D}{z_0} \qquad (117)$$

where $D=d+z_0$, or the "effective displacement parameter," and z_i is the nominal height above the ground surface.

The friction velocity, V^*, defined by:

$$V^*=\left(\frac{\tau_0}{\rho}\right)^{\frac{1}{2}} \qquad (118)$$

then:

$$V^*=\frac{ku}{\ln\frac{z_i+D}{z_0}} \qquad (119)$$

and,

$$Km=(z_i+D)kV^*. \qquad (120)$$

The preceding section (p. 28) takes up the method used here for the determination of the logarithmic wind profile parameters, V^*, z_0, and D from sufficient experimental data u on z_i. In that section, $V_*=\frac{1}{k}V^*$.

Alfalfa Investigations

Numerous wind profile measurements over alfalfa were taken with Sonoya Rotating Cup Anemometers on July 29, 30, and 31, 1960, when the alfalfa was 75 cm. high. The equipment and site have been fully described elsewhere (*14*). Mean wind velocities were measured over 5-minute periods at 90, 100, 120, and 160 cm. from the ground. Sampling times were selected when it was felt that thermal effects upon the profiles would be negligible (i.e., when temperature gradients were small). Three conditions minimizing this error were observed: (1) The measurements were made near the surface (within 160 cm. of the ground, or 85 cm. of the crop top); (2) the measurements were made during cloudy periods when the radiation load was small; and (3) the alfalfa was lush with plenty of soil moisture (soil moisture tension was 0.2 atm. at 6-inch depth).

Table 1 and figure 19 present the functional relationships between the mean windspeed at 160 cm. and the profile parameters z_0, D, and V^*. It can be seen that the roughness length, z_0, ranged from 28.5 to 1.3 cm., and the effective displacement, D, from −18.8 to −65.0 cm. The friction velocity, V^*, appeared fairly independent of windspeed. (Note that table 1 and figure 19 give values of V^*/k instead of V^*.) This would indicate that the shearing stress was fairly constant and independent of the windspeed at a given height above the alfalfa. One can conclude that within the range of windspeeds encountered, shearing stress is almost completely dependent upon the physical characteristics of the surface.

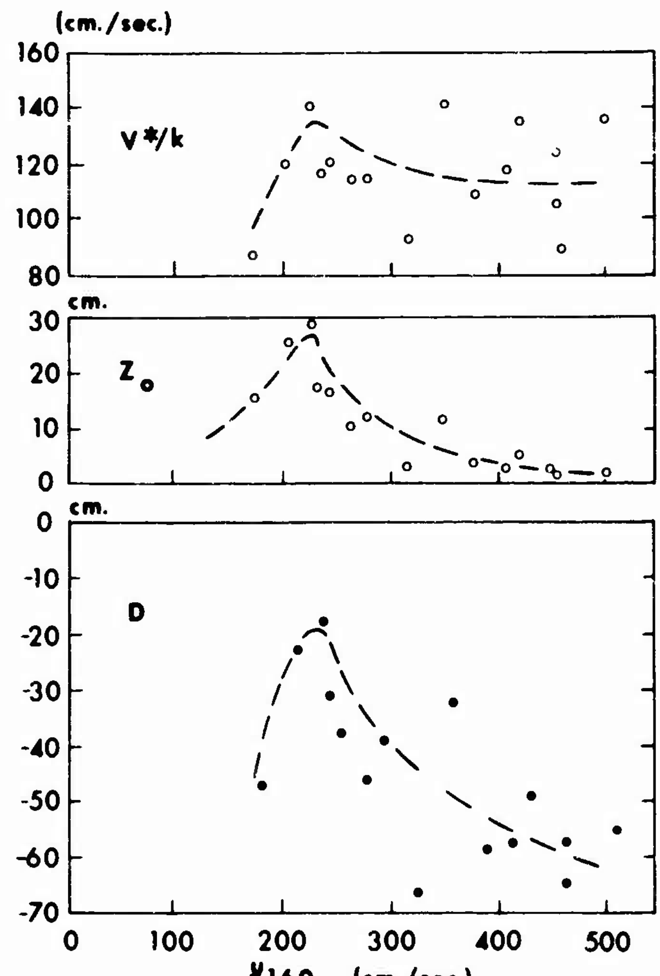

FIGURE 19.—Wind profile parameters for alfalfa, July 29–31, 1960.

TABLE 1.—*Functional relationships between windspeed and roughness length (z_0), effective displacement (D), and friction velocity (V^*) for alfalfa at Ithaca, N.Y., July 29–31, 1960*

Profile No.	Date and time	Height	Velocity	z_0	D	V^*/k
	E.s.t.	*Cm.*	*Cm./sec.*	*Cm.*	*Cm.*	*Cm./sec.*
1		90	87	15.6	−48.4	88.8
	7/30/60	100	107			
	1027	120	135			
		160	175			
2		90	118	25.2	−23.3	121.2
	7/30/60	100	135			
	1002	120	163			
		160	205			
3		90	130	28.5	−18.8	140.9
	7/30/60	100	145			
	0956	120	180			
		160	225			
4		90	138	17.8	−32.8	118.2
	7/30/60	100	156			
	1206	120	188			
		160	232			
5	7/29/60	90	140	16.4	−38.8	122.8
	1840	100	160			
	1852	120	197			
	1904	160	245			
6	7/29/60	90	158	11.0	−46.4	114.7
	1916	100	182			
	7/30/60	120	218			
	0950	160	268			
7	7/30/60	90	175	11.3	−39.8	117.6
	1008	100	197			
	1014	120	230			
		160	278			
8		90	212	3.5	−57.8	94.6
	7/29/60	100	235			
	1846	120	275			
		160	320			
9		90	235	10.7	−33.5	141.7
	7/29/60	100	260			
	1605	120	295			
		160	350			
10		90	250	3.2	−59.0	110.4
	7/31/60	100	280			
	1259	120	325			
		160	380			
11		90	270	3.2	−57.9	118.1
	7/31/60	100	305			
	1311	120	347			
		160	408			
12	7/31/60	90	280	5.3	−49.4	137.6
	1231	100	315			
	1353	120	355			
		160	420			
13		90	305	2.8	−57.8	125.0
	7/31/60	100	340			
	1317	120	387			
		160	450			
14		90	312	1.3	−65.0	106.2
	7/31/60	100	350			
	1247	120	395			
		160	455			
15	7/31/60	90	345	2.7	−55.8	137.1
	1219	100	385			
	1253	120	430			
		160	500			

When one observes the motion of the alfalfa plants in the field, two factors readily become apparent. As the wind velocity increases, the leaves orient themselves in the direction of the wind, and the field appears to consist of waves; i.e., "smoothing out effect."

Under low velocities, the plants stand nearly erect while each leaf acts as a momentum sink. The momentum loss is probably greatest in the area of the upper one-third of the plants; however, some wind movement is apparent down to the ground level. As wind velocities increase, however, the upper leaves orient themselves in the direction of the wind flow and the plants overlap each other. Thus, a complete surface of smooth leaves is approached and is accompanied by a drop in the roughness length, z_0. For the effect to occur, the plant must be high enough to provide a complete ground cover and consist of enough foliage to create the "wave" appearance under higher velocities.

Wheat Investigations

The air turbulence studies in a wheatfield were made on an open, nearly level hilltop (Mount Pleasant) located adjacent and to the north of Ellis Hollow Experimental site described elsewhere (*14*). The field has the approximate dimensions of 200 by 200 meters. As in the alfalfa investigations, measurements were made under conditions favoring small temperature gradients, and with the same equipment.

It was observed earlier that within the customary 5-minute averaging period there were periods of relatively steady wind. In an effort to separate the steady flow from the gusts, a series of 30-second sampling periods were used. When a series of two or more consecutive 30-second periods rendered similar readings from the cup anemometers, the profile was considered to be semi-steady. By selecting semi-steady periods the semi-log plotting of the wind profiles proved to be much more precise than when the 5-minute averaging period was employed.

On the first day of study (July 9, 1960), the wheat averaged almost 100 cm. in height at a density of 60 stalks per square foot. The heads were 10 cm. long, and located right above the upper leaves. Wind profiles were taken when the wind blew from a northeasterly direction. As can be seen in figure 20 and table 2, V^* and z_0 increased with an increase in wind velocity. Also, the effective displacement, D, decreased when the wind velocity above the crop increased.

In regard to these measurements, it must be mentioned that the wind velocities did not attain high enough values to cause appreciable bending of the wheat stalks. A different picture was obtained July 22 and 23, when measurements were taken at the same site. At this time, the average height of the wheat was approximately 130 cm. Most of the growth had taken place between the upper leaf and the head. Thus, the center of mass was displaced upward.

Figure 21 and tables 3 and 4 present the data showing that the roughness length, z_0, and effective displacement, D, decreased while the friction velocity, V^*, remained fairly constant with increasing windspeed above a "critical" level. Evidently, the wheat crop on July 22, 1960, acted similarly to alfalfa. The reversal in trends for the wheat crop during the two different stages of development has to be attributed both to a change in the physical characters of the crop, and to the diversity of range of windspeeds encountered. In the earlier stage (table 2), the winds were slower and the crop shorter, thus more rigid. This would permit some waving and leaf flutter, but little streamlining. At the later dates under the higher wind velocities when the crop was taller, streamlining probably occurred much as it did in alfalfa. It is of interest to point out that the trends observed in the wheat at the lower windspeeds on

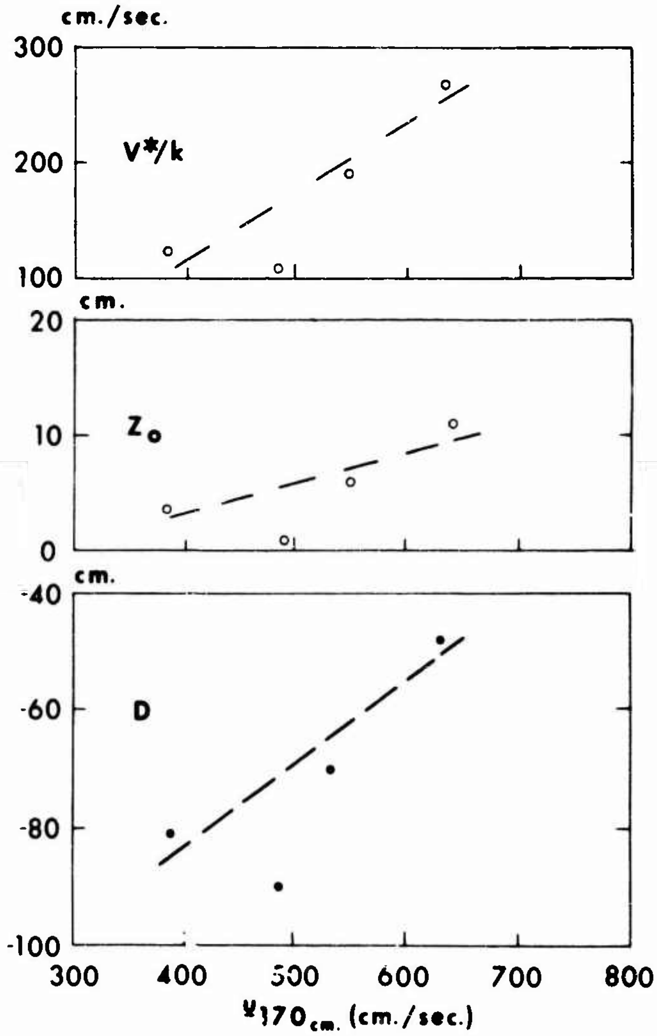

FIGURE 20.—Wind profile parameters for wheat, July 9, 1960.

TABLE 2.—*Wind profile data for wheat at Ithaca, N.Y., July 9, 1960*

Profile No.	Height	Velocity	V^*/k	D	z_0
	Cm.	*Cm./sec.*	*Cm./sec.*	*Cm.*	*Cm.*
1	100	180	125.3	−82.8	4.20
	110	225			
	130	310			
	170	380			
	250	460			
2	100	250	108.1	−91.9	0.788
	110	345			
	130	420			
	170	485			
	250	580			
3	100	320	195.6	−68.0	6.03
	110	390			
	130	455			
	170	545			
	250	670			
4	100	400	266.5	−49.4	10.9
	110	470			
	130	535			
	170	630			
	250	780			

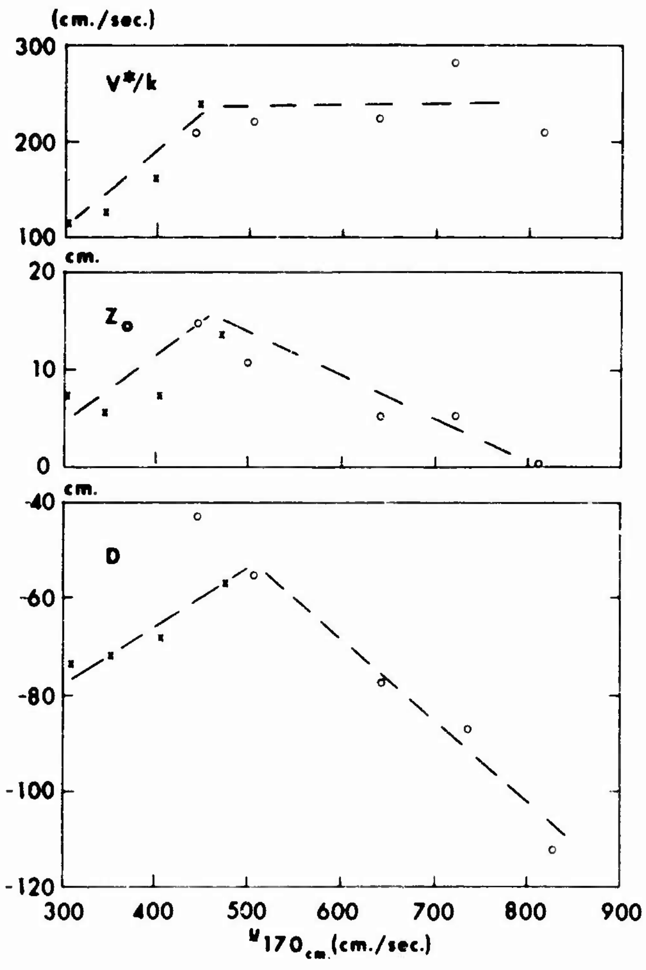

FIGURE 21.—Wind profile parameters for wheat, July 22-23, 1960.

the earlier date parallel those found in mature corn at higher windspeed in our 1959 investigations (*14*). A few values for corn of V^*, z_0, and D as a function of windspeed are given later in table 5. They are in agreement with the 1959 trends.

TABLE 3.—*Wind profile data for wheat at Ithaca, N.Y., July 22, 1960*

Profile No.	Height	Velocity	V^*/k	D	z_0
	Cm.	*Cm./sec.*	*Cm./sec.*	*Cm.*	*Cm.*
1	140	380	210.2	−46.6	15.0
	150	410			
	170	440			
	210	500			
	290	585			
2	140	440	221.6	−58.8	11.1
	150	470			
	170	500			
	210	585			
	290	670			
3	140	550	228.7	−82.2	5.24
	150	585			
	170	640			
	210	735			
	290	840			
4	140	585	285.8	−91.6	6.22
	150	640			
	170	725			
	210	840			
	290	990			
5	140	640	213.0	−118.0	1.09
	150	725			
	170	820			
	210	950			
	290	1080			

Figure 22 gives a qualitative diagram of the functional relationships for the three crops for comparative purposes. The trends on windspeed for the different crops are chiefly a matter of rigidity of momentum sink elements, whereas the order of magnitude of the values is attributed to the momentum sink geometry. The alfalfa is the least rigid, the taller wheat next, followed by the shorter wheat, with corn being the most rigid. A maximum Z_0 probably takes place in all three crops. Low enough windspeeds in alfalfa were not encountered to clearly define this point, whereas it might take very high winds to observe a reversal in corn. The wheat would fall between the alfalfa and corn in characteristics. Of course, all these relationships would depend upon stage of crop maturity, plant density, and a host of other factors too numerous to mention.

TURBULENT EXCHANGE WITHIN THE PLANT CANOPY

The exchange processes within the vegetative canopy are theoretically much more complex than

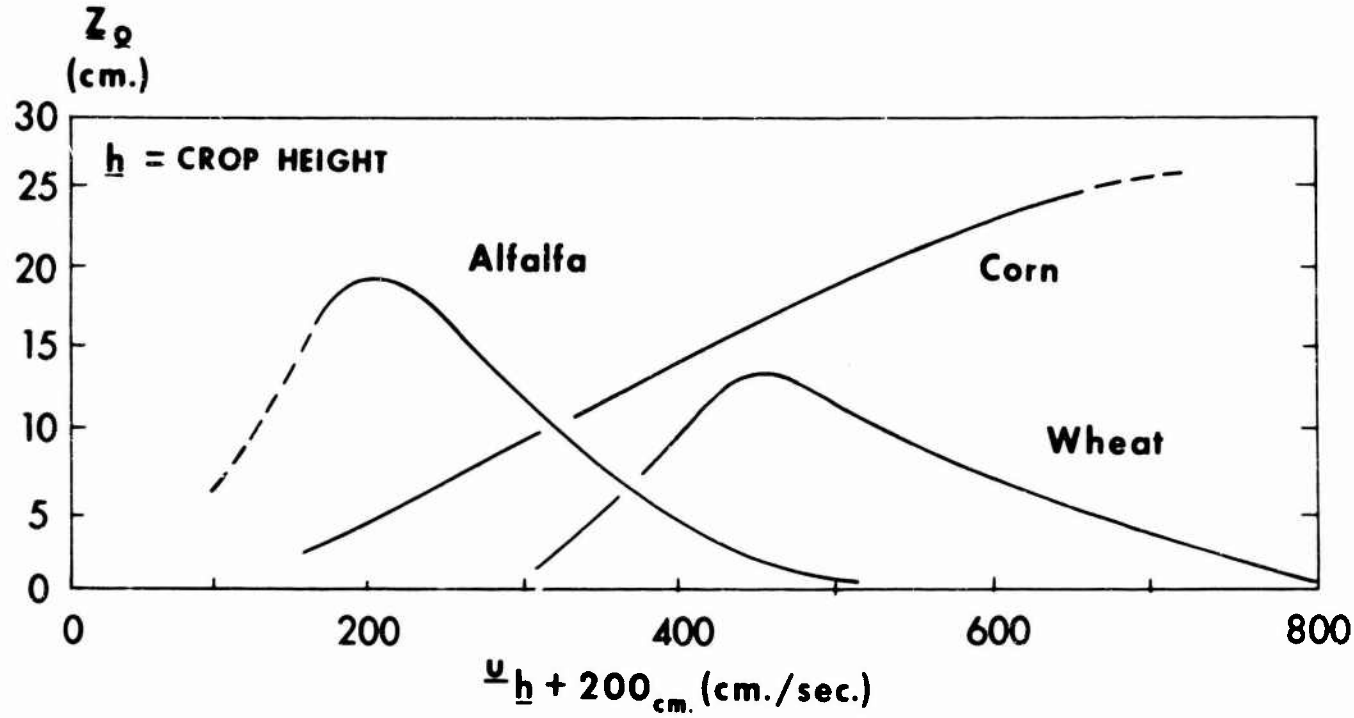

FIGURE 22.—Idealized roughness parameters for alfalfa, wheat, and corn as a function of windspeed.

those above, because of the complex distribution of sources and sinks within the "crop volume." Instrument and interpretative limitations on the experimental level are restrictive, too. Nonetheless, we have attempted to arrive at a semiquantitative picture, at least, of some transfer characteristics within the wheat and corn canopies.

Referring again to equation 113, we have

$$Q=K\frac{\partial c}{\partial z},$$

which states that the downward flux, Q, of some entity is equal to the product of the transfer coefficient, K, and the gradient of the entity across some plane, $\partial c/\partial z$. If we assume that the transfer coefficient for momentum is quantitatively equal to the transfer coefficient for, say CO_2, water vapor, and heat, then experimentally we need to determine the transfer coefficient for momentum from windspeed characteristics and the gradient for the entity in question (i.e., CO_2, water vapor or heat), in order to calculate the exchange rates for the latter.

Using Prandtl's model for rough flow in a pipe (*33*) and making the assumptions that turbulence is fully developed and isotropic within the vegetative canopy, we have:

$$K(z_t)=l\sqrt{\overline{(w')^2}} \qquad (121)$$

where $K(z_t)$ is the momentum transfer coefficient at nominal height, z_t; l is the "mixing length"; and w' is the vertical windspeed fluctuation, or "vertical eddy velocity." The eddy velocity, w', is defined as the difference between the instantaneous velocity, w, and a mean velocity, $\overline{w}$.

Experimentally, w' and l were evaluated from hot wire measurements made with a Hastings Model HR-2 nondirectional hot wire anemometer. The Hastings Model HR-2 is an instrument that measures all components of velocity in an additive manner. When measurements of the mean horizontal flow were made at a point, the values received on the recording chart were not actually true horizontal values. Looking at the flow pattern in two dimensions, the hot wire measures the mean horizontal flow (vector A) and the resolved component (vector D) of the horizontal fluctuation (vector B) and the vertical fluctuation (vector C).

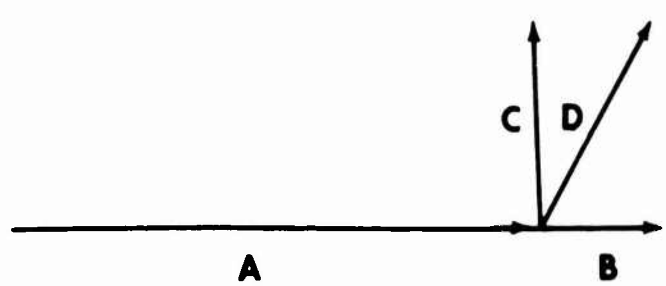

TABLE 4.—*Wind profile data for wheat at Ithaca, N.Y., July 23, 1960*

Profile No.	Height	Velocity [1]	V^*/k	z_0	D
	Cm.	*Cm./sec.*	*Cm./sec.*	*Cm.*	*Cm.*
	25	20.7*			
	50	34.6*			
	75	41.2*			
1	90	70†	123±5	7.2±.9	−77±
	100	140†			
	120	215†			
	160	305†			
	240	380†			
	25	------			
	50	37.7*			
	75	48.6*			
2	90	120†	131±7	5.9±1	−75±2
	100	195†			
	120	265†			
	160	345†			
	240	440†			
	25	24.6*			
	50	52.4*			
	75	54.3*			
3	90	140†	160±6	7.4±.8	−72±2
	100	215†			
	120	295†			
	160	400†			
	240	500†			
	25	25.6*			
	50	51.8*			
	75	64.5*			
4	90	180†	241±3	14.2±4	−60±1
	100	250†			
	120	345†			
	160	470†			
	240	610†			
	25	29.6*			
	50	89.9*			
	75	98.0*			
5	90	205†			
	100	280†			
	120	370†			
	160	490†			
	240	640†			

[1] * Hot wire data; † anemometer cup data.

A typical hot wire trace may be represented thus:

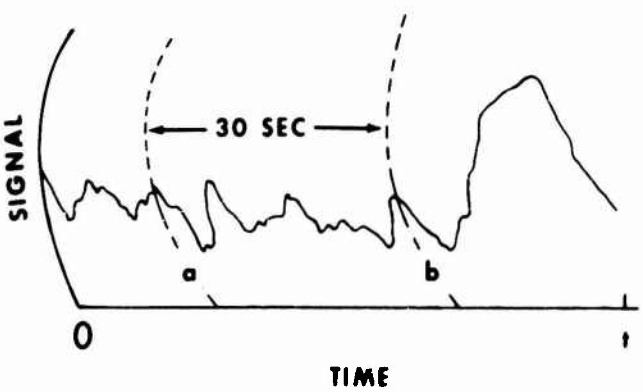

The mean velocity was determined by averaging the readings at intervals of two-thirds second over a 30-second run. If the horizontal wind, u, is considered in a steady state (a to b), the fluctuations during this period are assumed to be the fluctuations of the vertical wind component, w'. An averaging period, however, from 0 to t would include a large eddy regime. Then, averaging over this period would render a root mean square of the fluctuations for the horizontal component, $\sqrt{\overline{(u')^2}}$, of the large eddy. On the other hand, by selecting for steady periods, a good estimate of $\sqrt{\overline{(w')^2}}$ may be obtained (*33*).

Use is made of Taylor's Theorem (*34*), which employs a statistical approach to turbulence. Using an entire 30-second steady state hot wire record and displacing it two-thirds of a second for each time increment, t_1, we assigned the whole record equal weight in an autocorrelation, Rt, where Rt is the correlation between w'_{t_1} at the time t_1 and $w'_{t_1+2/3}$ at time $t_{1+2/3}$, etc. A good estimate for the mixing length, l, will then be:

$$l = u\int_0^{t_n} Rt\,dt, \qquad (122)$$

where t_n = time for $Rt=0$.

A typical autocorrelation curve is shown in figure 23. It is noticed that instead of $\lim_{t\to\infty} Rt = 0$, Rt crosses zero and then oscillates around it. This shows that the ideal case is approached in this evaluation, but never achieved.

Having estimated the vertical mixing length, l, and the vertical component of velocity, we may then determine the eddy diffusion coefficient at any point in space from equation 121. Then, from this relationship and the wind profile, we may estimate the shearing stress (momentum exchange) by:

$$\tau = \rho K(z_i)d\bar{u}/dz, \text{ or}$$
$$CO_2 \text{ exchange } P = K(z_i)d\,CO_2/dz, \qquad (123)$$

where P is the CO_2 exchange rate, and $d\,CO_2/dz$ is the gradient of CO_2.

Wheat Investigations

On July 23, the mast was placed so that the cup anemometers were at heights of 90, 100, 120, 160, and 240 cm. above the ground. The site was the same as that used for the previous measurements with the wheat 130 cm. high. On this day, however, a Hastings Model HR-2 hot wire anemometer with an 0.5-second time constant was used to obtain mean wind velocities at heights of 25, 50, and 75 cm. in the plant canopy.

Since there was only one hot-wire instrument to scan the chosen individual levels in the vegetative canopy of the wheat, a "normalizing" procedure had to be adopted to permit a complete mean windspeed profile evaluation. This consisted of taking numerous semisteady 30-second runs with

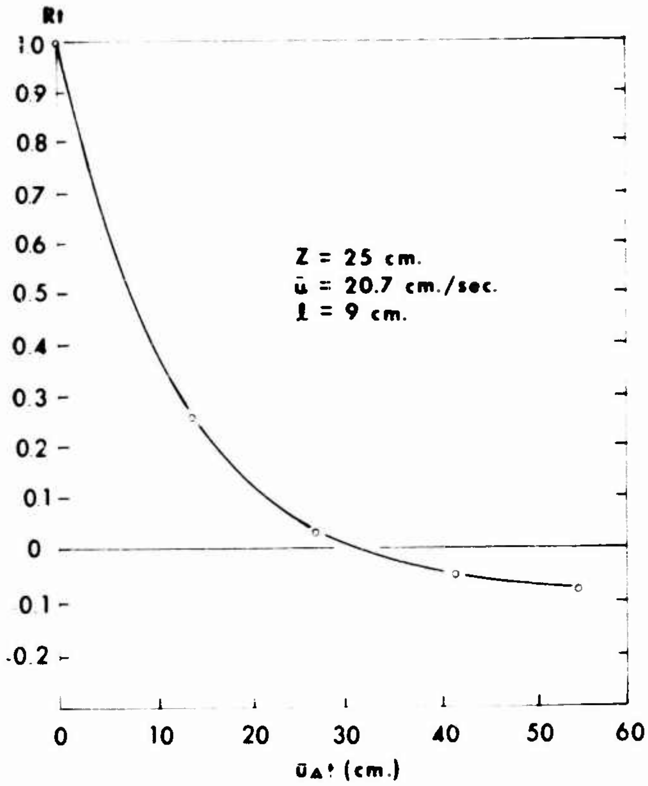

FIGURE 23.—Sample autocorrelation (Rt) as a function of lag time (Δt) times mean windspeed ($\bar{u}$) for wheat, July 23, 1960.

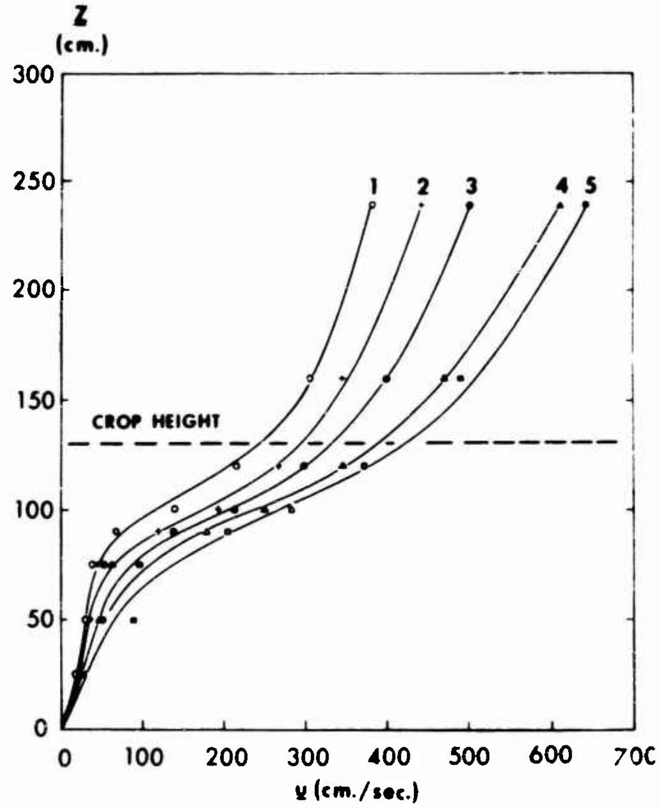

FIGURE 24.—Wind profiles in wheatfield, July 23, 1960.

the hot wire anemometer at a given level in the crop simultaneous to numerous semisteady 30-second profile runs with the cup anemometers above the crop. Hot wire measurements at the various levels in the canopy then were selected on nearly identical "above the crop profiles." Five complete profiles were selected in this way.

Values for the five profiles are given in table 4 and figure 24. There are three observations of immediate importance: (1), the velocities at 25 cm. are nearly the same for all wind regimes covered; (2), the values of $d\bar{u}/dz$ between 50 and 75 cm. are quite small for each profile; and (3), the point of inflection relative to the crop surface appears to be within 20 cm. below the crop top.

From hot wire measurements made in the wheat (130 cm. high) and cup measurements made in and above the wheat, two profiles that will be considered in detail in this section are plotted in figure 25. Using the method just described, we calculate the values for $K(z_i)$ for the three heights of 25, 50, and 75 cm. within the crop. Above the crop, $K(z_i)$ was calculated from the semilog profile, using equation 120.

Figure 26 shows the distribution of $K(z_i)$ increasing with height above the ground and increasing with windspeed above the crop. The distribution, $K(z_i)$, between 75 cm. and top of the crop was not determined, but it is believed to be rather complex, based upon the results found in corn.

Two items of importance should be pointed out. In contrast to the findings reported by Penman and Long (*22*) for wheat, the transport coefficient here is considerably larger than for molecular diffusion (10^4 greater) and the wheat crop did not appear to "seal itself" with increasing windspeed; i.e., the transport coefficient within the crop was sensitive to windspeed above the crop.

Calculations for shearing stress are given in figure 27. In this case, shear does appear to be considerably attenuated within the upper half of the crop.

Corn Investigations

On August 2, 1960, wind profiles were taken in Ellis Hollow cornfield (*14*) about 30 feet northwest of the central instrument line. Northwest winds blew approximately 45° to the corn rows. The sky became cloudy after 2:30 that afternoon, so that near isothermal conditions existed during the test period.

Wind profiles were taken with cup anemometers above the corn at heights of 250, 300, and 350 cm. The three cup anemometers were used as a reference for "normalizing" the hot wire measurements of 25, 50, 75, 100, 150, 200, 230, and 300 cm. above the ground. The crop averaged about 240 cm. high and was approximately 80 percent tasseled.

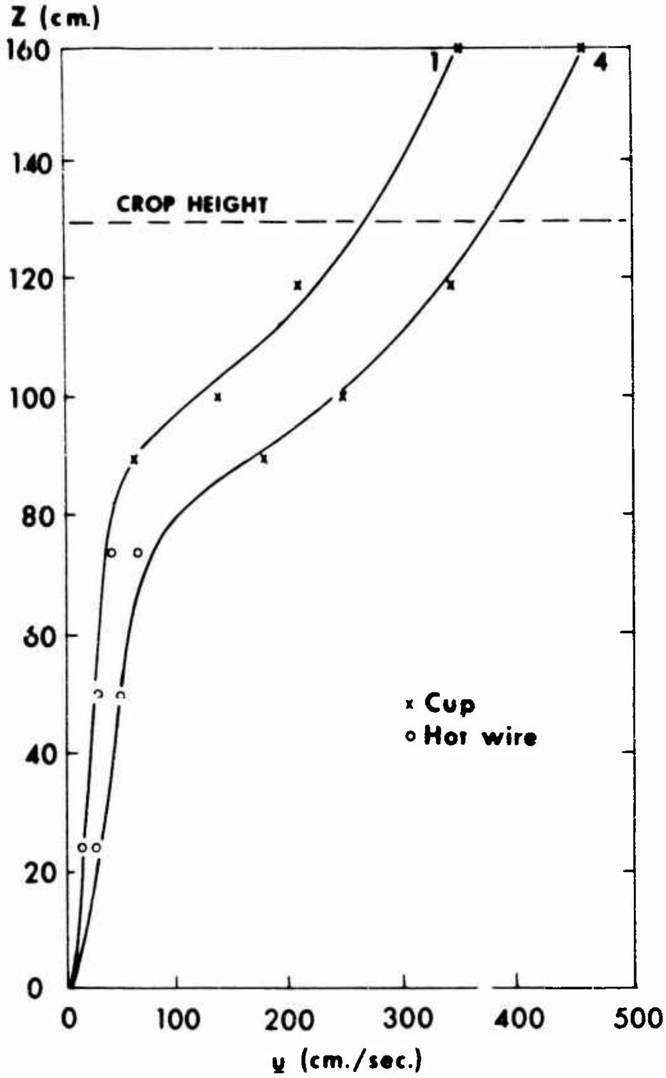

FIGURE 25.—Detailed wind profiles in wheatfield, July 23 1960.

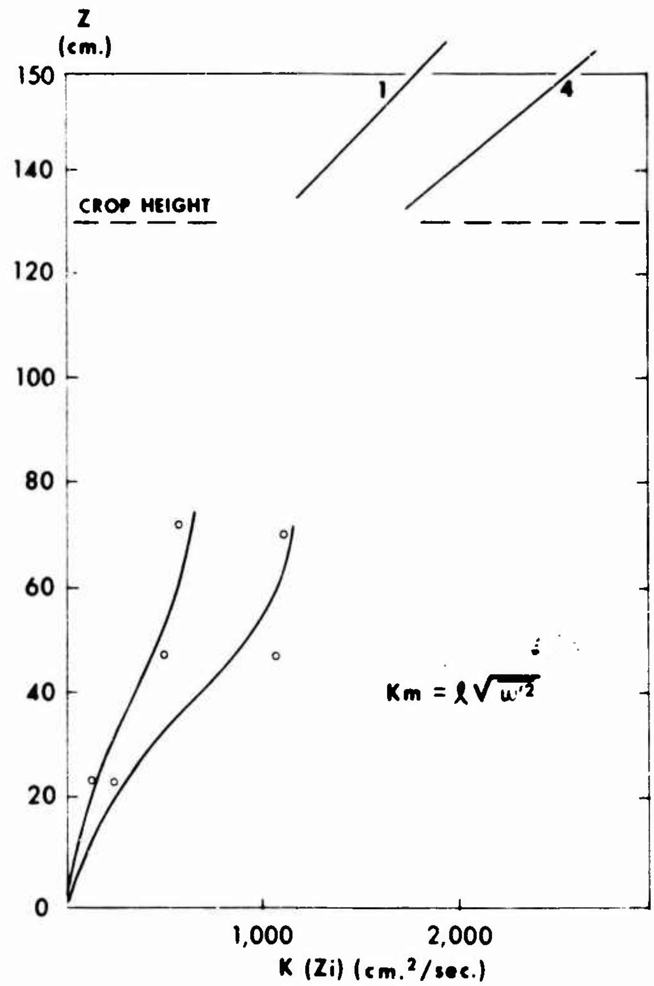

FIGURE 26.—Transfer coefficient for momentum (Km) as a function of height (z) in and above a wheat crop, July 23, 1960.

At this stage of development, there is an unusually high concentration of leaves at the top of the plant. Subsequent rapid vertical growth of the stem to full height eventually leads to a more even distribution of leaves along the stems.

Four wind profiles were chosen that cover the spectrum of winds that blew that afternoon. Figure 28 gives the graphical analyses of the turbulent boundary layer profiles above the crop. Too few levels—three—were taken to determine adequately the profile parameters, V^*, z_0, and D, by any statistical method. Nonetheless, by use of judgment from past experience in the graphical method with mature corn (*14*) realistic values were arrived at in this case. Pertinent data are given in table 5.

TABLE 5.—*Wind profile data taken above corn with cup anemometers at Ithaca, N.Y., August 2, 1960*

Profile No.	Height, z_i	Velocity, u	V^*/k	z_0	D
	Cm.	*Cm./sec.*	*Cm./sec.*	*Cm.*	*Cm.*
1	250	130	56.2	7.4	−180
	300	160			
	350	180			
2	250	215	98.5	9.6	−130
	300	385			
	350	350			
3	250	300	144.8	12.8	−100
	300	405			
	350	435			
4	250	420	177.7	17.0	−80
	300	470			
	350	505			

The measurements taken in and above the crop canopy under similar winds were plotted in figure 29. The solid lines were drawn in as a "best fit" approximation. Three points should be mentioned at this time:

(1) There is fairly good agreement between the cup anemometer and hot wire at the 300-cm. level;

(2) $d\bar{u}/dz$ is maximum just below the crop top; and

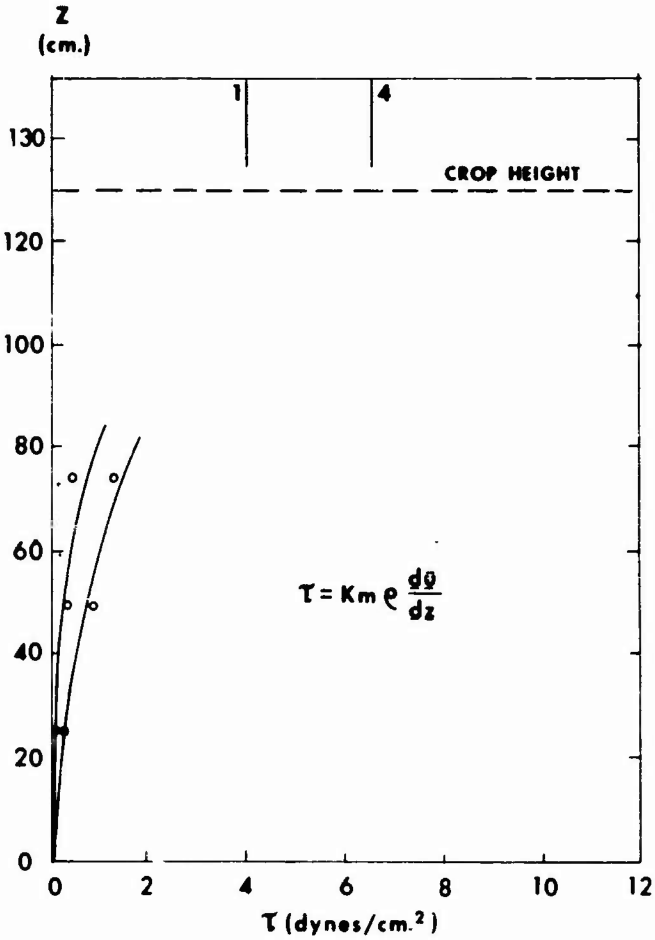

FIGURE 27.—Drag (τ) as a function of height (z) in and above a wheat crop, July 23, 1960.

(3) $d\bar{u}/dz$ is quite small between 25 and 100 cm.

In explanation of the last observation, it was determined that the vertical component of velocity was 8 percent of the mean horizontal component above the crop; however, this value increased as the height of the measurement was decreased. At the 25-cm. position, it was estimated that the vertical component was about 30 percent of the mean horizontal flow. Since the vertical component is additive, $d\bar{u}/dz$ between 25 and 100 cm. should be greater than shown in figure 29 and table 6. Therefore, the previous assumption of isotropic flow is less correct as the measurements approach the ground.

The statistical mixing lengths were calculated at each point, using the method described above. The values obtained are listed in table 7.

The values for above the crop (300 cm.) are at best approximate; however, they are in the right order of magnitude. Since the ratio of $l/z = 0.4$ within the turbulent boundary layer (Karman),

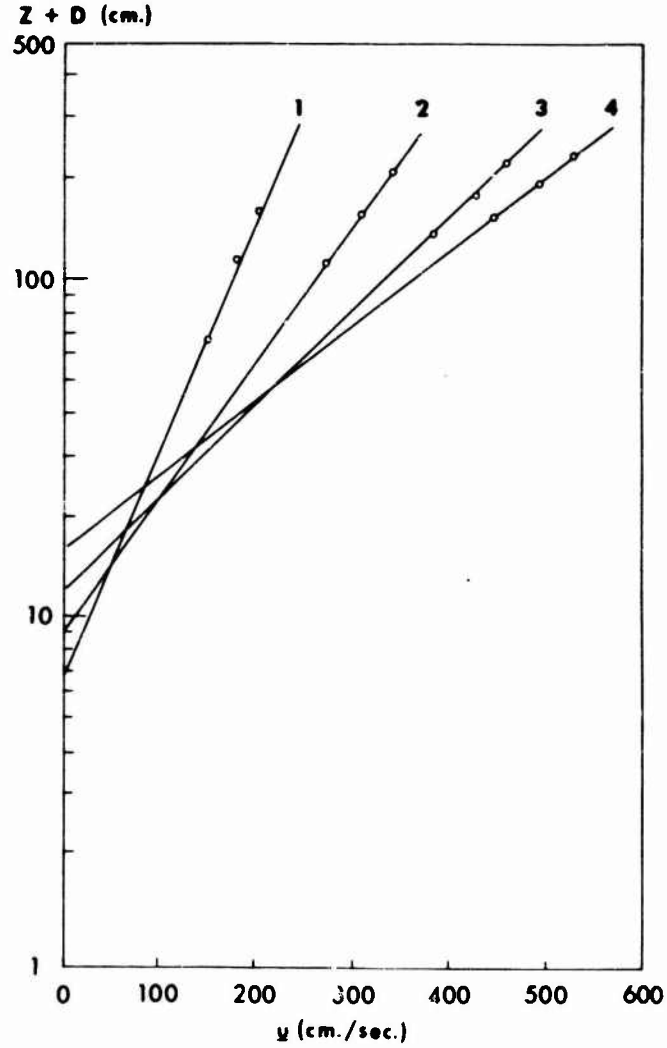

FIGURE 28.—Log profiles of wind above cornfield, August 2, 1960.

TABLE 6.—*Wind profile data taken with hot wire anemometer at Ithaca, N.Y., July 2, 1960*

Height, z_i (cm.)	Windspeed, u, according to profile No.—			
	1	2	3	4
	Cm./sec.	*Cm./sec.*	*Cm./sec.*	*Cm./sec.*
25	12. 6	18. 0	21. 0	43. 0
50	19. 0	20. 9	30. 0	48. 0
75	19. 7	26. 9	32. 0	----------
100	21. 5	30. 0	27. 4	60. 1
150	23. 5	44. 7	52. 0	100. 0
200	70. 4	124. 0	156. 7	249. 5
230	111. 2	166. 6	228. 4	300. 0
300	158. 5	266. 5	425. 7	488. 8

TABLE 7.—*Mixing length $l\ (z)_i$, as a function of height, at Ithaca, N.Y., Aug. 2, 1960*

Height, z_i (cm.)	Mixing length, l, for profile No.—			
	1	2	3	4
	Cm.	*Cm.*	*Cm.*	*Cm.*
25	21.0	25.0	25.5	30.0
50	31.0	33.0	36.0	47.0
75	39.5	45.0	47.5	----------
100	50.5	50.0	53.0	55.5
150	44.0	53.0	78.0	93.0
200	75.5	75.5	100.0	110.0
230	183.0	196.0	205.0	220.0
300	63.0	74.5	140.0	170.0

one would expect close to the same value at 300 cm. Using the ground as the reference plane, we obtain l/z range from 0.21 to 0.565. With the zero-plane displacement given as the reference, the values range from 0.485 to 0.71.

The mixing length values at 25 cm. are considered to be too large. This is attributed to the high fraction of vertical component of velocity when calculating the mean horizontal flow. Within this region, l/z is approximately 1.

The values for l/z are fairly constant between 50 and 200 cm. They are in the magnitude of 0.5. However, the most mysterious values were obtained at a point 10 cm. below the crop top ($z=230$). At this point, the mixing lengths are larger than those values obtained in the boundary layer above the crop, and are therefore suspect. The observation made while the data were being analyzed indicates that the reason for these high values originates from the abnormally long period of the cycle about the mean velocity.

At the position of 230 cm., the frequency of one cycle about the mean was from three to five times the ones previously encountered. It is suggested that this may be due to the elastic waving of the stalk and the upper leaves superimposed upon the normal frequency. The longer cycles were responsible for a much less rapid drop in the autocorrelation with time, and hence a larger value for:

$$\int_0^{t_n} Rt\,dt.$$

Values for the eddy diffusion coefficient, $K(z_i)$, were calculated from equation 121 (table 8). They were then plotted in figure 30. The dashed lines in figure 30 represent $K(z_i)$ as calculated from the semilog profile, and the solid lines are from the hot wire data. The shearing stress was calculated from equation 122 (table 9). Figure 31 shows the distribution of the shearing stress.

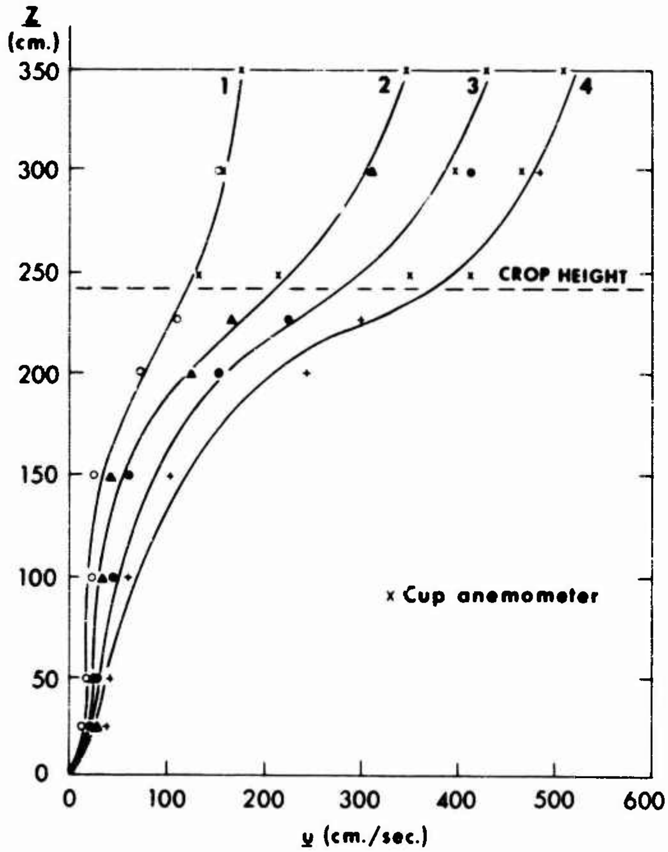

FIGURE 29.—Wind profiles in and above cornfield, August 2, 1960.

TABLE 8.—*Transfer coefficient, $K(z_i)$, as a function of height at Ithaca, N.Y., August 2, 1960*

Height, z_i (cm.)	$K(z_i)$ for profile No.—			
	1	2	3	4
	Cm.²/sec.	*Cm.²/sec.*	*Cm.²/sec.*	*Cm.²/sec.*
25	94	208	298	882
50	190	287	428	1,349
75	181	486	561	----------
100	359	540	1,039	1,576
150	339	1,211	2,223	2,818
200	1,306	1,910	2,700	3,894
230	5,106	5,606	6,724	7,854
300	1,796	2,712	5,250	7,208

SUMMARY

The determination of Km in and above the momentum sink elements using hot wire anemometer data affords an independent check on the semilog profile method for determining Km, and also permits a distribution analysis of where the momentum is being transferred in the vegetative s[illegible]. Of particular interest here is the com-

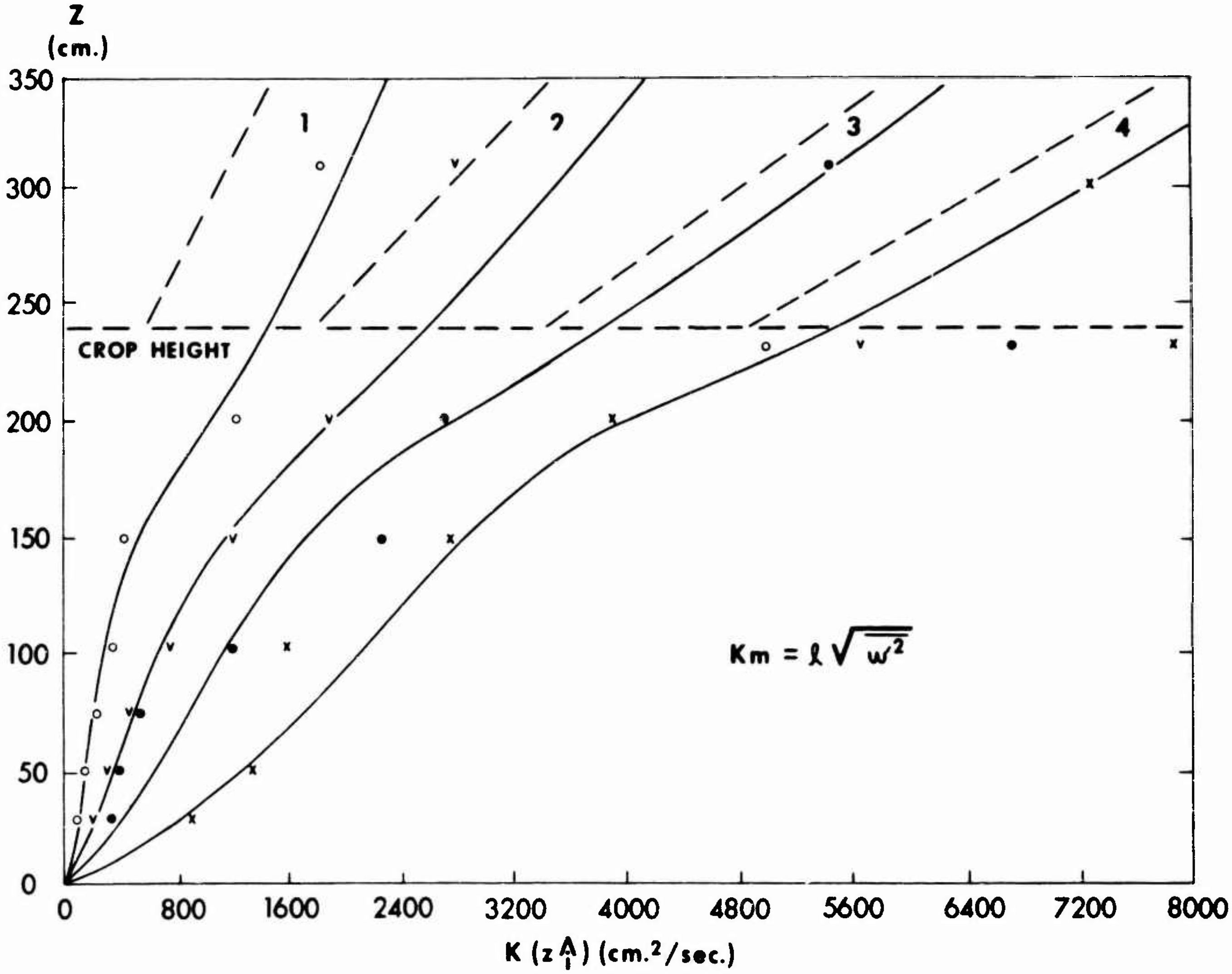

FIGURE 30.—Distribution of transfer coefficient for momentum (Km) in and above cornfield, August 2, 1960.

TABLE 9.—*Shearing stress as a function of height at Ithaca, N.Y., August 2, 1960*

Height, z, (cm.)	Shearing stress for profile No.—			
	1	2	3	4
	*Dynes/cm.*²	*Dynes/cm.*²	*Dynes/cm.*²	*Dynes/cm.*²
25	0.038	0.083	0.119	0.353
50	.076	.115	.171	.540
75	073	.194	.224	------
100	.143	.227	.499	.946
150	.203	.872	2.13	3.38
200	1.88	3.21	5.51	9.35
230	9.19	13.45	20.17	28.27
300	1.08	2.28	5.04	8.65

parison of the Km values derived by the two methods in the turbulent boundary layer above the corn (z_t=300 cm.) in figure 30. In three out of the four profiles the hot wire values are higher but of the same magnitude as the log profile values. The largest divergence occurs at the lowest windspeed, although there appears to be no consistent relation between divergence and windspeed. If the largest divergence at slow windspeed is indeed real, it should be anticipated from the following factors:

(1) Rotating cup anemometers are subject to greater errors at slow windspeeds;

(2) There are errors in estimating "free convection" from the log profile caused by thermal gradients; the latter are more pronounced at low windspeeds.

It should be pointed out, however, that temperature gradients were extremely small in the turbulent boundary layer over the corn (temperature gradients may have been significant within the canopy, however), and that the slowest wind measured above the crop was well above the stalling speed of the cup anemometers.

The distribution of shear in figure 31 can be considered. Realizing that the techniques used and the assumptions made are open to criticism, and that the results should be viewed as only semiquantitative, we should point out that the origin of shear from the log profiles falls on "planes" between 80 and 180 cm. above the ground ($-D$ values.) On the other hand, the hot wire evaluation of shear within the canopy demonstrates a "volume" distribution of shear in a complex but reasonable fashion. The hot wire quantitative values are obviously too high if the assumption is made that the total shear of the "surface" is accurately evaluated by the log wind profile characteristics above the "surface."

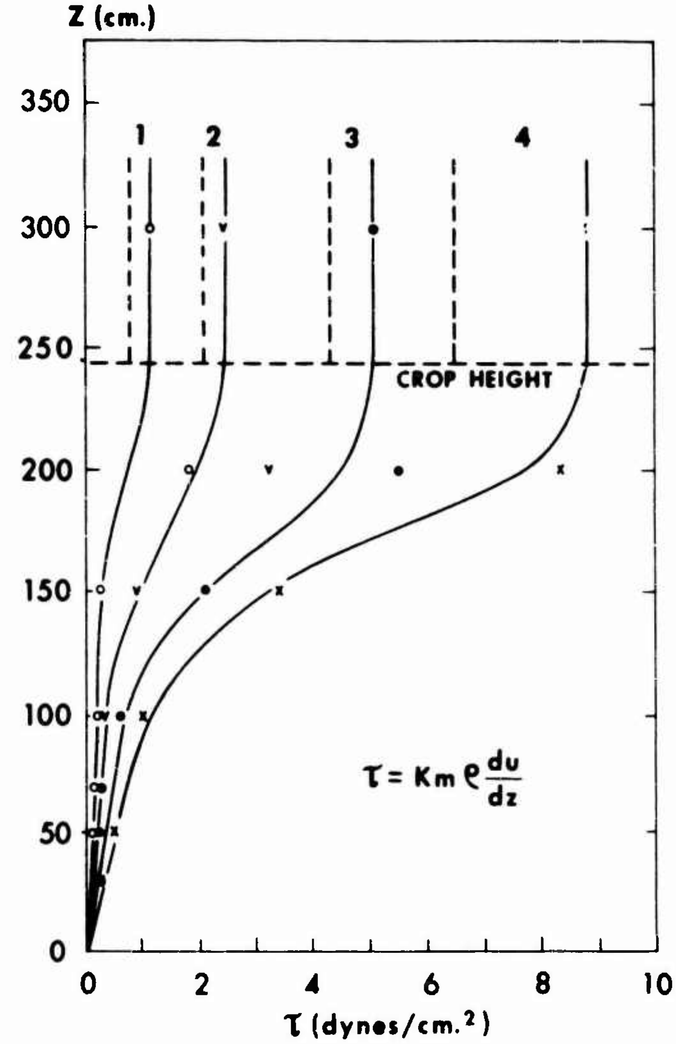

FIGURE 31.—Distribution of drag (τ) in and above cornfield, August 2, 1960.

SUMMARY AND CONCLUSIONS

1. Two theoretical models were developed for wind flow characteristics in plant canopies based upon a general type differential equation for the wind profile both inside and above the vegetative canopy at the earth's surface.

2. A testing of the theoretical models depended upon a breakdown of the wind structure into quasi-steady and transient states. It was assumed that the small scale eddies caused by the microstructure of the surfaces (plant surfaces) are responsible for vertical transport. For a beginning, the simpler case was studied experimentally. Wind flow in and above the vegetation at the quasi-steady state produced trends predicted by the turbulent flow model.

3. The turbulent canopy flow model postulated a linear growth of diffusivity within the turbulent canopy flow layer rather than the log velocity profile. This led to a realistic curvature reversal of the velocity profile deep in the canopy flow layer. This must be a basic characteristic of the turbulent wall flow within the roughness elements.

4. Studies of the log velocity wind profile characteristic over various kinds of vegetation revealed a complex coupling between windspeed, roughness length, friction velocity, and effective displacement and the surface geometric and elastic properties. In two cases, the friction velocity remained constant and independent of windspeed. To facilitate these and future studies, a machine computation method was developed that includes an evaluation of the standard errors of the logarithmic wind profile parameters.

5. An evaluation of the transfer coefficient and shear within the plant canopy revealed a reasonable picture of their spatial distribution within the "crop volume." This serves to emphasize that the concept of the roughness length, although very useful, is in reality an artifact.

LITERATURE CITED

(1) BATCHELOR, G. K.
1953. THE THEORY OF HOMOGENEOUS TURBULENCE. 197 pp., illus. Cambridge Univ. Press, London.

(2) CARSLAW, H. S., and JAEGER, J. C.
1947-48. CONDUCTION OF HEAT IN SOLIDS. 386 pp., illus. Oxford Press, London.

(3) CRAMER, H. E.
1952. PRELIMINARY RESULTS OF A PROGRAM FOR MEASURING THE STRUCTURE OF TURBULENCE FLOW NEAR THE GROUND. (Internatl. Symposium on Atmos. Turbulence in the Boundary Layer). U.S. Air Force Cambridge Research Center, Geophysics Res. Directorate, Cambridge, Mass. Geophysics Res. Papers (1951) 19: 187-205.

(4) ———
1959. MEASUREMENTS OF TURBULENCE STRUCTURE NEAR THE GROUND WITHIN THE FREQUENCY RANGE FROM 0.5 TO 0.1 CYCLES SEC.$^{-1}$. Adv. in Geophys. 6: 75-96.

(5) DAVIDSON, J. L., and PHILIP, J. R.
1958. LIGHT AND PASTURE GROWTH. *In* Climatology and Micro-Climatology, Canberra Symp. (Arid Zone Climatology) Proc. (181-187) (1956) 11: 355 pp., illus. Paris.

(6) HALSTEAD, M. H., et al.
1957. FORECASTING MICROMETEOROLOGICAL VARIABLES. U.S. Air Force Cambridge Res. Center, Geophysics Res. Directorate, Cambridge, Mass. Final Rpt. Contr. No. AF 19(604)—1117, 272 pp., illus. Texas A&M College, College Station, Tex.

(7) HEWSON, E. W. (Ed.)
1952. INTERNATIONAL SYMPOSIUM ON ATMOSPHERIC TURBULENCE IN THE BOUNDARY LAYER. U.S. Air Force Cambridge Research Center, Geophysics Res. Directorate, Cambridge, Mass. Geophysics Res. Papers (1951) 19: 23-25.

(8) HILL, P. G., and STENNING, H. H.
1960. LAMINAR BOUNDARY LAYER IN OSCILLATORY FLOW. Amer. Soc. Mech. Engin. Ser. D, Jour. Basic Engin. 82: 593-607.

(9) HINZE, J. O.
1959. TURBULENCE—AN INTRODUCTION TO ITS MECHANISM AND THEORY. 586 pp., illus. New York.

(10) INCE, E. L.
1944. ORDINARY DIFFERENTIAL EQUATIONS. 558 pp., illus. New York.

(11) KARLSSON, S. F.
1959. AN UNSTEADY TURBULENT BOUNDARY LAYER. Jour. Fluid Mech. 5: 622-636. (Discussion 607-608).

(12) KHINCHIN, A. I. (Trans. by G. Gamow)
1949 MATHEMATICAL FOUNDATION OF STATISTICAL MECHANICS. 179 pp. New York.

(13) LEE , LESTER.
1958. CONVECTIVE HEAT TRANSFER. *In* Combustion and Propulsion (3d Agaard Colloq.) 614 pp., illus. New York.

(14) LEMON, E. R., and others.
1963. THE ENERGY BUDGET AT THE EARTH'S SURFACE. PART I. U.S. Dept. Agr. Prod. Res. Rpt. 71, 33 pp., illus.

(15) LETTAU, H. H., and DAVIDSON, BEN (Eds.).
1957. EXPLORING THE ATMOSPHERE'S FIRST MILE. v. 1, pp. 332-336. London and New York.

(16) LIEPMANN, H. W.
1952. ASPECTS OF THE TURBULENCE PROBLEM. [Jour. Applied Math-Physics.] Ztschr. f. Angew. Math. u. Phys. 3: 321-342; 407-426.

(17) LIGHTHILL, M. J.
1954. RESPONSE OF LAMINAR SKIN FRICTION AND HEAT TRANSFER TO FLUCTUATION IN STREAM VELOCITY. Royal Soc. London, Proc., Ser. A, 224: 1-23.

(18) ———
1956. REVIEW: THE STRUCTURE OF TURBULENT SHEAR FLOW. A. A. Townsend. Jour. Fluid Mech. 1: 554-560.

(19) LIN, C. C.
1961. STATISTICAL THEORIES OF TURBULENCE, SECTION C—TURBULENT FLOWS AND HEAT TRANSFER. *In* High Speed Aerodynamics and Jet Propulsion. v. 5. The Princeton Series. Princeton, N.J.

(20) MONIN, A. S.
1959. GENERAL SURVEY OF ATMOSPHERIC DIFFUSION. (Internatl. Symposium on Atmos. Diffusion and Air Pollution.) Adv. in Geophys. 6: 29-40.

(21) OBUKHOV, A. M.
1959. DESCRIPTION OF TURBULENCE IN TERMS OF LAGRANGIAN VARIABLES. Adv. in Geophys. 6: 113-116.

(22) PENMAN, H. L., and LONG, I. F.
1960. WEATHER IN WHEAT: AN ESSAY IN MICRO-METEOROLOGY. Roy. Met. Soc. [London] Quart. Jour. 86: 16-50.

(23) PRANDTL, L.
1925. BERICHT ÜBER UNTERSUCHUNGEN ZUR AUSGEBILDETEN TURBULENZ. Ztschr. f. Angew. Math. u. Mech. 5: 136-139.

(24) PRIESTLEY, C. H. B.
1952. ATMOSPHERIC TURBULENCE IN THE BOUNDARY LAYER. (Internalt. Symposium on Atmos. Turbulence in the Boundary Layer.) U.S. Air Force Cambridge Res. Center, Geophysics Res. Directorate, Cambridge, Mass. Geophysics Res. Papers (1951) 19: 33-43.

(25) ———
1959. TURBULENT TRANSFER IN THE LOWER ATMOSPHERE. 130 pp., illus. Chicago.

(26) ROBINSON, S. M.
1961. A METHOD FOR MACHINE COMPUTATION OF WIND PROFILE PARAMETERS. Wis. Univ. Dept. of Meteor. (Contract DA-36-039-SC-80282 with Meteor. Dept., U.S. Army Electronics Prov. Ground, Fort Huachuca, Ariz.) Tech. Note 1: 1-10. Madison.

(27) SCHLICHTING, H. (Trans. by J. KESTIN)
1960. BOUNDARY LAYER THEORY. 647 pp., illus. New York.

(28) SHAW, F. S.
1953. RELAXATION METHODS. 396 pp., illus. New York.

(29) SHEPPARD, P. A.
1958. TRANSFER ACROSS THE EARTH'S SURFACE AND THROUGH THE AIR ABOVE. Roy. Met. Soc. [London] Quart. Jour. 84: 205-224.

(30) Spalding, D. B.
1960. Heat and mass transfer in aeronautical engineering. Aeronaut. Quart. 11: 105-136.

(31) Spence, D. A.
1960. Distributions of velocity and enthalpy in the compressible turbulent boundary layer. Jour. Fluid Mech. 9: 368-387.

(32) Sutton, O. G.
1953. Micrometeorology. 333 pp., illus. New York.

(33) ———
1955. Atmospheric turbulence. Ed. 2. 111 pp., illus. Methuen & Co., London and New York.

34) Tan, H. S., and Ling, S. C.
1960. Quasi-steady micro-meteorological atmospheric boundary layer over a wheat field. Therm. Adv. Res., Rpt. TAR-IR 602: 1-16. Ithaca, N.Y.

(35) ——— Ritter, A., and Ordway, D. E.
1960. The effects of turbulence and photosynthesis on CO_2 profiles in the lower atmosphere. Therm. Adv. Res., Rpt. TAR-IR 601: 1-22. Ithaca, N.Y.

(36) Tepper, M.
1959. Mesometeorology. The link between macroscale atmospheric motions and local weather. Amer. Meteor. Soc. Bul. 40: 56-72.

(37) Townsend, A. A.
1956. The structure of turbulent shear flow. 315 pp., illus. London.

(38) Watson, J.
1958. A solution of the Navier-Stokes equations illustrating the response of a laminar boundary layer to a given change in the external stream velocity. Jour. Mech. and Appl. Math. Quart. 2: 302-325.

(39) Whittaker, E. T., and Watson, G. N.
1945. Modern analysis. 1st Amer. Ed. 608 pp. London.

U.S. GOVERNMENT PRINTING OFFICE 1963 O—673-752